Universidad de Concepción
Dirección de Postgrado
Facultad de Ingeniería -Programa de Doctorado en Ciencias de la Ingeniería con mención en Ingeniería Eléctrica

MODELLING AND CONTROL OF CO-ROTATING TWIN-SCREW EXTRUSION PROCESS

(Modelación y control de procesos de extrusión bi-tornillo)

Tesis para optar al grado de:

Doctor en Ciencias de la Ingeniería con Mención en Ingeniería Eléctrica

GEIMER FERNANDO LOTERO GARNICA

CONCEPCIÓN-CHILE

2017

Profesor guía: Dr. Daniel Sbarbaro Hoffer
Departamento de Ingeniería Eléctrica, Facultad de Ingeniería
Universidad de Concepción

Autor:

Geimer Fernando Lotero Garnica

Profesor Guía:

Dr. Daniel Sbarbaro Hoffer

Director de Programa:

Miguel Figueroa Toro

Esta tesis ha sido revisada por los señores:

Dr. Daniel Sbarbaro Hoffer, Profesor Guía
Departamento de Ingeniería Eléctrica-Facultad de Ingeniería
Universidad de Concepción

Dr. Alejandro Rojas Norman
Departamento de Ingeniería Eléctrica-Facultad de Ingeniería
Universidad de Concepción

Dr. Bernhard Maschke
Laboratoire d'Automatique et de Génie des Procédés
Université Claude Bernard Lyon-1

y ha sido ---

To my wife

Abstract

In this work a distributed parameter bi-zone dynamic model with moving interface of an extrusion process is presented. The interconnection of the moving interface is performed under the assumption of variable viscosity along the extruder. A finite volume method is proposed for discretizing the dynamic model. The steady state values of the variables were calculated by using an efficient optimization algorithm without the need of performing back calculations. Experimental tests performed with an industrial type twin screw extruder are compared against simulations for the case of variable screw speed and constant feed rate. The comparison shows good qualitative agreement between experimental and simulation results. An energy based controller for the validated extrusion process model is derived using internal energy as a storage function and controlled variable with the screw speed as control input. The stability of the controller is proved through the use of a Lyapunov-like candidate function. Finally, the practical usefulness of the method is illustrated by closed-loop simulations of the experimentally verified model of the extrusion process. This model can be used to design observers for estimating non-measurable variables as well as advanced control strategies.

Acknowledgements

I would like to thank to all those people who helped me in the process of completing my PhD thesis. Especially, I express my appreciation to my thesis director Professor Daniel Sbarbaro who support me since the beginning of this endeavor. I am really grateful with my co-supervisors Professor Bernhard and Doctor Françoise Couenne for of all the help, patience and guidance through this process. Their experience helped me a lot.

I wish to thank Professor Flavien Melis a the IMP Laboratory of the Université de Lyon for all his kind support with the experimental tests, also Hatim Aboulbaraket and Professor Hamroum Boussad for their help with the data adquisition system for the extrusion process. I am also grateful with Professor Alejandro Rojas for his recommendations at the begining of this project. I acknowledge all the people from the Laboratoire d'Automatique et de Génie des Procédés (LAGEP) and the Université Claude Bernard Lyon 1 for receiving me in his lab during all my visits to France. I am also very grateful with the University of Concepción because of this opportunity.

I would like to appreciate the support received from the ANR sponsored project HAMEC-MOPSYS under Reference Code ANR-11-BS03-0002 and by the French-Chilean ECOS/-CONICYT project C12E08. Also, I am very thankful with the Chilean Government and CONICYT for their support with the Scholarship for Doctoral Studies in Chile.

I express my deepest appreciation to my family, who supported me in this crazy idea of start my doctoral studies far away from home. And finally, I thank my wife, Lina, for all her advises, support, patience and unconditional love. Without her, this thesis would not be completed.

Contents

List of Figures

List of Tables

Symbols

PP	Polypropylene
PFZ	Partially filled zone
FFZ	Fully filled zone
A_1	WLF temperature dependency
A_2	WLF temperature dependency
B	Coefficient of pressure flow
c	Concentration
C_l	Distance between axes of screws
C_p	Heat capacity
D	External diameter
D_s	Internal diameter
D_1	WLF reference viscosity
D_2	WLF reference temperature
e	Tip width
$I(l)$	Quadratic error function
f	Filling ratio
F_{in}	Input flow
F_d	Flow at the die
H	Channel depth of the screw
k	Color function
K_d	Die conductance
L	Screw length
L_d	Die length
$l(t)$	Interface position
M	Total Mass
n	Number of screw flights
N	Screw speed
N_d	Number of discretization elements
P	Pressure

P_0	Atmospheric pressure
R_{ext}	External radius of the screw
R_d	Die radius
S_{eff}	Effective surface
S_{exc}	Exchange surface
T	Temperature
T_b	Barrel temperature
T_{in}	Input temperature
V_0	Occupied volume by the material
V_{eff}	Effective volume of the extruder
W	Channel width
α	Thermal exchange coefficient
α_w	Fligth angle
γ	Shear rate
η	Viscosity of the matter
ξ	Screw pitch
μ	Viscous dissipation coefficient
ρ_0	Material density
τ	Critical shear stress
ϕ	Helix angle
ψ	Inter-meshing angle

Subscripts

$_{in}$	Subscript for inlet
$_d$	Subscript for the die
$_f$	Subscript for FFZ
$_p$	Subscript for PFZ
$_b$	Subscript for the barrel
$_*$	Subscript for steady state

Chapter 1

Introduction

1.1 Introduction

The extrusion processes are mainly used in food and chemical industry for mixing, processing and molding of either polymers or raw materials for products such as cereals, potato chips and cookie dough. Basically, an extruder is made of a barrel and a screw who rotates inside and forces the product according to the Archimedes principle. At the end of the barrel, there is a die where the material comes out of the process. There exist two type of extruders, the single screw and the twin-screw extruders. Single screw extruders have poor mixing capability and are limited in their ability to transport high viscous materials. On the other side, twin-screw extruders, are divided in two additional types: counter-rotating and co-rotating screws. In the counter-rotating type, the screws are moving in opposite directions, while in the co-rotating type, screws are moving in the same direction. The co-rotating extruders are by far, the most used type thanks to its high mixing capabilities and self-cleaning capabilities. The counter-rotating and co-rotating screws can be inter-meshing or non-inter-meshing. In the first one, one screw penetrates the channel of the other screw producing a positive pumping action, better mixing capabilities and self-cleaning characteristics. Meanwhile, in the non-inter-meshing configuration the screws do not interfere between each other and their behaviour is very similar to the single screw extruders.

The extrusion process implies different interacting factors that increase the complexity and difficult the task of modelling and control. These interacting factors are related to material properties (i.e. rheology, thermal conductivity,etc.), operating conditions (screw speed, feed rate, barrel temperature, etc.) and the geometry of the machine (screws, barrel, die, etc.). In addition, being an energy intensive production method, process energy efficiency is one of the major concerns and the selection of the most

energy efficient processing conditions is a key to reducing operating costs [1]. Fig. 1.1 shows an open loop diagram of a typical twin-screw extrusion process with manipulated variables, disturbance variables, process output variables, and product quality variables [2].

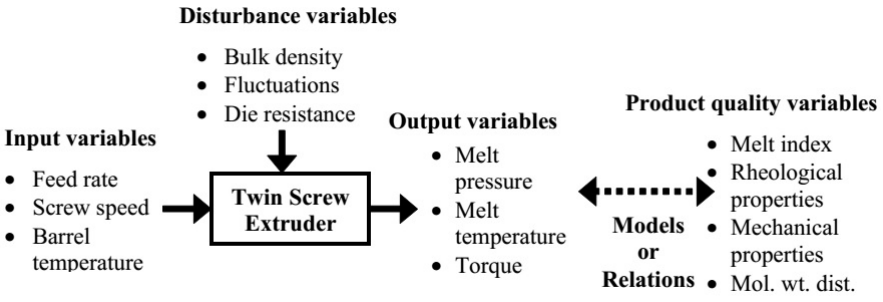

FIGURE 1.1: Open Loop Diagram of the extrusion process [2].

Thanks to its complexity, the task of control and modelling the extrusion process is challenging and has been of constant interest through years. Modelling challenges include complex screw geometry, moving interfaces and flow boundaries. Problems such as the identification of an equivalent geometry of the screws and the modelling of systems of PDE's with a moving interface are analyzed through this work in detail. On the other hand, although several empirical and phenomenological approaches for modelling the extrusion process have been proposed in literature, the majority of control strategies presented are related only to predictive control and linearized multivariable control. However, so far in most cases the authors present some experimental validation and different simulation methods but no steady state computations are discussed. Additional control challenges are related with the problem of modelling and simulation of systems of PDE's with a moving interface, the control of nonlinear PDE's, nonlinear systems with delays and passivity based control.

1.2 Objectives

The main objective of this project is to design and implement an energy-based control methodology that provide consistent operation of a twin-screw extruder process bi-zone model with non-constant viscosity. The objective was accomplished by performing the following steps:

- An infinite dimensional model for the extrusion process was obtained based on previous works in order to obtain a model that provides a reasonable description of a twin-screw extrusion process.
- A finite volume method approach adapted to deal with a moving interface with variable viscosity was presented in order to perform dynamical simulations on the extrusion process model.
- Dynamical simulations were developed using the discretized extrusion process model with variable viscosity.
- The bi-zone model with variable viscosity was validated trough experimental tests performed with an industrial type twin-screw extruder.
- An energy-based control strategy was designed for the bi-zone extrusion process model. Stability of the closed loop was proved using Lyapunov-like arguments and the controller was validated through closed-loop simulations.

This work was supported in part by the ANR sponsored project HAMECMOPSYS under Reference Code ANR-11-BS03-0002 and by the French-Chilean ECOS/CONICYT project C12E08.

1.3 Organization and contribution of the thesis

This thesis is divided into four chapters:

- In Chapter 2 general aspects regarding to the modelling of the twin-screw extrusion process are presented. The proposed bi-zone model based on mass and energy balances with the assumption of variable viscosity is explained in detail. This model comprises a moving interface which separates a region where the material is accumulated behind the die and fills completely the available volume which is called the Fully Filled Zone (FFZ) from another spatial domain that is not completely filled by the material which is called Partially Filled Zone (PFZ). A discretization scheme for the proposed model based on the finite volume method is used in order to deal with the moving interface. In addition interface relations and boundary conditions are considered.
- In Chapter 3 dynamic simulations of the bi-zone model with variable screw-speed and variable input flow are presented in order to perform a physical validation of the model. It is worth to point out that two different conditions for viscosity are taken into account: constant and variable viscosity.

- In Chapter 4 the bi-zone model is adapted experimentally to an industrial twin-screw extruder. In this study the extrusion of Polypropylene has been chosen. The material properties and equipment are described in details in this Chapter. In addition, the steady state of the extrusion process model is studied through the implementation of an optimization problem using a golden search algorithm. The conservativeness of the finite volume method is explained. Simulation and experimental tests for the extrusion of Polypropylene are presented.

- Chapter **??** is related to the control of the extrusion process. First the entropy balance for the extrusion process is developed which could be useful for control purposes in future works. Later, the energy-based control for the validated extrusion process using the internal energy as a storage function and controlled variable is explained with detail. A section dedicated to the stability analysis of the closed-loop system is included in this chapter. Finally, a simulation example showing the behaviour of the model-based controller is presented. The thesis concludes with final remarks and perspectives on future work in Chapter 6.

1.4 Publications

1. **International Journal papers:**
   F. Lotero, F. Couenne, B. Maschke, and D. Sbarbaro, *Distributed parameter bi-zone model with moving interface of an extrusion process and experimental validation*, Mathematical and Computer Modelling of Dynamical Systems (2017),0(0):1-19. doi:10.1080/13873954.2016.1278393.
   F. Lotero, F. Couenne, B. Maschke, and D. Sbarbaro, *Energy-based control of a distributed parameter bi-zone model with moving interface*, (2017), Submitted to the International Journal of Control.

2. **International conference papers:**
   F. Lotero, F. Couenne, B. Maschke, and D. Sbarbaro, *Bi-zone modelling and simulation of twin-screw extrusion process with variable screw speed*, 8th Vienna International Conference on Mathematical Modelling 8 (2015), pp. 592–597.

Chapter 2

Extrusion process modelling

2.1 Introduction

The earliest developments of the extruder technology are not new. In 1797, Joseph Bramah developed the earliest industrial extruder in 1797 through a patent in which he described a press for the production of pipes of a specific diameter and length without joints in lead and other soft metals [3]. Later, in 1869 the first known twin-screw extruder was developed by Follows and Bates for the sausage manufacture [4]. The first screw extruder designed especially for processing thermoplastic materials was developed in 1935 by Paul Troester [5], and further developments are based on improving product quality, adapting the process to new type of materials, reduce energy consumption, minimize manufacturing costs, etc. Although there exist several developments since the invention of the first screw extruder, the main idea of the process remains, that is, as an Archimedes screw that rotates into a barrel.

Although screw extruders have been used commercially for many years, the task of modelling and control is complex due to strong interactions that exist between a large number of factors such as material properties (rheology, thermal conductivity, etc.), geometrical factors (screw design, screw wear, etc.) and operating conditions (screw speed, barrel temperature, flow rate, etc.). Modelling challenges include complex screw geometry, moving interfaces and flow boundaries. This complexity has lead in recent years to an increase in the interest to provide suitable models for analysis and control [6].

This chapter is organized as follows: Section 2.2 deals with some fundamentals on screw-extruders such as classification, geometrical properties and process description. A brief bibliographic synthesis regarding to the modelling of the extrusion process together with the presentation of the bi-zone model and interface relations is presented on Section 2.3.

Finally, Section 2.4 presents the discretization of this moving interface model using a finite volume method.

2.2 Extrusion process overview

2.2.1 Extruders description and classification

It is possible to describe two types of extruders, the single screw extruders and the twin-screw extruders. A single screw extruder consists of one screw rotating into a barrel. The material is transported due to the friction with the channel walls. The main disadvantage yields in the fact that if the material slip at the barrel wall, it will rotate with the screw without being pushed forward [2]. Therefore, the effect of the extrusion is null if the material adheres to the screw. The above statement can be used to say that the single screw extruders have poor mixing capability and are limited in their ability to transport high viscous materials. In order to address these problems, the twin-screw extruder technology was implemented. The presence of a second screw allows to move forward the material in the extruder, making the propulsion of materials less dependent on friction, temperature and pressure. However, the twin-screw extruders heavily depends on the geometry of the machine (screw inter-meshing, direction of rotation, etc). Table 2.1 shows some of the advantages and limitations of industrial twin-screw extruders.

2.2.2 Process description of a twin-screw extruder

The extrusion process can be basically described in terms of four main zones. The feeding zone, the conveying zone, the melting or transition zone and the pumping zone. Fig. 2.1 shows a schematic of the extrusion process.

- Initially, at the feeding zone, the raw material is charged into the machine trough a hopper at room temperature. There could be several hoppers in the process in order to obtain different compositions of the final product.
- The rotation of the screws is made using an electric motor attached to a reducer. The material is transported from the hopper to the end of the barrel due to the friction between the screw and the material. In addition, the use of a twin screw helps to achieve a positive displacement of the material.
- In the conveying zone the material is compacted and transported to the transition zone. The barrel is connected to electrical heating and water-cooling systems which helps to melt the material. In the transition zone the material is mixed and melted

Twin-Screw Extrusion Process	
Advantages	**Limitations**
-Better mixing and homogenization capacity	-Parasite secondary reactions if the temperature is too high
-A large heat transfer surface area that allows good control of the stock temperature	-Air-entrapment
-There is a good control over residence times and stock temperatures for the profile extrusion of thermally sensitive materials	-Capital costs are higher due to more frequent and costly maintenance requirements and more complicated operations
-Residence time distribution is short and narrow	
-Interchangeable screw and barrel sections can be arranged to serve distinct and precise processing requirements	
-High pressure and temperature support: 0 to 500 bar and 400-500 °C	
-The possibility of injection of reagents along the extruder	

TABLE 2.1: Advantages and limitations of a twin-screw extruder. (Source: Personal collection).

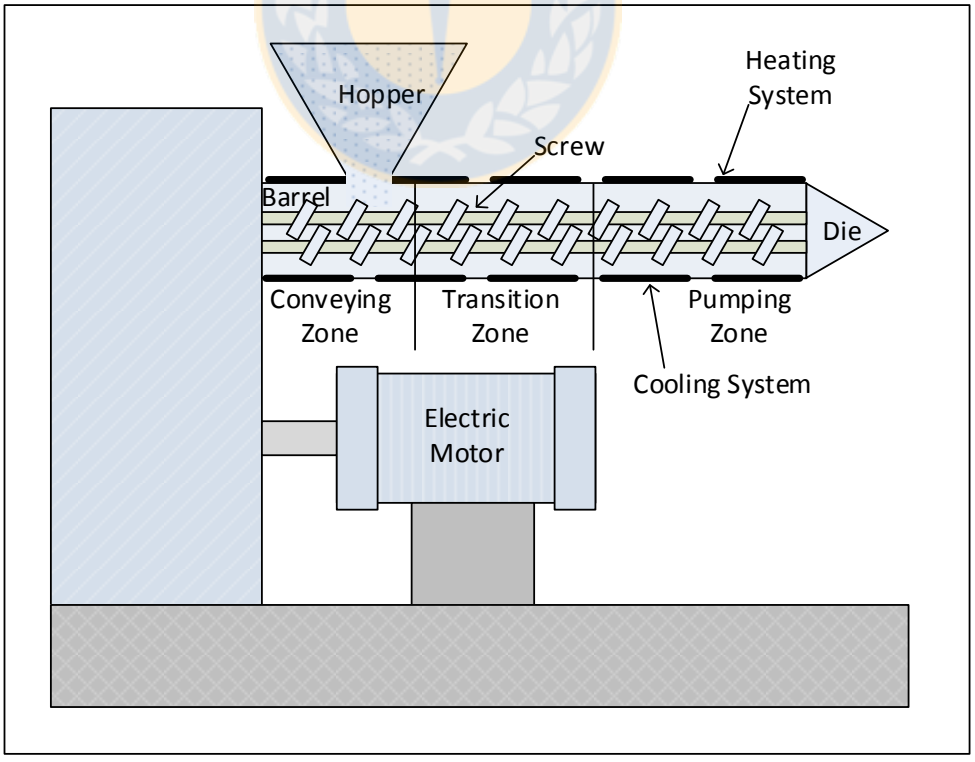

FIGURE 2.1: Schematic view of a twin-screw extrusion process. (Source: Personal collection).

thanks to a chemical reaction that occurs due to the heat of the barrel, viscous dissipation and friction.

- In the pumping zone the material gets completely melted and the pressure increases because of the screw rotation and the change of diameter at the die. The melt is finally extruded trough the die in the desired form. It is worth to point out that the geometry of the screws is different in each zone in order to improve the melting properties of the product.

2.2.3 Twin-screw extruders classification

According to its name, a twin screw extruder contains two parallel screws located into a barrel. Due to this main characteristic, a twin-screw extruder can be classified according to the direction of rotation and the engagement of the screw as follows:

- Direction of rotation: If the screws are rotating in the same direction, the extruder is called co-rotating. On the other hand, if the screws are rotating in opposite directions, the extruder is called counter-rotating. Fig. 2.2 shows a schematic view of this screw classification.

FIGURE 2.2: Co-rotating and counter-rotating twin-screws [7].

- Inter-penetration: This classification is related to the degree of inter-penetration of the two screws into each other. A twin screw extruder could be classified as an inter-meshing extruder if the separation between the screw axes is less than the outer screw diameter [4]. On the other hand if the separation between the screw axes is at least equal to the screw outer diameter the extruder is called non-inter-meshing. The inter-meshing configuration provides a positive pumping action, better mixing capabilities and self-cleaning characteristics. Meanwhile in the non-inter-meshing configuration the behaviour is very similar to single screw extruders.

The selection of each type of twin-screw extruders basically depends on the type of application. For example, high speed co-rotating twin screw extruders are used for compounding resin with additives (colorants, fillers, flame retardants, reinforcements,

stabilizers), devolatization to remove solvents, and reactive extrusion. Low-speed co-rotating and counter-rotating extruders are used to produce profiles and pipe. Counter-rotating twin screws are used for compounding PVC and other resin systems. Non-intermeshing counter-rotating extruders are principally used for devolatilization and chemical reactions [7]. In food industry applications, the co-rotating twin screw extruders are commonly used due to its self-cleaning capacity, the excellent mixing quality and a very high degassing rate.

2.2.4 Principal elements of a twin-screw extruder

2.2.4.1 Barrel

The barrel represents the fixed external cover in which the screws rotate. In modern equipments, the barrel and the screw are constructed in a modular way. That characteristic allows more flexibility on applications because every section of the barrel can be used according to their function, i.e. feeding, degassing, etc. In addition, due to the importance of the temperature control in the extrusion process, the barrel plays an important role because it contains the heating and cooling systems of the machine. Fig. 2.3 shows a schematic view of a barrel, note that there could be barrel sections with cylindrical shape.

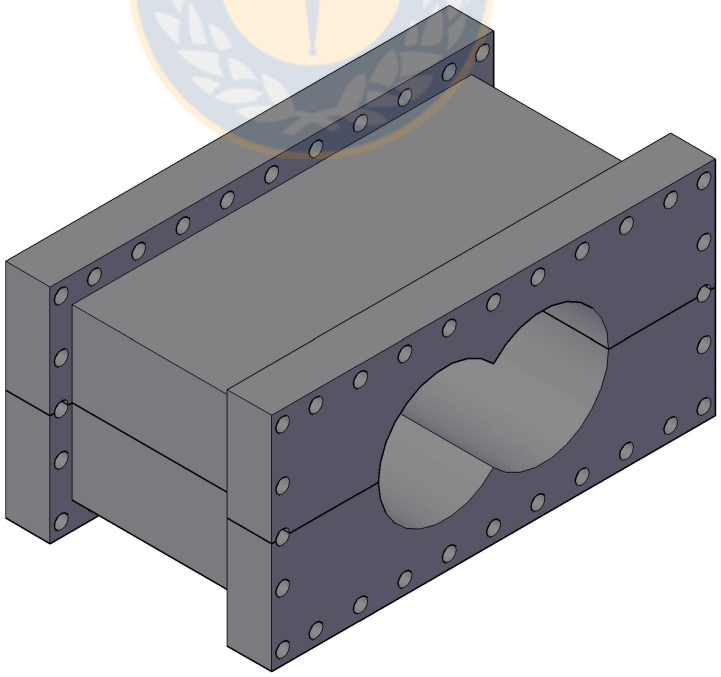

FIGURE 2.3: Example of a barrel section of a twin-screw extruder. (Source: Personal collection).

2.2.4.2 The screw

As stated above, the screws are constructed in a modular way. This property allows composing different geometrical configurations in order to localize the feeding, melting, conveying, mixing, pumping and venting at specific locations along the extruder barrel [7], and also allows to easily change the screw designs in order to adapt the system to different material processing and requirements. It is possible to have three different types of screws: Conveying, or right handed, elements drag material forward due to their positive helix angle; the higher the angle, the higher the conveying capacity. Left handed elements have a negative helix, thus impose a restriction to the flow that can induce local fully-filled flow conditions, heat transfer becoming more efficient and the flow pattern much more complex [8]. The kneading blocks are a combination of different kneading disks, which can have negative, neutral and positive angles. Positive and negative angles are very efficient in terms of mixing and induce conveying capacity. Neutral angles have no drag capacity; therefore, the local flow residence time increases and both distributive and dispersive mixing take place. Fig. 2.4 shows a screw profile in which different types of screw elements can be observed. In addition, Fig. 2.5 shows a detail of an interface

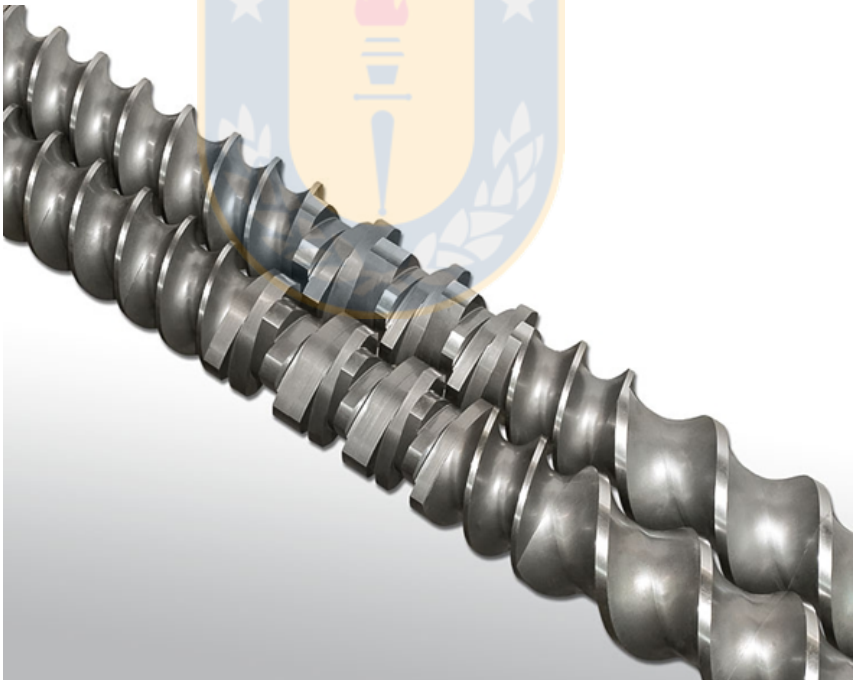

FIGURE 2.4: Example of different screw elements.(Source: Online. Avalaible from: `www.binovapm.it`).

generated by the presence of the melt behavior when inverse screw profiles are used in the extruder. Note that a fully filled region is generated because of the geometry of the screw sections.

FIGURE 2.5: Example of different screw sections. (Source: Personal collection).

2.2.4.3 Screw geometry

The screw geometry of twin-screw extruders have been studied by different authors trough last years [9][10]. It is possible to describe the geometry of a twin-screw extruder with the following parameters which can be seen in Fig. 2.6 and 2.7:

- External ratio of the screw: R_{ext}
- The distance between axes: C_l
- The number of screw flights: n
- The screw pitch: ξ

With those parameters it is possible to define the following variables:

- Channel width: Is the channel extension, in terms of the number of screw flights and the screw pitch

$$W = \frac{\xi \cos \phi}{n} - e. \tag{2.1}$$

- Helix angle: Is the angle of the screw flight

$$\phi = \arctan \frac{\xi}{2\pi R_{ext}}. \tag{2.2}$$

- Tip width: Is the width of the flight tip

$$e = \alpha_w R_{ext} \sin \phi. \tag{2.3}$$

- Inter-meshing angle: Is the angle of the zone of interpenetration

$$\psi = \arccos \frac{C_l}{2R_{ext}}. \tag{2.4}$$

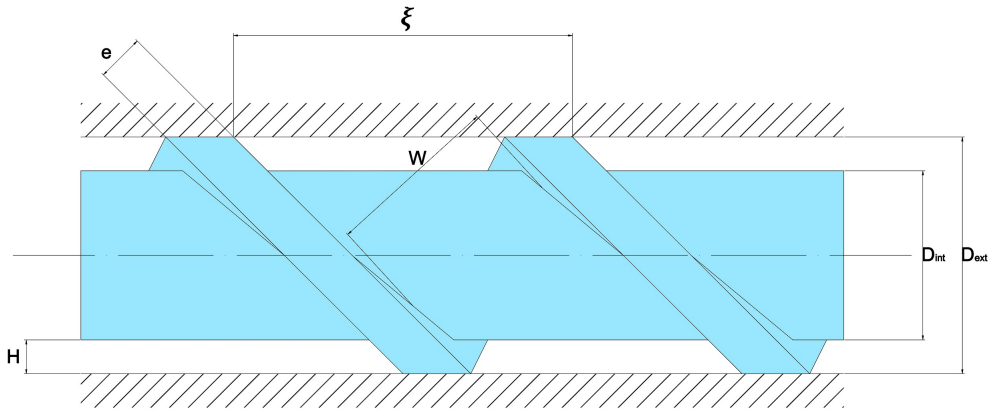

FIGURE 2.6: Screw geometry and characteristic dimensions: Side view. (Source: Personal collection).

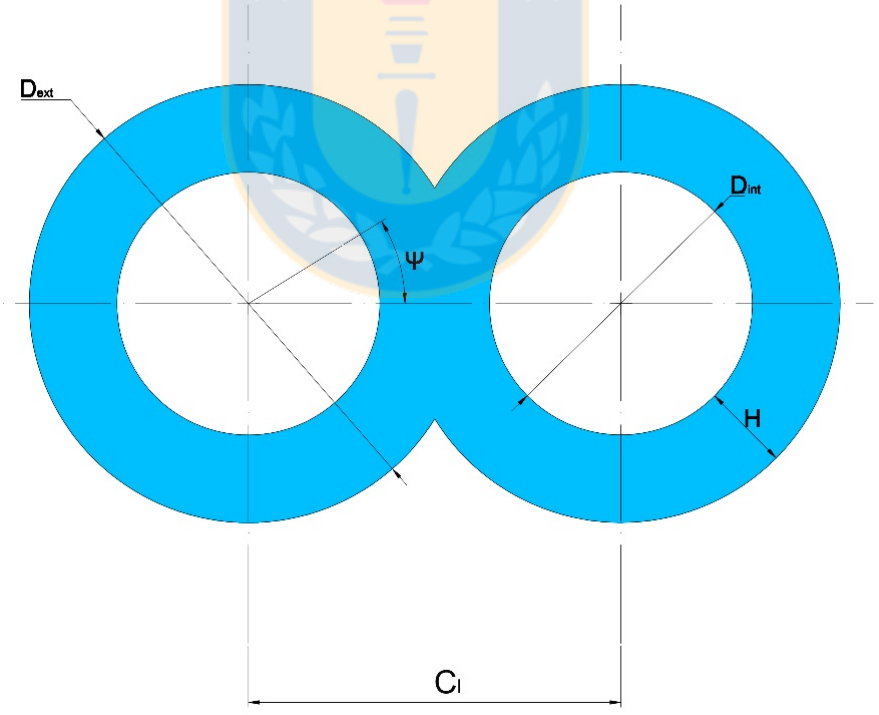

FIGURE 2.7: Screw geometry and characteristic dimensions: Front view. (Source: Personal collection).

2.3 Bi-zone model of the extrusion process

2.3.1 Extrusion process modelling overview

As stated at the beginning of this chapter, modelling and control of the extrusion process is challenging because of its complexity and the strong interactions that exist between a large number of factors such as material properties, geometrical factors and operating conditions. This complexity has lead in recent years to an increase in the interest to provide suitable models for analysis and control.

Several empirical and phenomenological approaches for modelling the extrusion process have been proposed. For instance, Wang [11] proposed a continuous time empirical model based on Laguerre functions described by transfer functions identified from experimental data. Garge [12] presented a systematic procedure for identifying a control-relevant model for reactive extrusion processes. Iqbal [13] proposed a gray box model, which essentially incorporates both phenomenological and empirical approaches, to predict the behavior of output variables due to changes in the co-rotating twin screw extruders. In this work a steady-state study was carried out in order to analyze the rheological behavior of the melt. On the other hand, several phenomenological models have been described in literature. Tayeb et al. [14] developed a phenomenological model based on solving the thermal balance and Stokes equation for a co-rotating twin-screw extruder with deep screw channels. In this work, the model was based on a division of the twin-screw extruder into four functional sections. The steady state values of the variables were computed by assuming a constant viscosity with numerical values chosen accordingly to the local shear rate and temperature. Zuilichem [15] presented a detailed heat transfer model for twin-screw extruders. However, neither experimental nor simulated results were presented.

On the other hand, Kulshreshtha [16] presented dynamic model for twin screw extruders based on mass and energy balances with experimental validation. An alternative numerical method was developed to solve the governing equations by using a simplified steady state profile. First, the solution on the solid conveying zone is found and later this information provides the boundary conditions for the solution at the melt zone. However, this numerical method was not efficient, because it requires repeated iterations to calculate the position of the moving boundary between each solid conveying zones and melt zone.

On the other hand, a non-linear infinite dimensional model obtained by using transport equations through a moving interface was presented in [17]. In this case, the authors proposed a model based on the works by Kulshreshtha, with constant viscosity. The dynamical model is solved using a finite volume method scheme. However, no experimental results are presented and the assumption of constant viscosity is not quite useful

since the rheology of the melt influences the dynamic behaviour of the extrusion process. More complex models using quasi-3D spatial profiles of the degree of fill are described in [18][19]. Several models representing the extrusion process as a series of Continuous Stirred Tank Reactors (CSTR) [20], [21], [22] were also presented. The advantage of this modelling approach is that it gives rise to a precise model since each piece of screw can be taken into account. Moreover, any stage (such start-up) of the extrusion process can be simulated. The authors, presented an experimental validation of this model with good quantitative results. However, the main disadvantage of this modelling approach lies on the fact, that dividing the extrusion process in several CSTR is tedious and complicated.

In those works, the authors present some experimental validation and different simulation methods. However, steady state computations are not discussed. In fact, as far as modelling issues are concerned, one can find many papers devoted to steady-state modelling for design purpose, but works devoted to the dynamic modelling of extruders are less common [17].

2.3.2 Bi-zone model of the extrusion process

This work extends those previous works developed by [16], [23], [24], [25] and [26] in which the extrusion process is simplified into a bi-zone model. In this case, the phenomenological modelling of the extrusion process is performed with the assumption of variable viscosity with moving interface, which adds more complexity to the analysis because of the temperature and shear rate dependency of the viscosity. In this particular case, the resulting bi-zone model has a non-linear infinite dimensional structure and can be described as follows:

A region where the material is accumulated behind the die and fills completely the available volume which is called the fully filled zone *(FFZ)*. At the *FFZ* the flow depends both on the pumping capacity of the screw and the pressure flow. This region can be related to the transition and pumping zone on the extruder. The extruder may also comprise a spatial domain that is not completely filled by the material. This region corresponds to the feeding and conveying region and is called partially filled zone *(PFZ)*. In this domain, the pressure gradient is zero and the pressure inside the barrel is approximately equal to the atmospheric pressure. These two zones are coupled with a very thin moving interface which characterizes the spatial domains where the pressure gradient is null or not. Assuming the interval of the spatial domain of the extruder as $[0, L]$ where $L > 0$ is the length of the extruder, and calling $l(t) \in [0, L]$ as the position of the thin interface, the domain of the *PFZ* is $[0, l(t)[$ and the *FFZ* is defined in the interval $]l(t), L]$. Fig. 2.8 shows a schematic view of the bi-zone model.

On the other hand, the extrusion of Polypropylene *(PP)* has been chosen in this work since it is a shear sensitive material [27]. When the shear stress is increased, the viscosity of the melt decreases. This is very important in the case of variable screw speed since at higher values the shear heating provided by the screw rotation becomes the main heating source [28].

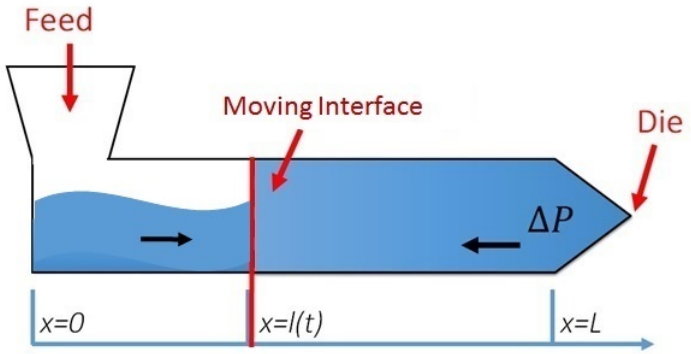

FIGURE 2.8: Bi-zone model of the extrusion process. (Source: Personal collection).

2.3.3 Assumptions

The following assumptions are considered:

- **i.** The considered melt is formed of PP and another constituent. The latter can be an additive chosen in order to obtain the right quality of the final product or a tracer that can be introduced in order to characterize the flow in the extruder.
- **ii.** The heat capacity C_p and the density ρ_0 of the *PP* are assumed to be constant and identical for PP and the additive. This statement is related to the fact that, on the extrusion processes, the percentages of additive used are very small compared to the concentration of *PP*.
- **iii.** The equivalent screw pitch ξ is assumed to be uniform along the extruder.
- **iv.** The *PFZ* is submitted to atmospheric pressure P_0.
- **v.** The heat exchange with the barrel is modeled with the following constitutive relation $\alpha(T_b(x,t) - T_p(x,t))$ where α is the thermal exchange coefficient.

Remark 2.1. Regarding to assumption (*iii*), it worth to point out that real screw profiles are formed by an arrangement of screw sections which have different properties in order to adapt the system to a given material or processing conditions. In this study we have considered the mean value of ξ in order to use the simplest model for control purposes.

A variable pitch could be included for future works. However, some screw sections such as the kneading blocks should be analyzed in detail since its geometry is different ar more complex than the direct screw.

2.3.4 Definition of variables

The extrusion process can be used for the production of different products that may vary in their physical properties. Depending on the desired product, the extrusion process can combine different functions such as transport, mixing, compression, chemical reactions, cooking, drying, etc. Depending of each of these functions, different modelling parameters can be used; in this case, for a non-reactive polymer extrusion, the following variables are considered:

- Filling ratio $f_p(x,t)$: Is defined as the ratio between the occupied volume by the material in the extruder (V_0) and the effective volume (V_{eff}) between the barrel and the screws. The effective volume (V_{eff}) is the total volume that can be occupied by the material.

$$f_p(x,t) = \frac{V_0(x,t)}{V_{eff}}. \tag{2.5}$$

  It is worth to point out that, in the PFZ the filling ratio is less than the total available volume, i.e. $0 < f_p(x,t) < 1$. Meanwhile, at the FFZ the filling ratio is $f_f(x,t) = 1$.

- Concentration $c(x,t)$: Represents the volume fraction of tracer in the transported homogeneous mixture.

- Temperature $T(x,t)$: It depends both on the heat exchange between the barrel and the extruded material and the viscous dissipation phenomena due to the transformation of mechanical energy into heat.

- Pressure $P(x,t)$: In the PFZ the pressure is supposed to be equal to the atmospheric pressure P_0. On the other hand, in the FFZ, the pressure depends on the die flow F_d and the geometry of the die.

- Viscosity $\eta(T_p(x,t))$: Several models can be found in literature regarding the viscosity, which basically depends on temperature, shear rate and material physical properties. In this work, the viscosity of the material on both PFZ and FFZ was simulated using the Cross-WLF model. This model provides a representation of viscosity over a wide range of processing conditions [29]. Further details regarding to the Cross-WLF model can be found in Section 4.2.

2.3.5 Model of the partially filled zone

In the *PFZ*, the mass balance equation belongs to the domain $[0, l(t)[$ and it is written in terms of the filling ratio $f_p(x,t)$ with $l(t)$ the position of the interface. $f_p(x,t)$ is defined as the ratio between the volume filled by the material in the extruder (V_0) and the free volume or effective volume between the barrel and the screw (V_{eff}). In other words, V_{eff} is the total volume that can be occupied by the material.
The position of the interface will change due to the difference between the incoming and the outgoing flow rates. With these assumptions, the variation of the amount of material in time is derived as the change of the inflows and outflows through the effective section between the screw and the barrel (S_{eff}) defining an elementary volume in this area. Fig. 2.9 shows a Cartesian representation of the variation of the elementary volume between x_2 and x_1 with $0 < x_1 < x_2 < l(t)$ which can be written as:

$$\frac{d}{dt}\int_{x_1}^{x_2}\int_{0}^{z_{max}f_p(x,t)} \rho_0 y_{max} dz dx = F_m(x_1,t) - F_m(x_2,t), \tag{2.6}$$

with $F_m(x_1,t)$ an $F_m(x_2,t)$ as the inflow and outflow at x_1 and x_2 respectively. The integral form of the right term of the equation is $F_m(x_1,t) - F_m(x_2,t) = \int_{x_1}^{x_2} \partial_x F_m(x,t) dx$. On the other hand, distributing equation (2.6) and using Leibniz formula we have:

$$\int_{x_1}^{x_2}\left[\rho_0 y_{max} z_{max}\frac{\partial f_p(x,t)}{\partial t} + \int_{0}^{z_{max}f_p(x,t)}\frac{d}{dt}(\rho_0 y_{max} z_{max})\right]dx = -\int_{x_1}^{x_2}\frac{\partial F_m(x,t)}{\partial x}dx. \tag{2.7}$$

In equation (2.7) ρ_0 and $S_{eff} = y_{max} z_{max}$ are constant, then:

$$\rho_0 S_{eff}\frac{\partial f_p(x,t)}{\partial t} = -\frac{\partial F_m(x,t)}{\partial x}. \tag{2.8}$$

Extending to a global formulation of the mass balance in the *PFZ* and considering

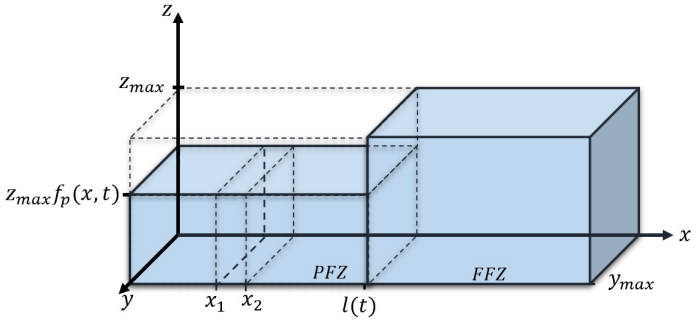

FIGURE 2.9: Cartesian representation of the effective volume V_{eff}. (Source: Personal collection).

the transport phenomena for screw elements of pitch ξ, we have the material flow as a

function of $f_p(x,t)$ and the screw speed $N(t)$ with $V_{eff} = \xi S_{eff}$:

$$F_m(x,t) = N(t)\rho_0 V_{eff} f_p(x,t). \tag{2.9}$$

Finally, replacing equation (2.9) we have the following mass balance equation:

$$\frac{\partial f_p(x,t)}{\partial t} = -\xi N(t)\frac{\partial f_p(x,t)}{\partial x}. \tag{2.10}$$

In addition, the concentration (c) represents the volume fraction of tracer in the transported homogeneous mixture. Since this variable has the same behavior as the homogeneous mixture because the mass density is supposed to be constant, its evolution can also be described by a transport equation in the *PFZ* as it follows:

$$\frac{\partial c_p(x,t)}{\partial t} = -\xi N(t)\frac{\partial c_p(x,t)}{\partial x}. \tag{2.11}$$

Defining $u(x,t)$ as the internal energy per unit of volume, $h(x,t)$ the enthalpy and $P(x,t)$ as the pressure (assumed to be uniform), we have:

$$u(x,t) = h(x,t) - P(x,t). \tag{2.12}$$

According to the first law of thermodynamics, the variation of energy per unit depends on the enthalpy inflow and outflow $F_h(x,t)$, the thermal power generated by viscous dissipation $Q_c(x,t)$ and the convective heat form the barrel to the melt $\phi_e(x,t)$. Then, the expression for the energy balance at the *PFZ* with transport velocity $\xi N(t)$ is as follows:

$$\rho_0 V_{eff}\frac{\partial}{\partial t}\Big((h(x,t) - P(x,t))f_p(x,t)\Big) = -\rho_0\xi N(t)\frac{\partial}{\partial x}(h(x,t)f_p(x,t)) - \rho_0 P_0\frac{\partial f_p(x,t)}{\partial t} + Q_c(x,t) + \phi_e(x,t), \tag{2.13}$$

with,

$$\begin{aligned} Q_c(x,t) &= \mu\eta(T_p(x,t))N^2(t), \\ \phi_e(x,t) &= S_{ech}\alpha(T_b(x,t) - T_p(x,t)), \end{aligned} \tag{2.14}$$

where μ is the viscous dissipation coefficient, η is the viscosity of the material, $S_{ech} = \pi D^2 L$ is the total exchange surface (the real exchange surface is proportional to the percentage of melt $f_p(x,t)$). Recalling that the pressure at the *PFZ* is equal to the atmospheric pressure P_0 and using equation (2.10) we have:

$$\rho_0 S_{eff}\frac{\partial h(x,t)}{\partial t} = -\rho_0\xi N(t)\frac{\partial h(x,t)}{\partial x} + (Q_c(x,t) + \phi_e(x,t)), \tag{2.15}$$

Finally, recalling the relationship betweeen $h(x,t)$ and the T_p of the homogeneous mixture with constant density ρ_0 as $\partial h(x,t) = C_p \partial T_p(x,t)$ we have the following:

$$\frac{\partial T_p(x,t)}{\partial t} = -\xi N(t) \frac{\partial T_p(x,t)}{\partial x} + \Omega(f_p, N, T_b, T_p)\,, \tag{2.16}$$

with

$$\Omega(f_p, N, T_b, T_p) = \frac{Q_c(x,t)}{\rho_0 V_{eff} C_p f_p(x,t)} + \frac{\phi_e(x,t)}{\rho_0 V_{eff} C_p}. \tag{2.17}$$

2.3.6 Model of the fully filled zone

In this section, the available volume is completely filled, so the filling ratio have no dynamics, i.e. $f_f = 1$. Since in this zone a pressure drop is assumed, the momentum balance equation in the *FFZ* is expressed in terms of the pressure gradient as:

$$\frac{\partial P(x,t)}{\partial x} = \eta(T_f(x,t)) \frac{V_{eff} N(t) \rho_0 - F_d(t)}{B \rho_0} \quad (t,x) \in (\mathbb{R},^+, [l(t), L])\,, \tag{2.18}$$

where B is the pressure flow coefficient and $F_d(t)$ is the net forward flow [24], [30]:

$$F_d(t) = \frac{K_d}{\eta_d(t)} \Delta P(t), \tag{2.19}$$

with $\Delta P(t) = (P(L,t) - P_0)$ and $\eta_d(t)$ as the melt viscosity at the die; $\eta_d(t) = \eta(T_f(L,t))$. The mass and energy balances provides the equations for the concentration $c_f(x,t)$ and the temperature $T_f(x,t)$ on the *FFZ* since the transport and thermal phenomena are similar to those which occur in the *PFZ*:

$$\frac{\partial c_f(x,t)}{\partial t} = -\frac{F_d(t)\xi}{\rho_0 V_{eff}} \frac{\partial c_f(x,t)}{\partial x}, \tag{2.20}$$

$$\frac{\partial T_f(x,t)}{\partial t} = -\frac{F_d(t)\xi}{\rho_0 V_{eff}} \frac{\partial T_f(x,t)}{\partial x} + \Omega(1, N, T_f, T_b). \tag{2.21}$$

2.3.7 Moving Interface

The interface that separates the *FFZ* from the *PPZ* is located at $l(t)$ where a pressure gradient from atmospheric pressure to a greater value occurs and the filling ratio changes from less than one to one. The position of the interface will change due to the difference between the incoming and the outgoing flow rates. Taking into account the assumption of a material composed by a homogeneous mixture and no chemical reactions in the process. In other words, no species are produced or destroyed and the variation of the amount of material in time is derived as the change of the inflows and outflows through

the cross section S_{eff} defining an elementary volume in this area. This cross section is the effective section between the screws and the barrel. Then considering a fixed domain $[l^-, l^+]$, which contains strictly the position of the interface, i.e. $l^- < l(t) < l^+$. The variation of the elementary volume between l^- and l^+ in Cartesian coordinates (x, y, z) can be seen in Fig. 2.9. Then, the dynamics of the moving boundary is obtained from the global mass balance on the FFZ:

$$\frac{d}{dt}\int_{l^-}^{l^+}\int_0^{z_{max}f_p(x,t)} \rho_0 y_{max} dz dx = F(l^-) - F(l^+) = \Delta F. \tag{2.22}$$

Recalling, $f_p(x,t)$ with $x \in [l^-, l(t)]$ as the filling ratio at the PFZ and $f_f(x,t) = 1$ with $x \in [l(t), l^+]$ as the filling ratio at the FFZ, it is possible to rewrite equation (2.22) as:

$$\int_0^{z_{max}f_p(x,t)} \left[\frac{d}{dt}\int_{l^-}^{l(t)} \rho_0 y_{max} dx + \frac{d}{dt}\int_{l(t)}^{l^+} \rho_0 y_{max} dx\right] dz = \Delta F. \tag{2.23}$$

Distributing and using the Leibniz Rule:

$$\int_{l^-}^{l^+} \left[\frac{d}{dt}\int_0^{z_{max}f_p(x,t)} \rho_0 y_{max} dz + \rho_0 y_{max} z_{max}\frac{\partial f_p(x,t)}{\partial t}\right] dx = \Delta F, \tag{2.24}$$

then,

$$\int_{l^-}^{l^+} \frac{d}{dt}\int_0^{z_{max}f_p(x,t)} \rho_0 y_{max} dz dx + \int_{l^-}^{l^+} \rho_0 y_{max} z_{max}\frac{\partial f_p(x,t)}{\partial t} dx = \Delta F. \tag{2.25}$$

Solving the integrals using the relationship $S_{eff} = y_{max} z_{max}$:

$$\rho_0 S_{eff}(f_p(l^-,t) - (f_p(l^+,t))\frac{dl(t)}{dt} + \int_{l^-}^{l^+}\frac{d}{dt}\int_0^{z_{max}f_p(x,t)} \rho_0 y_{max} dz dx = \Delta F, \tag{2.26}$$

$$\frac{dl(t)}{dt}\rho_0 S_{eff}(f_p(l^-,t) - 1) + \int_{l^-}^{l^+}\frac{\partial f_p(x,t)}{\partial t}\rho_0 y_{max} dx = \Delta F, \tag{2.27}$$

redistributing terms,

$$\frac{dl(t)}{dt}\rho_0 S_{eff}(f_p(l^-,t) - 1) + \int_{l^-}^{l(t)}\frac{\partial f_p(x,t)}{\partial t}\rho_0 y_{max} dx + \int_{l(t)}^{l^+}\frac{\partial f_f(x,t)}{\partial t}\rho_0 S_{eff} dx = \Delta F. \tag{2.28}$$

Recalling that at the FFZ the filling ratio is equal to one,

$$\frac{dl(t)}{dt}\rho_0 S_{eff}(f_p(l^-,t) - 1) + \int_{l^-}^{l(t)}\frac{\partial f_p(x,t)}{\partial t}\rho_0 S_{eff} dx = \Delta F, \tag{2.29}$$

using the relationship $\frac{\partial f_p(x,t)}{\partial t} = -\xi N(t)\frac{\partial f_p(x,t)}{\partial x}$

$$\frac{dl(t)}{dt}\rho_0 S_{eff}((f_p(l^-,t)-1) - \int_{l^-}^{l(t)} \xi N(t)\rho_0 S_{eff}\frac{\partial f_p(x,t)}{\partial x}dx = \Delta F, \tag{2.30}$$

rewriting,

$$\frac{dl(t)}{dt}\rho_0 S_{eff}(f_p(l^-,t)-1) + \xi N(t)\rho_0 S_{eff}(f_p(l^+,t) - f_p(l^-,t)) = \Delta F, \tag{2.31}$$

using the first order approximation of the filling ratio $f_p(l^-,t)$ and the flow rate $F(l^-,t)$:

$$\frac{f_p(l^-,t) - f_p(l(t),t)}{l(t)-l^-} = \frac{\partial f_p(l(t),t)}{\partial t}, \tag{2.32}$$

$$\frac{F(l^-,t) - F(l(t),t)}{l(t)-l^-} = \frac{\partial F(l(t),t)}{\partial t}, \tag{2.33}$$

then, it is possible to obtain:

$$\begin{aligned}\frac{dl(t)}{dt}\left(f_p(l(t,t) + (l(t)-l^-)\frac{\partial f_p(l(t),t)}{\partial x} - 1\right) + \xi N(t)\left((l(t)-l^-)\frac{\partial f_p(l(t),t)}{\partial x}\right) \\ = \frac{1}{\rho_0 S_{eff}}\left[F(l(t),t) - (l(t)-l^-)\frac{\partial F(l(t),t)}{\partial x} - F(l^+,t)\right].\end{aligned} \tag{2.34}$$

In the case that $l^- \to l(t)$

$$\frac{dl(t)}{dt} = \frac{F(l^+) - F(l(t),t)}{\rho_0 S_{eff}(1-f_p(l(t),t))}. \tag{2.35}$$

Taking into account that at the *FFZ* the net flow rate is uniform and equal to the net flow at the die, i.e. $F_d(t)$, see equation (2.19). In addition, the flow rate $F(l(t),t)$ is defined by the maximum pumping capacity of the screw,

$$F(l(t),t) = \rho_0 N(t) V_{eff} f_p(l(t),t). \tag{2.36}$$

Furthermore, the ordinary differential equation of the moving interface is:

$$\frac{dl(t)}{dt} = \frac{F_d(t) - \rho_0 N(t) V_{eff} f_p(l(t),t)}{\rho_0 S_{eff}(1-f_p(l(t),t))}. \tag{2.37}$$

2.3.8 Interface relations

To describe the coupling that exists between the two zones of the extrusion process model it is necessary to consider physical coupling relations. In this work, the coupling relationship for the homogeneous mixture mass balance is established taking into account

the continuity of pressure at the interface. In addition, it is possible to assume the viscosity of the matter, η, as variable or constant. In the case of constant viscosity it is simple to establish an analytical solution for the pressure at the interface. However, it is well known that the polymer rheology is directly related to temperature and pressure [7]. Within the extruder, increasing the temperature of the melt at a constant pressure results in a lower viscosity of the melt which in turn impedes the flow of the melt within the barrel [31]. Therefore, using time-varying viscosity should be useful for modelling purposes, since the dynamical behaviour of the extrusion process could be predicted properly. However, finding an analytical solution for the pressure at the interface is more difficult when time-varying viscosity is used because of that temperature dependency. The coupling relationship taking into account the continuity of pressure at the interface is shown as follows:

2.3.8.1 Continuity of the pressure at the interface

Recalling the expression for the pressure gradient from equation (2.18) with variable viscosity as:

$$P(L,t) - P(l(t),t) = \int_{l(t)}^{L} \eta(T_f(x,t)) \frac{\rho_0 V_{eff} N(t) - F_d(t)}{B\rho_0} dx. \tag{2.38}$$

It worth to point out that, the assumption of continuity of pressure at the interface is a state coupling relation. Therefore, taking into account that the pressure at the *PFZ* is equal to the atmospheric pressure P_0 we have: $P(l(t),t) = P_0$.

$$P(L,t) = P_0 + \frac{\rho_0 V_{eff} N(t) - F_d(t)}{B\rho_0} \int_{l(t)}^{L} \eta(T_f(x,t)) dx. \tag{2.39}$$

The term $\int_{l(t)}^{L} \eta(T_f(x,t))dx$ can be interpreted as the (time-varying) total viscosity of the fully filled part. On the other hand, the flow at the die is given by:

$$F_d(t) = \frac{K_d \Delta P}{\eta_d(t)} = \frac{K_d}{\eta_d(t)} \left(\frac{\rho_0 V_{eff} N(t) - F_d(t)}{B\rho_0} \int_{l(t)}^{L} \eta(T_f(x,t)) dx \right), \tag{2.40}$$

rearranging terms,

$$F_d(t) + F_d(t) \frac{K_d}{B\rho_0 \eta_d(t)} \int_{l(t)}^{L} \eta(T_f(x,t)) dx = \frac{K_d V_{eff} N(t)}{B\eta_d(t)} \int_{l(t)}^{L} \eta(T_f(x,t)) dx, \tag{2.41}$$

and finally,

$$F_d(t) = \frac{K_d \rho_0 V_{eff} N(t) \int_{l(t)}^{L} \eta(T_f(x,t)) dx}{B\rho_0 \eta_d(t) + K_d \int_{l(t)}^{L} \eta(T_f(x,t)) dx}. \tag{2.42}$$

Remark 2.2. Assuming constant viscosity, the pressure gradient from equation (2.18) can be written as:

$$\frac{\partial P(x,t)}{\partial x} = \eta \frac{\rho_0 V_{eff} N(t) - F_d(t)}{B\rho_0}. \tag{2.43}$$

Using the first order approximation of the pressure, and knowing that in the *PFZ* the pressure is equal to P_0,

$$\frac{P(L,t) - P_0}{L - l(t)} = \frac{\partial P(x,t)}{\partial x}, \tag{2.44}$$

then replacing (2.43) in equation (2.44),

$$\frac{P(L,t) - P_0}{L - l(t)} = \eta \frac{\rho_0 V_{eff} N(t) - K_d(P(L,t) - P_0)/\eta}{B\rho_0}. \tag{2.45}$$

By rearranging items, is it possible to obtain the die pressure $P(L,t)$ or the die flow $F_d(t)$ as a function of screw speed $N(t)$ and the position of the interface $l(t)$,

$$\begin{cases} P(L,t) = P_0 + \dfrac{\eta\rho_0 V_{eff} N(t)(L - l(t))}{(B\rho_0 + K_d(L - l(t)))} \\ F_d(t) = \dfrac{K_d\rho_0 V_{eff} N(t)(L - l(t))}{(B\rho_0 + K_d(L - l(t)))} \end{cases} \tag{2.46}$$

2.3.8.2 Continuity of the temperature and the concentration at the interface

The temperature and the concentration are supposed to be continuous at the interface.

$$\begin{cases} T_p(l^-, t) = T_f(l^+, t) \\ c_p(l^-, t) = c_f(l^+, t). \end{cases} \tag{2.47}$$

Then, recalling the interface relation concerning the energy balance, the following equation for the temperature at the interface can be written:

$$\frac{d}{dt}\int_{l^-}^{l^+} T(x,t)dx = \frac{d}{dt}\int_{l^-}^{l(t)} T_p(x,t)dx + \frac{d}{dt}\int_{l(t)}^{l^+} T_f(x,t)dx. \tag{2.48}$$

Applying the Leibniz Rule:

$$\begin{aligned} \frac{d}{dt}\int_{l^-}^{l^+} T(x,t)dx = \int_{l^-}^{l(t)} \frac{\partial}{\partial t} T_p(x,t)dx + \int_{l(t)}^{l^+} \frac{\partial}{\partial t} T_f(x,t)dx \\ + [T_p(l(t),t) - T_f(l(t),t)]\frac{dl(t)}{dt}. \end{aligned} \tag{2.49}$$

Finally, with the assumption of continuity of the temperature at the interface:

$$\frac{d}{dt}\int_{l^-}^{l^+} T(x,t)dx = \int_{l^-}^{l(t)} \frac{\partial}{\partial t} T_p(x,t)dx + \int_{l(t)}^{l^+} \frac{\partial}{\partial t} T_f(x,t)dx. \tag{2.50}$$

2.3.9 Boundary conditions

The boundary conditions associated to equations (2.10), (2.11) and (2.16) are derived from continuity assumptions as follows:

$$\begin{aligned} f_p(0,t) &= \tfrac{F_{in}(t)}{\rho_0 N(t) V_{eff}} \\ T_p(0,t) &= T_{in}(t) \\ c_p(0,t) &= c_{in}(t), \end{aligned} \tag{2.51}$$

where F_{in}, T_{in} and c_{in} are the feed rate, the inlet temperature and concentration of the matter respectively.

2.4 Finite volume method discretization

2.4.1 Summary of the extrusion process model

Recalling the extrusion process model at the *PFZ* and the *FFZ* as it follows:

A. For the *PFZ*, from equations (2.10), (2.11), (2.16):

$$\begin{cases} \dfrac{\partial f_p(x,t)}{\partial t} = -\xi N(t) \dfrac{\partial f_p(x,t)}{\partial x} \\ \dfrac{\partial c_p(x,t)}{\partial t} = -\xi N(t) \dfrac{\partial c_p(x,t)}{\partial x} \\ \dfrac{\partial T_p(x,t)}{\partial t} = -\xi N(t) \dfrac{\partial T_p(x,t)}{\partial x} + \Omega(f_p, N, T_b, T_p), \end{cases} \tag{2.52}$$

where,

$$\Omega(f_p, N, T_b, T_p) = \frac{\mu\eta(T_p(x,t))N^2(t)}{f_p(x,t)\rho_0 V_{eff} C_p} + \frac{S_{exc}\alpha}{\rho_0 V_{eff} C_p}(T_b(x,t) - T_p(x,t)), \tag{2.53}$$

B. For the *FFZ*, from equations (2.20) and (2.21):

$$\begin{cases} \dfrac{\partial c_f(x,t)}{\partial t} = -\dfrac{F_d(t)\xi}{\rho_0 V_{eff}} \dfrac{\partial c_f(x,t)}{\partial x} \\ \dfrac{\partial T_f(x,t)}{\partial t} = -\dfrac{F_d(t)\xi}{\rho_0 V_{eff}} \dfrac{\partial T_f(x,t)}{\partial x} + \Omega(1, N, T_f, T_b), \end{cases} \tag{2.54}$$

where,

$$\Omega_f(1, N, T_b, T_f) = \frac{\mu\eta(T_f(x,t))N^2(t)}{\rho_0 V_{eff} C_p} + \frac{S_{exc}\alpha}{\rho_0 V_{eff} C_p}(T_b(x,t) - T_f(x,t)). \tag{2.55}$$

C. Moving Interface

$$\frac{dl(t)}{dt} = \frac{F_d(t) - \rho_0 N(t) V_{eff} f_p(l(t), t)}{\rho_0 S_{eff}(1 - f_p(l(t), t)}. \tag{2.56}$$

D. For the interface relations, recalling the continuity of the pressure and the temperature at the interface with variable viscosity:

$$\begin{cases} P(L,t) = P_0 + \dfrac{\rho_0 V_{eff} N(t) - F_d(t)}{B\rho_0} \int_{l(t)}^{L} \eta(x,t)dx \\ F_d(t) = \dfrac{K_d \rho_0 V_{eff} N(t) \int_{l(t)}^{L} \eta(x,t)dx}{B\rho_0 \eta_d(t) + K_d \int_{l(t)}^{L} \eta(x,t)dx}. \end{cases} \tag{2.57}$$

D. Boundary conditions

$$\begin{cases} f_p(0,t) = \frac{F_{in}(t)}{\rho_0 N(t) V_{eff}} \\ T_p(0,t) = T_{in}(t) \\ c_p(0,t) = c_{in}(t). \end{cases} \tag{2.58}$$

2.4.2 Discretization of the extrusion process model

A finite volume method approach is adapted to deal with a moving interface with variable viscosity. Although, using a finite volume scheme is quite standard, since it has been widely used in science and engineering [32], dealing with a moving interface is challenging due to the difficulties of having a very non-linear coupled system with a moving interface. The dynamics of $l(t)$ depends on the coupling between the filling ratio $f_p(l(t), t)$ and the pressure $P(L, t)$. The main difference between fixed and moving interface appears in the analysis of inter-facial topological changes which are introduced by the interface motion. In addition difficulties arises during numerical simulation as the interface position must be computed as part of the process solution and discontinuities in material properties across the interface should be preserved. Most recent works in literature have been focused on the use of marker-cells, volume of fluids [33], height functions or level set methods [34]. In this study in order to deal with the moving interface we use a fixed mesh on which a color function whose values are 1 or 0 according to the *PFZ* and the *FFZ*. This method is similar to the height functions method. Therefore, all the states and flux variables which describe the extruder model on both the *PFZ* and the *FFZ* are extended over the whole domain $[0, L]$ through the use of the color function.The approach used in this work is similar to the one presented on [35], but with the use of a non-constant viscosity term.

Recalling the interval $[0, L]$ as the length of the extruder and dividing it into N_d elements of size Δ as it is shown on Fig. 2.10. It is worth to point out that close to the boundaries, i.e. 0 and L, the size of those elements must be $\Delta_b = \Delta/2$. The moving interface is located at $x = l(t)$, that means, there are two interconnected sub-domains, the *PFZ*

$x \in [0, l^-]$and the *FFZ* $x \in [l^+, L]$. For instance, if the screw length is $L = 1$ m and $N_d = 100$, then $\Delta = L/N_d = 0.01$ and $\Delta_b = 0.005$ as it is shown on Fig. 2.11. Using this discretization it is possible to derive the discrete dynamics of the energy and the mass balance equations using the finite volume method in each sub-domain, as it is described in the next sections.

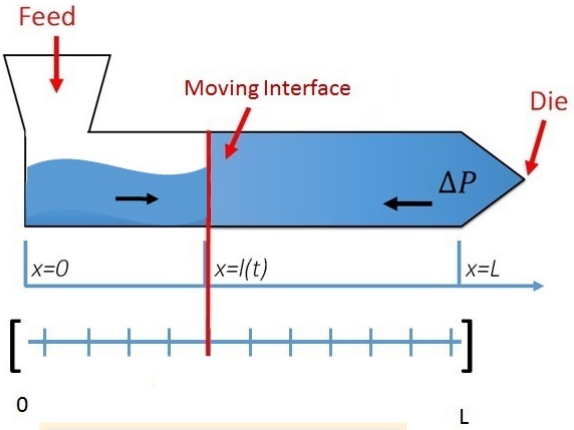

FIGURE 2.10: Division of the domain $[0, L]$. (Source: Personal collection).

2.4.2.1 Discretization of the model of the *PFZ*

2.4.2.1.1 Discretization of the energy balance:

Considering the energy balance from equation (2.52) defined in a fixed interval $[a, b] \in [0, l(t)]$:

$$\frac{\partial T_p(x,t)}{\partial t} = -\xi N(t)\frac{\partial T_p(x,t)}{\partial x} + \Omega_p(f_p, N, T_b, T_p). \tag{2.59}$$

Writing the equation on integral form:

$$\frac{d}{dt}\int_a^b T_p(x,t)dx = -\int_a^b \xi N(t)\frac{\partial T_p(x,t)}{\partial x}dx + \int_a^b \Omega_p(f_p, N, T_b, T_p)dx, \tag{2.60}$$

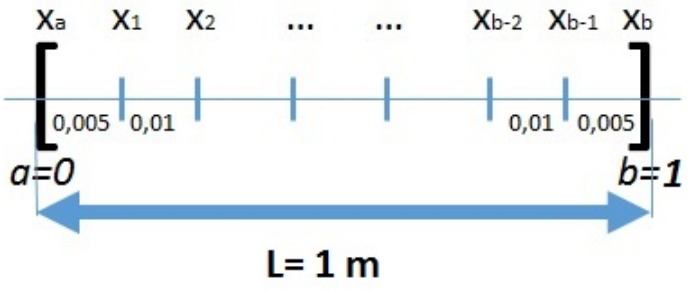

FIGURE 2.11: Division of the domain $[0, L]$ for $N_d = 100$ elements. (Source: Personal collection).

using the relationship $F(T_p(x,t)) = \xi N(t) T_p(x,t)$ in order to obtain:

$$\frac{d}{dt}\int_a^b T_p(x,t)dx = -\int_a^b \frac{\partial F(T_p(x,t))}{\partial x}dx + \int_a^b \Omega_p(f_p, N, T_b, T_p)dx. \tag{2.61}$$

The discretization of the energy balance can be carried out as it follows:

i. Dividing the domain $[a,b]$ into N_d elements with center x_i and size $h_i = x_{i+1/2} - x_{i-1/2}$ as it is shown on Fig. 2.12.

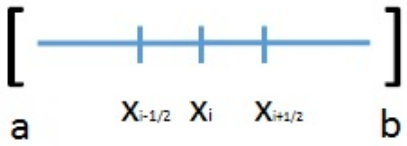

FIGURE 2.12: Division of the domain $[a,b]$. (Source: Personal collection).

ii. Suppose that $T_p(x,t)$ is constant in each mesh and equal to an approximate value of the mean temperature written as T_p^i for the ith mesh.

$$h_i T_p^i = \int_{x_{i-1/2}}^{x_{i+1/2}} T_p(x,t)dx. \tag{2.62}$$

The approximated value of the mean is equal to the value of the function T_p at the center x_i of the mesh.

iii. Discretizing for the ith mesh we have from equation (2.61):

$$\frac{d}{dt}\int_{x_{i-1/2}}^{x_{i+1/2}} T_p(x,t)dx + \int_{x_{i-1/2}}^{x_{i+1/2}} \frac{\partial F(T_p(x,t))}{\partial x}dx - \int_{x_{i-1/2}}^{x_{i+1/2}} \Omega_p(f_p, N, T_b, T_p)dx = 0. \tag{2.63}$$

This can be written as:

$$h_i \frac{dT_p^i}{dt} + F_{i+1/2} - F_{i-1/2} - h_i\Omega_i = 0, \tag{2.64}$$

with $\Omega_i = \Omega(f_p^i, N, T_p^i, T_b^i) = \dfrac{\mu\eta(T_p^i)N^2(t)}{f_p^i \rho_0 V_{eff} C_p} + \dfrac{S_{exc}\alpha}{\rho_0 V_{eff} C_p}(T_b^i - T_p^i)$.

iv. Now, $F_{i+1/2}$ is an approximation of the flow F_{T_p} as a function of the mean values of T_p in the interval $[x_{i-1/2}, x_{i+1/2}]$, that means:

$$F_{i+1/2} = \xi N(t) T_p^{i+1/2}, \tag{2.65}$$

and using the following approximation for $T_p^{i+1/2}$

$$T_p^{i+1/2} = (\lambda T_p^i + (1-\lambda)T_p^{i+1}). \tag{2.66}$$

then,

$$F_{i+1/2} = \xi N(t)(\lambda T_p^i + (1-\lambda)T_p^{i+1}), \tag{2.67}$$

and similarly:

$$F_{i-1/2} = \xi N(t)(\lambda T_p^{i-1} + (1-\lambda)T_p^i). \tag{2.68}$$

Now, assuming $\lambda = 1$

$$\begin{cases} F_{i+1/2} = \xi N(t) T_p^i \\ F_{i-1/2} = \xi N(t) T_p^{i-1}. \end{cases} \tag{2.69}$$

v. Replacing on equation (2.64) in order to obtain:

$$h_i \frac{dT_p^i}{dt} + \xi N(t) T_p^i - \xi N(t) T_p^{i-1} - h_i \Omega_i = 0, \tag{2.70}$$

that is,

$$h_i \frac{dT_p^i}{dt} + \xi N(t)(T_p^i - T_p^{i-1}) - h_i \Omega_i = 0, \tag{2.71}$$

then,

$$\frac{dT_p^i}{dt} = -\frac{\xi N(t)}{h_i}(T_p^i - T_p^{i-1}) + \Omega_i, \tag{2.72}$$

with,

$$\Omega_i = \frac{\mu\eta(T_p^i)N^2(t)}{f_p^i \rho_0 V_{eff} C_p} + \frac{S_{exc}\alpha}{\rho_0 V_{eff} C_p}(T_b^i - T_p^i). \tag{2.73}$$

Replacing,

$$\frac{dT_p^i}{dt} = -\frac{\xi N(t)}{h_i} T_p^i + \frac{\xi N(t)}{h_i} T_p^{i-1} + \frac{\mu\eta N^2(t)}{f_p^i \rho_0 V_{eff} C_p} + \frac{S_{exc}\alpha}{\rho_0 V_{eff} C_p}(T_b^i - T_p^i). \tag{2.74}$$

Rearranging items and using the relationship $\theta_{exc} = \dfrac{S_{exc}\alpha}{\rho_0 V_{eff} C_p}$:

$$\frac{dT_p^i}{dt} = \frac{\xi N(t)}{h_i} T_p^{i-1} - (\frac{\xi N(t)}{h_i} + \theta_{exc}) T_p^i + \frac{\mu\eta(T_p^i)N^2(t)}{f_p^i \rho_0 V_{eff} C_p} + \theta_{exc} T_b^i. \tag{2.75}$$

vi. Rewriting using the following state vectors into $K+1$ elements, where K is the element associated to the interval where the interface lies; i.e. $x_k - h_k/2 \leq l^- \leq x_k + h_k/2$:

$$\begin{cases} T_p = \begin{pmatrix} T_p^0 & T_p^1 & T_p^2 ... T_p^K \end{pmatrix}^T \\ f_p = \begin{pmatrix} f_p^0 & f_p^1 & f_p^2 ... f_p^K \end{pmatrix}^T, \end{cases} \tag{2.76}$$

and the barrel temperature:

$$T_b = \begin{pmatrix} T_b^0 & T_b^1 & T_b^2 ... T_b^K \end{pmatrix}^T. \tag{2.77}$$

The energy balance can be written as

$$\frac{\partial T_p}{\partial t} = A_p T_p + B_p T_b + P_p T_p^{ext} + S^p. \tag{2.78}$$

where,

$$A_p = \begin{pmatrix} -D_0^p & 0 & 0 & \cdots & 0 & 0 & 0 \\ \xi N(t)/h_1 & -D_1^p & 0 & \cdots & 0 & 0 & 0 \\ \vdots & \vdots & \vdots & \ddots & \vdots & \vdots & \vdots \\ \vdots & \vdots & \vdots & \ddots & \vdots & \vdots & \vdots \\ 0 & 0 & 0 & \cdots & \xi N(t)/h_{K-1} & -D_{K-1}^p & 0 \\ 0 & 0 & 0 & \cdots & 0 & \xi N(t)/h_K & -D_K^p \end{pmatrix}, \tag{2.79}$$

with, $D_i^p = \xi N(t) h_i^{-1} + \theta_{exc}$, $B_p = \theta_{exc} I_{[K+1]}$, with $I_{[K+1]}$ is an identity matrix of dimension $K \times K$, and P_p a matrix with dimension $[K+1] \times 2$ which its only non-zero element is $P_p(1,1) = \xi N(t)/h_0$. Also $T_p^{ext} = [T_p^{in}, T_p^{(l(t))}]$ and elements of S^p are defined as:

$$S^p = \frac{\mu \eta(T_p^i) N(t)^2}{f_p^i \rho_0 V_{eff} C_p}. \tag{2.80}$$

2.4.2.1.2 Discretization of the local mass balance: Considering the dynamics of the filling ratio from equation (2.52) defined in a fixed interval $[a,b] \in [0, l(t)]$:

$$\frac{\partial f_p(x,t)}{\partial t} = -\xi N(t) \frac{\partial f_p(x,t)}{\partial x}. \tag{2.81}$$

Writing the equation in integral form:

$$\frac{d}{dt} \int_a^b f_p(x,t) dx = -\int_a^b \xi N(t) \frac{\partial f_p(x,t)}{\partial x} dx, \tag{2.82}$$

then the discretization process can be written in the same way as for the temperature at the *PFZ*:

i. Using the relationship $F(f_p(x,t)) = \xi N(t) f_p(x,t)$ in order to obtain:

$$\frac{d}{dt} \int_a^b f_p(x,t) dx = -\int_a^b \frac{\partial F(f_p(x,t))}{\partial x} dx, \tag{2.83}$$

ii. Using the same division of the domain $[a, b]$ and assuming $f_p(x,t) = f_p^i$:

$$\frac{d}{dt}\int_{x_{i-1/2}}^{x_{i+1/2}} f_p(x,t)dx = -\int_{x_{i-1/2}}^{x_{i+1/2}} \frac{\partial F(f_p(x,t))}{\partial x}dx, \tag{2.84}$$

then,

$$h_i \frac{df_p^i}{dt} = -F_{i+1/2} + F_{i-1/2}. \tag{2.85}$$

iii. Taking into account the same procedure as before on Section 2.4.2.1.1,

$$\begin{cases} F_{i+1/2} = \xi N(t) f_p^i \\ F_{i-1/2} = \xi N(t) f_p^{i-1}. \end{cases} \tag{2.86}$$

iv. Then the mass balance can be written as:

$$\frac{\partial f_p}{\partial t} = A_p^{fp} f_p + B_p^{fp} f_p^{in}, \tag{2.87}$$

where,

$$A_p^{fp} = \begin{pmatrix} -D_0^{fp} & 0 & 0 & \cdots & 0 & 0 & 0 \\ \xi N(t)/h_1 & -D_1^{fp} & 0 & \cdots & 0 & 0 & 0 \\ \vdots & \vdots & \vdots & \ddots & \vdots & \vdots & \vdots \\ \vdots & \vdots & \vdots & \ddots & \vdots & \vdots & \vdots \\ 0 & 0 & 0 & \cdots & \xi N(t)/h_{K-1} & -D_{K-1}^{fp} & 0 \\ 0 & 0 & 0 & \cdots & 0 & \xi N(t)/h_K & -D_K^{fp} \end{pmatrix}, \tag{2.88}$$

with, $D_i^{f_p} = \dfrac{\xi N(t)}{h_i}$ and $B_p^{f_p}$ is a matrix of dimensions $[K+1] \times 1$ in which its only non-zero element is $B_p^{f_p}(1,1) = \xi N(t) h_0^{-1}$.

2.4.2.1.3 Discretization of the concentration: Considering the dynamics of the concentration from equation (2.11) defined in a fixed interval $[a, b] \in [0, l(t)]$:

$$\frac{\partial c_p(x,t)}{\partial t} = -\xi N(t) \frac{\partial c_p(x,t)}{\partial x}. \tag{2.89}$$

Writing the equation on integral form:

$$\frac{d}{dt}\int_a^b c_p(x,t)dx = -\int_a^b \xi N(t) \frac{\partial c_p(x,t)}{\partial x}dx. \tag{2.90}$$

Then the discretization process can be made as it follows:

i. Using the relationship $F(c_p(x,t)) = \xi N(t) c_p(x,t)$ in order to obtain:

$$\frac{d}{dt}\int_a^b c_p(x,t)dx = -\int_a^b \frac{\partial F(c_p(x,t))}{\partial x}dx. \tag{2.91}$$

ii. Using the same division of the domain $[a,b]$ and making $c_p(x,t) = c_p^i$ it is possible to obtain:

$$\frac{d}{dt}\int_{x_{i-1/2}}^{x_{i+1/2}} c_p(x,t)dx = -\int_{x_{i-1/2}}^{x_{i+1/2}} \frac{\partial F(c_p)}{\partial x}dx, \tag{2.92}$$

then,

$$h_i \frac{dc_p^i}{dt} = -F_{i+1/2} + F_{i-1/2}. \tag{2.93}$$

iii. Taking into account the same procedure as before on Section 2.4.2.1.1,

$$\begin{cases} F_{i+1/2} = \xi N(t) c_p^i \\ F_{i-1/2} = \xi N(t) c_p^{i-1}. \end{cases} \tag{2.94}$$

iv. Then it results in the following equation:

$$\frac{dc_p^i}{dt} = -\frac{\xi N(t)}{h_i}(c_p^i - c_p^{i-1}). \tag{2.95}$$

v. The concentration of solvent can be written as,

$$\frac{\partial c_p}{\partial t} = A_p^{cp} c_p + B_p^{cp} c_p^{in}, \tag{2.96}$$

where,

$$A_p^{cp} = \begin{pmatrix} -D_0^{cp} & 0 & 0 & \cdots & 0 & 0 & 0 \\ \xi N(t)/h_1 & -D_1^{cp} & 0 & \cdots & 0 & 0 & 0 \\ \vdots & \vdots & \vdots & \ddots & \vdots & \vdots & \vdots \\ \vdots & \vdots & \vdots & \ddots & \vdots & \vdots & \vdots \\ 0 & 0 & 0 & \cdots & \xi N(t)/h_{K-1} & -D_{K-1}^{cp} & 0 \\ 0 & 0 & 0 & \cdots & 0 & \xi N(t)/h_K & -D_K^{cp} \end{pmatrix} \tag{2.97}$$

with, $D_i^{c_p} = \dfrac{\xi N(t)}{h_i}$ and $B_p^{c_p}$ is a matrix of dimensions $[K+1]\times 1$ in which its only non-zero element is $B_p^{c_p}(1,1) = \xi N(t) h_0^{-1}$.

2.4.2.2 Discretization of the model of the *FFZ*

2.4.2.2.1 Discretization of the energy balance: Considering the energy balance of the *FFZ* from equation (2.54) defined in a fixed interval $[a, b] \in [l(t), L]$:

$$\frac{\partial T_f(x,t)}{\partial t} = -\frac{F_d(t)\xi}{\rho_0 V_{eff}} \frac{\partial T_f(x,t)}{\partial x} + \Omega_f(1, N, T_b, T_f). \tag{2.98}$$

The integral form of the energy balance is:

$$\frac{d}{dt}\int_a^b T_f(x,t)dx = -\int_a^b \frac{F_d(t)\xi}{\rho_0 V_{eff}} \frac{\partial T_f(x,t)}{\partial x} dx + \int_a^b \Omega_f(1, N, T_b, T_f)dx, \tag{2.99}$$

using the relationship $F(T_f(x,t)) = \dfrac{F_d(t)\xi}{\rho_0 V_{eff}} T_f(x,t)$ in order to obtain:

$$\frac{d}{dt}\int_a^b T_f(x,t)dx = -\int_a^b \frac{\partial F(T_f(x,t))}{\partial x} dx + \int_a^b \Omega_f(1, N, T_b, T_f)dx. \tag{2.100}$$

Then, the discretization process can be made as it follows:

i. Suppose that T_f is constant in each mesh and equal to an approximate value of the mean temperature written as T_f^i for the ith mesh.

$$h_i T_f^i = \int_{x_{i-1/2}}^{x_{i+1/2}} T_f(x,t)dx. \tag{2.101}$$

ii. Discretizing for the ith mesh we have from equation (2.100):

$$\frac{d}{dt}\int_{x_{i-1/2}}^{x_{i+1/2}} T_f(x,t)dx + \int_{x_{i-1/2}}^{x_{i+1/2}} \frac{\partial F(T_f(x,t))}{\partial x} dx - \int_{x_{i-1/2}}^{x_{i+1/2}} \Omega_f(1, N, T_b, T_f)dx = 0, \tag{2.102}$$

this can be written as:

$$h_i \frac{dT_f^i}{dt} + F_{i+1/2} - F_{i-1/2} - h_i\Omega_i = 0, \tag{2.103}$$

with $\Omega_i = \Omega(1, N, Tb^i, T_f^i) = \dfrac{\mu\eta(T_f^i)N^2(t)}{\rho_0 V_{eff} C_p} + \dfrac{S_{exc}\alpha}{\rho_0 V_{eff} C_p}(T_b^i - T_f^i)$.

iii. Using the following relation:

$$F_{i+1/2} = \frac{F_d\xi}{\rho_o V_{eff}} T_f^{i+1/2}, \tag{2.104}$$

and,

$$T_f^{i+1/2} = (\lambda T_f^i + (1-\lambda)T_f^{i+1}), \tag{2.105}$$

then,

$$F_{i+1/2} = \frac{F_d(t)\xi}{\rho_o V_{eff}}(\lambda T_f^i + (1-\lambda)T_f^{i+1}), \tag{2.106}$$

And similarly:

$$F_{i-1/2} = \frac{F_d(t)\xi}{\rho_o V_{eff}}(\lambda T_f^{i-1} + (1-\lambda)T_f^{i}). \tag{2.107}$$

Now, assuming $\lambda = 1$, then:

$$\begin{cases} F_{i+1/2} = \dfrac{F_d(t)\xi}{\rho_o V_{eff}} T_f^i \\ F_{i-1/2} = \dfrac{F_d(t)\xi}{\rho_o V_{eff}} T_f^{i-1}. \end{cases} \tag{2.108}$$

iv. Replacing those results on eq. 2.103:

$$h_i \frac{dT_f^i}{dt} + \frac{F_d(t)\xi}{\rho_o V_{eff}} T_f^i - \frac{F_d(t)\xi}{\rho_o V_{eff}} T_f^{i-1} - h_i \Omega_i = 0, \tag{2.109}$$

then,

$$h_i \frac{dT_f^i}{dt} + \frac{F_d(t)\xi}{\rho_o V_{eff}}(T_f^i - T_f^{i-1}) - h_i \Omega_i = 0. \tag{2.110}$$

Rearranging items:

$$\frac{dT_f^i}{dt} = -\frac{F_d(t)\xi}{\rho_o V_{eff} h_i}(T_f^i - T_f^{i-1}) + \Omega_i. \tag{2.111}$$

That gives,

$$\frac{dT_f^i}{dt} = -\frac{F_d(t)\xi}{\rho_o V_{eff} h_i}(T_f^i - T_f^{i-1}) + \frac{\mu\eta(T_f^i)N^2(t)}{\rho_0 V_{eff} C_p} + \frac{S_{exc}\alpha}{\rho_0 V_{eff} C_p}(T_b^i - T_f^i). \tag{2.112}$$

Rearranging:

$$\frac{dT_f^i}{dt} = \frac{F_d(t)\xi}{\rho_o V_{eff} h_i} T_f^{i-1} - (\frac{F_d(t)\xi}{\rho_o V_{eff} h_i} + \theta_{exc})(T_f^i) + \frac{\mu\eta(T_f^i)N^2(t)}{\rho_0 V_{eff} C_p} + \theta_{exc} T_b^i. \tag{2.113}$$

v. Thus, the discretized equation for the energy balance at the *FFZ* is defined in the interval defined by the elements $K+1$ and N_d, where the element K is so that $x_k - h_k/2 \leq l^+ \leq x_k + h_k/2$

$$\frac{\partial T_f^i}{\partial t} = A_f T_f + B_f T_b + P_f T_f^{ext} + S^f, \tag{2.114}$$

where,

$$A_f = \begin{pmatrix} -D_{l+}^f & 0 & 0 & \cdots & 0 & 0 & 0 \\ E_{K+2}^f & -D_{K+2}^f & 0 & \cdots & 0 & 0 & 0 \\ \vdots & \vdots & \vdots & \ddots & \vdots & \vdots & \vdots \\ \vdots & \vdots & \vdots & \ddots & \vdots & \vdots & \vdots \\ 0 & 0 & 0 & \cdots & E_{L-1}^f & -D_{L-1}^f & 0 \\ 0 & 0 & 0 & \cdots & 0 & E_L^f & -D_L^f \end{pmatrix} \tag{2.115}$$

with, $D_i^f = \dfrac{F_d(t)\xi}{\rho_o V_{eff} h_i} + \theta_{exc}$ and $E_i^f = \dfrac{F_d(t)\xi}{\rho_o V_{eff} h_i}$ and $B_f = \theta_{exc} I_{[K+1]}$, and P_f is a matrix of dimension $[K+1] \times 2$ in which its only non-zero element is $P_f(1,1) = (F_d(t)\xi)(\rho_o V_{eff} h_{l+})^{-1}$. Finally, $T_f^{ext} = [T_f^{in}, T_f^L]$ and the elements of S^f are defined as:

$$S^f = \frac{\mu\eta(T_f^i)N(t)^2}{\rho_0 V_{eff} C_p}\,. \tag{2.116}$$

2.4.2.2.2 Discretization of the concentration: Considering the concentration dynamics at the *FFZ* from equation 2.20 defined in a fixed interval $[a,b] \in [l(t), L]$:

$$\frac{\partial c_f(x,t)}{\partial t} = -\frac{F_d(t)\xi}{\rho_0 V_{eff}} \frac{\partial c_f(x,t)}{\partial x}, \tag{2.117}$$

the integral form is:

$$\frac{d}{dt}\int_a^b c_f(x,t)dx = -\int_a^b \frac{F_d(t)\xi}{\rho_0 V_{eff}} \frac{\partial c_f(x,t)}{\partial x} dx. \tag{2.118}$$

Using the relationship $F(c_f(x,t)) = \dfrac{F_d(t)\xi}{\rho_0 V_{eff}} c_f(x,t)$ in order to obtain:

$$\frac{d}{dt}\int_a^b c_f(x,t)dx = -\int_a^b \frac{\partial F(c_f(x,t))}{\partial x} dx, \tag{2.119}$$

then, the discretization process can be made as it follows:

i. Suppose that c_f is constant in each mesh and equal to an approximate value of the mean concentration written as c_f^i for the ith mesh.

$$h_i c_f^i = \int_{x_{i-1/2}}^{x_{i+1/2}} c_f(x,t)dx. \tag{2.120}$$

ii. Discretizing for the ith mesh:

$$\frac{d}{dt}\int_{x_{i-1/2}}^{x_{i+1/2}} c_f(x,t)dx + \int_{x_{i-1/2}}^{x_{i+1/2}} \frac{\partial F(c_f(x,t))}{\partial x}dx = 0, \tag{2.121}$$

this can be written as:

$$h_i\frac{dc_f^i}{dt} + F_{i+1/2} - F_{i-1/2} = 0. \tag{2.122}$$

iii. Writing the following relation:

$$F_{i+1/2} = \frac{F_d(t)\xi}{\rho_o V_{eff}} c_f^{i+1/2}, \tag{2.123}$$

and,

$$c_f^{i+1/2} = (\lambda c_f^i + (1-\lambda)c_f^{i+1}), \tag{2.124}$$

then,

$$F_{i+1/2} = \frac{F_d(t)\xi}{\rho_o V_{eff}}(\lambda c_f^i + (1-\lambda)c_f^{i+1}). \tag{2.125}$$

And similarly:

$$F_{i-1/2} = \frac{F_d(t)\xi}{\rho_o V_{eff}}(\lambda c_f^{i-1} + (1-\lambda)c_f^{i}). \tag{2.126}$$

Now, assuming $\lambda = 1$, then:

$$\begin{cases} F_{i+1/2} = \dfrac{F_d(t)\xi}{\rho_o V_{eff}} c_f^i \\ F_{i-1/2} = \dfrac{F_d(t)\xi}{\rho_o V_{eff}} c_f^{i-1}. \end{cases} \tag{2.127}$$

iv. Replacing those results on equation (2.122):

$$h_i\frac{dc_f^i}{dt} + \frac{F_d(t)\xi}{\rho_o V_{eff}} c_f^i - \frac{F_d(t)\xi}{\rho_o V_{eff}} M_f^{i-1} = 0. \tag{2.128}$$

Then,

$$h_i\frac{dc_f^i}{dt} = -\frac{F_d(t)\xi}{\rho_o V_{eff}}(c_f^i - c_f^{i-1}). \tag{2.129}$$

v. The concentration of solvent can be written as:

$$\frac{\partial c_f^i}{\partial t} = A_f^{cf} c_f + P_f^{cf} c_f^{ext}, \tag{2.130}$$

where,

$$A_f^{cf} = \begin{pmatrix} -D_{l+}^{cf} & 0 & 0 & \cdots & 0 & 0 & 0 \\ E_{K+2}^{cf} & -D_{K+2}^{cf} & 0 & \cdots & 0 & 0 & 0 \\ \vdots & \vdots & \vdots & \ddots & \vdots & \vdots & \vdots \\ \vdots & \vdots & \vdots & \ddots & \vdots & \vdots & \vdots \\ 0 & 0 & 0 & \cdots & E_{L-1}^{cf} & -D_{L-1}^{cf} & 0 \\ 0 & 0 & 0 & \cdots & 0 & E_L^{cf} & -D_L^{cf} \end{pmatrix} \tag{2.131}$$

with, $D_i^{cf} = E_i^{cf} = \dfrac{F_d(t)\xi}{\rho_o V_{eff} h_i}$ and

$$P_f^{cf} = \begin{pmatrix} \dfrac{F_d(t)\xi}{\rho_o V_{eff} h_{l+}} & 0 \\ 0 & 0 \\ \vdots & \vdots \\ 0 & 0 \end{pmatrix} \tag{2.132}$$

where $c_f^{ext} = [c_f^{in}, c_f^K]$.

2.4.2.3 Interconnection of the Moving Interface

In Section 2.4.1 the interface relation assuming the continuity of the pressure at the interface was made as it follows:

$$\begin{cases} P(L,t) = P_0 + \dfrac{\rho_0 V_{eff} N(t) - F_d(t)}{B\rho_0} \int_{l(t)}^{L} \eta(x,t)dx \\ F_d(t) = \dfrac{K_d \rho_0 V_{eff} N(t) \int_{l(t)}^{L} \eta(x,t)dx}{B\rho_0 \eta_d(t) + K_d \int_{l(t)}^{L} \eta(x,t)dx}. \end{cases} \tag{2.133}$$

The treatment of interfaces between materials of different properties remains a formidable challenge to the computation of fluid dynamics. Generally, color functions are used to distinguish the regions where different materials fall in. To accurately reproduce the physical processes across the interface transition region, keeping the compact thickness of the interface is of great importance [36]. Therefore, in order to simplify the analysis of the dynamics of the temperature at the moving interface the following color function that represents both the *PFZ* and *FFZ* can be proposed as it follows:

$$k(x,l(t)) = \begin{cases} 1 & \text{if } x \in [0,l(t)[\\ 0 & \text{if } x \in [l(t),L] \end{cases} \text{ and } \overline{k}(x,l(t)) = \begin{cases} 0 & \text{if } x \in [0,l(t)[\\ 1 & \text{if } x \in [l(t),L]. \end{cases} \tag{2.134}$$

This color function is used to extend over the whole domain $[0, L]$ all the states and flux variables which describe the extruder model in *PFZ* and *FFZ* as it follows:

$$\mathcal{N}(x,t) = k(x,\, t)\mathcal{N}_p(x,t) + \overline{k}(x, l(t))\mathcal{N}_f(x,t), \tag{2.135}$$

where, $\mathcal{N}$ denotes the flux or state. Omitting x in k and $\overline{k}$ for simplicity, in the case of the temperature along the extruder, the following definition should be considered:

$$T(x,t) = k(l(t))T_p(x,t) + \overline{k}(l(t))T_f(x,t). \tag{2.136}$$

Recalling the assumption of continuity of the temperature as stated on Section 2.3.8.2 and the interface position on $l(t) \in]l^-, l^+]$ with $l^- = K$ and $l^+ = K+1$ the following equation for the temperature in the domain $[K-1/2, K+3/2]$ can be written:

$$\frac{\partial}{\partial t}\int_{x_{K-1/2}}^{x_{K+3/2}} T(x,t)dx = \frac{\partial}{\partial t}\int_{x_{K-1/2}}^{l(t)} k(l(t))T_p(x,t)dx + \frac{\partial}{\partial t}\int_{l(t)}^{x_{K+3/2}} \overline{k}(l(t))T_f(x,t)dx, \tag{2.137}$$

distributing terms:

$$\begin{aligned}\frac{\partial}{\partial t}\int_{x_{K-1/2}}^{x_{K+3/2}} T(x,t)dx = &\frac{\partial}{\partial t}\int_{x_{K-1/2}}^{l^-} k(l(t))T_p(x,t)dx + \frac{\partial}{\partial t}\int_{l^-}^{l(t)} k(l(t))T_p(x,t)dx \\ &+\frac{\partial}{\partial t}\int_{l(t)}^{l^+} \overline{k}(l(t))T_f(x,t)dx + \frac{\partial}{\partial t}\int_{l^+}^{x_{K+3/2}} \overline{k}(l(t))T_f(x,t)dx.\end{aligned} \tag{2.138}$$

Approximating $l(t) \simeq l^+$ then,

$$\begin{aligned}\frac{\partial}{\partial t}\int_{x_{K-1/2}}^{x_{K+3/2}} T(x,t)dx = &\frac{\partial}{\partial t}\int_{x_{K-1/2}}^{l^-} k(l(t))T_p(x,t)dx + \frac{\partial}{\partial t}\int_{l^-}^{l(t)} k(l(t))T_p(x,t)dx \\ &+\frac{\partial}{\partial t}\int_{l(t)}^{x_{K+3/2}} \overline{k}(l(t))T_f(x,t)dx.\end{aligned} \tag{2.139}$$

Recalling that $l^- = K$ and $l^+ \simeq l(t) = K+1$:

$$\begin{aligned}\frac{\partial}{\partial t}\int_{x_{K-1/2}}^{x_{K+3/2}} T(x,t)dx = &\frac{\partial}{\partial t}\int_{x_{K-1/2}}^{x_K} k(l(t))T_p(x,t)dx + \frac{\partial}{\partial t}\int_{x_K}^{x_{K+1}} k(l(t))T_p(x,t)dx \\ &+\frac{\partial}{\partial t}\int_{x_{K.+1}}^{x_{K+3/2}} \overline{k}(l(t))T_f(x,t)dx\end{aligned} \tag{2.140}$$

Then, the integrals on the fluxes become

$$\begin{aligned}\int_{x_{K-1/2}}^{x_K} \frac{\partial}{\partial x} F_p(x,t)dx + \int_{x_K}^{x_{K+1}} \frac{\partial}{\partial x} F_p(x,t)dx + \int_{x_{K+1}}^{x_{K+3/2}} \frac{\partial}{\partial x} F_f(x,t)dx \\ = F_p^K - F_p^{K-1/2} + F_p^{K+1} - F_p^K + F_f^{K+3/2} - F_f^{K+1},\end{aligned} \tag{2.141}$$

simplifying:

$$\begin{aligned}\frac{\partial}{\partial t}\int_{x_{K-1/2}}^{x_K} \frac{\partial}{\partial x} F_p(x,t)dx + \int_{x_K}^{x_{K+1}} \frac{\partial}{\partial x} F_p(x,t)dx + \int_{x_{K+1}}^{x_{K+3/2}} \frac{\partial}{\partial x} F_f(x,t)dx \\ = -F_p^{K-1/2} + F_p^{K+1} + F_f^{K+3/2} - F_f^{K+1}.\end{aligned} \tag{2.142}$$

Recalling the continuity of heat flux at the the interface, i.e at $K+1$:

$$F_p^{K+1} - F_f^{K+1} = 0, \tag{2.143}$$

then,

$$\begin{aligned}\int_{x_{K-1/2}}^{x_K} \frac{\partial}{\partial x} F_p(x,t)dx + \int_{x_K}^{x_{K+1}} \frac{\partial}{\partial x} F_p(x,t)dx + \int_{x_{K+1}}^{x_{K+3/2}} \frac{\partial}{\partial x} F_f(x,t)dx \\ = -F_p^{K-1/2} + F_f^{K+3/2},\end{aligned} \tag{2.144}$$

that is,

$$\frac{\partial}{\partial t}\int_{x_{K-1/2}}^{x_{K+3/2}} T(x,t)dx = -F_p^{K-1/2} + F_f^{K+3/2}, \tag{2.145}$$

Using the approximation for the fluxes $F_p^{K-1/2}$ and $F_p^{K+3/2}$ in the same way as in equations (2.68) and (2.106):

$$\frac{\partial}{\partial t}\int_{x_{K-1/2}}^{x_{K+3/2}} T(x,t)dx = -\xi N(t) T_p^{K-1} + \frac{F_d(t)\xi}{\rho_0 V_{eff}} T_f^K. \tag{2.146}$$

Using the initial approximation for temperature as in equation (2.62), the definition of $2h = x_{K+3/2} - x_{K-1/2}$ and taking into account the interface relationship defined on Section 2.3.8.2:

$$2h\frac{d}{dt}T_f^{K+1} = -\xi N(t) T_p^{K-1} + \frac{F_d(t)\xi}{\rho_0 V_{eff}} T_f^K, \tag{2.147}$$

Then,

$$\frac{d}{dt}T_f^{K+1} = -\frac{1}{2h}\xi N(t) T_p^{K-1} + \frac{1}{2h}\frac{F_d(t)\xi}{\rho_0 V_{eff}} T_f^K. \tag{2.148}$$

By replacing the definition of temperature from equation (2.136), assuming that k and $\overline{k}$

are constant in each mesh and equal to an approximate value of each color function written as k_i and $\overline{k}_i$ for the ith mesh respectively and taking into account the approximation $l^+ \simeq l(t) = K+1$ we have:

$$\frac{d}{dt}T_{l(t)} = -\frac{k_{K-1}}{2h}\xi N(t)T_{K-1} + \frac{\overline{k}_K}{2h}\frac{F_d(t)\xi}{\rho_0 V_{eff}}T_K. \tag{2.149}$$

2.4.3 Summary of the total discrete model

Summarizing and taking into account the use of the color functions k and $\overline{k}$, the discretized system equations for the extrusion process model are the following:

- Recalling equations (2.78), (2.87) and (2.96) at the *PFZ* with $i \in [0, K+1[$:

$$\frac{d}{dt}k_i T_i = k_i A_p T_i + B_p T_{b,i} + P_p T_i^{ext} + S^p, \tag{2.150}$$

$$\frac{d}{dt}f_{p,i} = A_p^{fp} f_{p,i} + B_p^{fp} f_p^{in}, \tag{2.151}$$

$$\frac{\partial}{\partial t}k_i c_p^i = k_i A_p^{cp} c_p^i + B_p^{cp} c_p^{in}. \tag{2.152}$$

- For the *FFZ* with $i \in]K+1, L]$:

$$\frac{d}{dt}\overline{k}_i T_i = \overline{k}_i A_f T_i + B_f T_{b,i} + P_f T_i^{ext} + S^f, \tag{2.153}$$

$$\frac{\partial}{\partial t}\overline{k}_i c_f^i = \overline{k}_i A_f^{cf} c_f^i + P_f^{cf} c_f^{ext}. \tag{2.154}$$

- The temperature at the interface:

$$\frac{d}{dt}T_{K+1} = -\frac{k_{K-1}}{2h}\xi N(t)T_{K-1} + \frac{\overline{k}_K}{2h}\frac{F_d(t)\xi}{\rho_0 V_{eff}}T_K. \tag{2.155}$$

- The position of the interface is defined by:

$$\frac{dl(t)}{dt} = \frac{F_d(t) - \rho_0 N(t) V_{eff} f_p(K+1,t)}{\rho_0 S_{eff}(1 - f_p(K+1,t))}. \tag{2.156}$$

- The interface relations assuming the continuity of pressure:

$$\begin{cases} P(L,t) = P_0 + \dfrac{\rho_0 V_{eff} N(t) - F_d(t)}{B\rho_0}\int_{l(t)}^{L}\eta(x,t)dx \\ F_d(t) = \dfrac{K_d \rho_0 V_{eff} N(t)\int_{l(t)}^{L}\eta(x,t)dx}{B\rho_0\eta_d(t) + K_d\int_{l(t)}^{L}\eta(x,t)dx}. \end{cases} \tag{2.157}$$

2.5 Summary

In this chapter some fundamental on screw-extruders were presented, among a brief description of the extrusion process, its classification and geometrical properties. A brief bibliographic synthesis regarding the modelling of the extrusion process together with the presentation of the bi-zone model and interface relations was presented. This model is derived from balance laws expressing conservation of mass, concentration of solvent and energy with non-constant viscosity. This last condition implies a new approach on the discretization process, that has not been addressed before, since the viscosity is temperature and shear rate dependable. A finite volume method approach is adapted to the bi-zone model in order to deal with a moving interface. A discretization method for the system was presented taking into account the difficulties of having a non-linear coupled system with a moving interface. The dynamics of the moving interface depends on the coupling between the filling ratio $f_p(l(t), t)$ and the pressure $P(L, t)$. In the next chapter, some simulations of the proposed bi-zone extrusion process model are performed in order to analyze its behavior for different initial conditions.

Chapter 3

Analysis and dynamic simulations

3.1 Introduction

In this chapter, dynamical and steady state simulations of the extrusion process are presented in order to analyze the behaviour of the discretized model. Two different approaches where used: A first approach, similar than the one adopted by [25] in which the viscosity is supposed as a constant where the steady state of the model is analyzed in order to compute the equilibrium points upon a given set of initial conditions. Then different open-loop simulations are presented with variable screw speed and variable input flow in order to test different operational conditions. A second, more complex approach is presented in which the viscosity is assumed as variable. A power-law model for viscosity is used, with dependency on the temperature of the melt. In this case the equilibrium points of the extrusion process are also computed, and some open-loop simulations for variable screw speed and variable input flow are presented.

3.2 Extrusion process model with constant viscosity

3.2.1 Description of the simulated model

In this section, some simulation tests for the mass and energy balance equations of the extrusion process model with constant viscosity are presented. The simulations were made using $Matlab^{®}$ and the Solver Function used was $Ode113$. The latter was chosen because is more efficient at problems with stringent error tolerances and ODE functions that are expensive to evaluate [37]. In order to test the behaviour of the discretized model two different simulations were made:

- Test No.1: variable feed rate $F_{in}(t)$ with constant screw speed $N(t) = N_0$
- Test No.2: variable screw speed $N(t)$ with constant feed rate F_{in}

Table 3.1 shows some input variables used on the simulation process, most of the data are obtained from Diagne [17].

Initial screw speed	$N_0 = 250[rpm]$
Barrel temperature	$T_b(x) = 330[K]$
Input temperature	$T_{in} = 293[K]$
Extruder length	$L = 2[m]$
Initial feed rate	$F_{in} = 270/3600[kg/s]$
Initial filling ratio	$f_p^{in} = \dfrac{F_{in}}{\rho_0 V_{eff} N_0} = 0.6139$

TABLE 3.1: Input values used on the simulation process for constant viscosity. (Amended from [17]).

In addition, some screw and thermodynamical parameters were used on the simulation process which are detailed in Table 3.2 and 3.3 respectively.

External diameter	$D = L/15 = 0.133[m]$
Internal diameter	$D_s = 0.001[m]$
Screw pitch	$\xi = 30 \times 10^-4[m]$
Effective surface	$S_{eff} = \frac{\pi}{4}(D^2 - D_s^2) = 0.01396[m^2]$
Effective volume	$V_{eff} = S_{eff}\xi = 4.188 \times 10^-5[m^3]$

TABLE 3.2: Screw parameters used on the simulation process for constant viscosity. (Source: Personal collection).

Thermal exchange coefficient	$\alpha = 10.41 \times 10^1[J/(m^2Ks)]$
Material density	$\rho_0 = 1400/2[kg/m^3]$
Exchange surface	$S_{exc} = \pi D^2 L[m^2]$
Initial viscosity	$\eta = 500/4[Pa/s]$
Heat capacity	$C_p = 3.6 \times 10^3[J/(kgK)]$

TABLE 3.3: Thermodynamical Parameters used on the simulation process.(Source: Personal collection).

The simulations where performed based on the equations shown in Section 2.4.1 and the discretization process presented in Section 2.4.2 with constant viscosity.

3.2.2 Equilibrium Points Computation

Recalling the extrusion process model and the boundary conditions shown in Section 2.4.1, it is possible to find the equilibrium points, i.e. $\partial/\partial t = 0$, for the filling ratio, the temperature and the moving interface:

3.2.2.1 Filling Ratio

For the filling ratio we have the following expression at the steady state:

$$-\xi N^* \frac{\partial f_p^*(x)}{\partial x} = 0, \tag{3.1}$$

then,

$$\frac{\partial f_p^*(x)}{\partial x} = 0, \tag{3.2}$$

that is,

$$f_p^* = \kappa, \tag{3.3}$$

with κ as a constant.

3.2.2.2 Moving Interface

Assuming $dl(t)/dt = 0$ we have the following expression at steady state:

$$\frac{F_d^*(l^*) - \rho_0 N^* V_{eff} f_p^*(l^*)}{\rho_0 S_{eff}(1 - f_p^*(l^*))} = 0. \tag{3.4}$$

Then, solving for the filling ratio we can have an equilibrium value for the given parameters as it follows:

$$f_p^{in} = f_p^*(l^*) = \frac{F_{in}}{\rho_0 N^* V_{eff}} = \kappa = 0.6139. \tag{3.5}$$

Then, the equilibrium of the interface position is,

$$l^* = L - \frac{B\rho_0 f_p^*(l^*)}{K_d(1 - f_p^*(l^*))} = 1.1095 \text{ m}. \tag{3.6}$$

Using the equation (3.6) it is possible to compute the filling ratio at the equilibrium f_p^* as function of the position of the interface $l^* \in [0, L]$ trough the following expression:

$$f_p^*(l^*) = \frac{(l^* - L)K_d}{-B\rho_0 + K_d(l^* - L)}. \tag{3.7}$$

Fig. 3.1 shows the equilibrium of the filling ratio as a function of the moving interface. Note that in the case when the extruder is empty, i.e. the moving interface is at $l(t) = L = 2$ m, the filling ratio on steady state is $f_p^*(L) = 0$. Also note that when the extruder gets filled the filling ratio at equilibrium reaches its maximum, i.e. approximately at $f_p^*(0) = 0.78$. This is basically due to the configuration of the screw and the parameters of the extruder. Therefore, based upon the geometrical properties of the screws the equilibrium of the filling ratio can be changed in order to optimize the process. In addition, the circular dot on the figure represents the computed filling ratio on steady state of the moving interface as stated on equations (3.5) and (3.6) with the initial values shown on Table 3.1. Also, the steady state of the input flow can be computed using

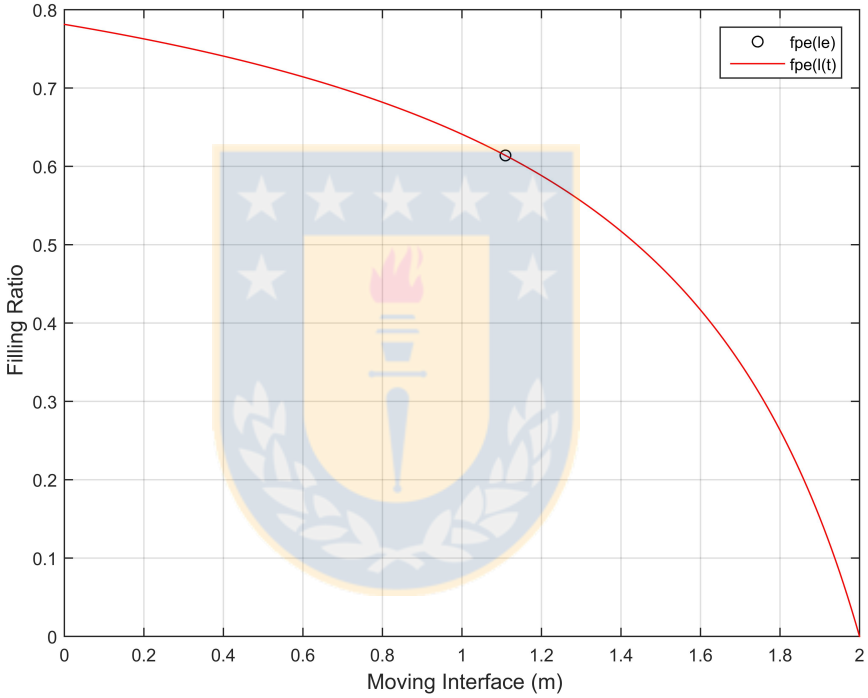

FIGURE 3.1: Filling ratio as a function of the moving interface.(Source: Personal collection).

equation 2.18 as it follows:

$$\Delta P = V_{eff}\eta N^* \rho_0 \left[\frac{L - l^*}{B\rho_0 + K_d(L - l^*)}\right] = 31250 \text{ Pa}, \tag{3.8}$$

$$F_d^* = \frac{K_d}{\eta}\Delta P = 270/3600 \text{ kg/s}. \tag{3.9}$$

3.2.2.3 Temperature of the melt

3.2.2.3.1 Temperature at the *PFZ*:

On steady state, i.e. $\partial T_p(x,t)/\partial t = 0$, the temperature at the *PFZ* is given by:

$$-\xi N^* \frac{\partial T_p^*(x)}{\partial x} + \Omega_p(f_p^*, N^*, T_b^*, T_p^*) = 0, \tag{3.10}$$

where,

$$\Omega_p(f_p^*, N^*, T_b^*, T_p^*) = \frac{\mu\eta N^{*2}}{f_p^*\rho_0 V_{eff} C_p} + \frac{S_{exc}\alpha}{\rho_0 V_{eff} C_p}(T_b^* - T_p^*(x)), \tag{3.11}$$

then,

$$-\xi N^* \frac{\partial T_p^*(x)}{\partial x} + \frac{\mu\eta N^{*2}}{f_p^*\rho_0 V_{eff} C_p} + \frac{S_{exc}\alpha}{\rho_0 V_{eff} C_p}(T_b^* - T_p^*(x)) = 0, \tag{3.12}$$

redistributing terms,

$$\frac{\partial T_p^*(x)}{\partial x} = \frac{\mu\eta N^*}{\xi f_p^*\rho_0 V_{eff} C_p} + \frac{S_{exc}\alpha}{\xi N^*\rho_0 V_{eff} C_p}(T_b^* - T_p^*(x)). \tag{3.13}$$

This equation can be written as:

$$\frac{\partial T_p^*(x)}{\partial x} + \frac{S_{exc}\alpha}{\xi N^*\rho_0 V_{eff} C_p} T_p^*(x) = \frac{\mu\eta N^*}{\xi f_p^*\rho_0 V_{eff} C_p} + \frac{S_{exc}\alpha}{\xi N^*\rho_0 V_{eff} C_p} T_b^*. \tag{3.14}$$

Which is a linear differential equation. Then, the solution for the temperature on steady state on the domain of the *PFZ*, i.e $[0, x]$, is the following:

$$T_p^*(x) = \zeta_1 \left(1 - \exp\left(\frac{-S_{exc}\alpha x}{\rho_0 V_{eff} C_p \xi N^*}\right)\right) + T_{in} \exp\left(\frac{-S_{exc}\alpha x}{\rho_0 V_{eff} C_p \xi N^*}\right), \tag{3.15}$$

with,

$$\zeta_1 = \left(\frac{\mu\eta N^*}{f_p^*} + \frac{S_{exc} T_b^*}{N^*}\right) \frac{N^*}{S_{exc}\alpha}. \tag{3.16}$$

3.2.2.3.2 Temperature at the *FFZ*: Using $\partial T_f(x,t)/\partial t = 0$, in order to find the temperature on steady state for the *FFZ*:

$$-\frac{F_d^*\xi}{\rho_0 V_{eff}} \frac{\partial T_f(x)}{\partial x} + \Omega_f(1, N^*, T_b^*, T_f^*) = 0, \tag{3.17}$$

where,

$$\Omega_f(1, N^*, T_b^*, T_f^*) = \frac{\mu\eta N^{*2}}{\rho_0 V_{eff} C_p} + \frac{S_{exc}\alpha}{\rho_0 V_{eff} C_p}(T_b^* - T_f^*(x)), \tag{3.18}$$

then,

$$-\frac{F_d^*\xi}{\rho_0 V_{eff}} \frac{\partial T_f^*(x)}{\partial x} + \frac{\mu\eta N^{*2}}{\rho_0 V_{eff} C_p} + \frac{S_{exc}\alpha}{\rho_0 V_{eff} C_p}(T_b^* - T_f^*(x)) = 0 \tag{3.19}$$

redistributing terms,

$$\frac{\partial T_f^*(x)}{\partial x} + \frac{S_{exc}\alpha}{F_d^*\xi C_p} T_f^*(x) = \frac{\mu\eta N^{*2} + S_{exc}\alpha T_b^*}{F_d^*\xi C_p}. \tag{3.20}$$

The equation (3.20) is a linear differential equation for which the solution for the temperature at steady state on the domain of the *FFZ*, i.e. $[l^*, x]$, is the following:

$$T_f^*(x) = \zeta_2 + \left(T_p^* - \zeta_2\right) \exp\left(\frac{-S_{exc}\alpha(x - l^*)}{F_d^*\xi C_p}\right), \tag{3.21}$$

with

$$\zeta_2 = \frac{\mu\eta N^{*2} + S_{exc}\alpha T_b^*}{S_{exc}\alpha} \tag{3.22}$$

With equations (3.15) and (3.21) it is possible to compute the temperature at steady state in the extruder for a given set of parameters. Fig. 3.2 shows the temperature at the interface for different values of the equilibrium point of the moving interface. Note that, when the moving interface gets closer to the die output, i.e. close to $x = 2$ m, the temperature grows asymptotically towards the die. This is related to the chosen parameters of the extrusion process and imposes a restriction from the modelling point of view since the moving interface cannot be closer to the die. The black circular point in the figure, represents the temperature at the interface $T(l^*) = 345.73$ K with $l^* = 1.1095$ m.

In addition, Fig. 3.3 shows the melt temperature in the extruder in steady state for different equilibrium points, i.e. $l_1^* = 0.4331$,$l_2^* = 1.1095$ and $l_3^* = 1.4595$ where it is possible to note that the melt temperature changes accordingly with the equilibrium of the moving interface on the *PFZ* and the *FFZ*. If the moving interface is closer to the die, the melt temperature will be higher. That means, the melt temperature is intrinsically related to the moving interface which can be used for control purposes as it was shown by [17].

3.2.3 Dynamic simulation with constant viscosity and variable input flow

In this case a variable input flow was used in order to test three important operational conditions:

- Initial operation starting from a theoretical equilibrium of the interface position and the filling ratio using an input flow of $F_{in} = 324/3600$ kg/s.
- After 50 s of operation up to 600 s, the input flow decreases to $F_{in} = 216/3600$ kg/s in order to empty the extruder.

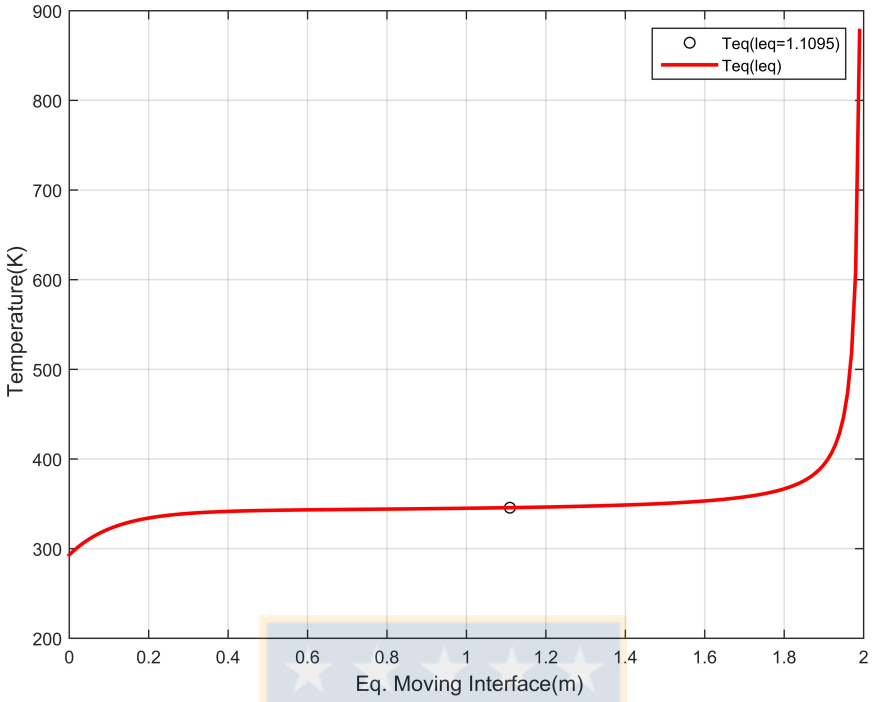

FIGURE 3.2: Temperature vs. equilibrium of the moving interface. (Source: Personal collection).

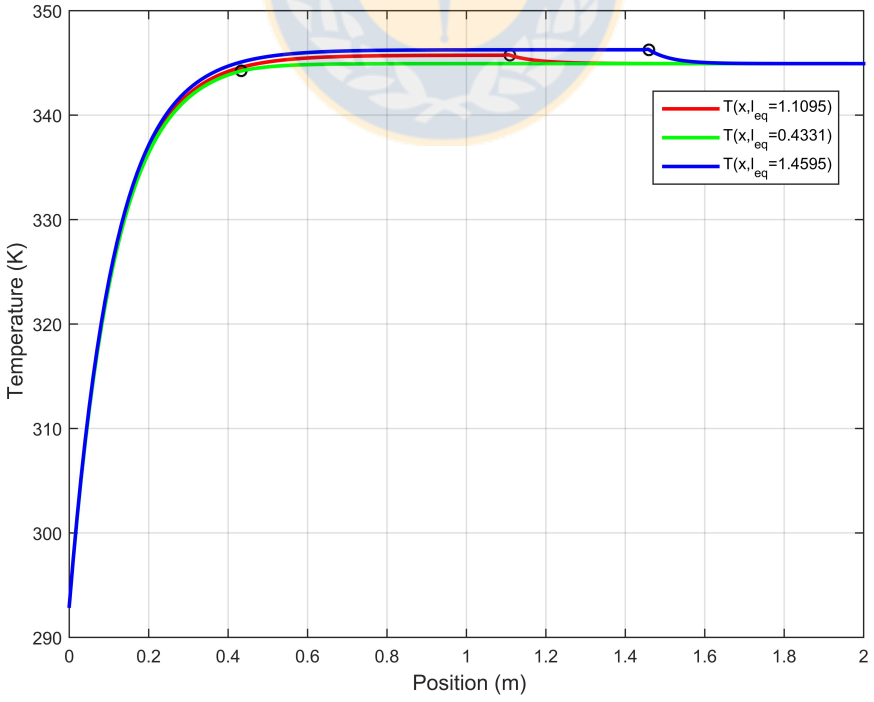

FIGURE 3.3: Temperature at steady state for different equilibrium points. (Source: Personal collection).

- After 600 s of operation up to 1200 s, the input flow changes to its initial value $F_{in} = 270/3600$ kg/s in order to fill up the extruder.

A spatial discretization N_d of 200 elements and a simulation time of 1200 s were used. Summarizing, the initial conditions defined for the filing ratio, the interface position and the input flow along the extruder are f_p^0, l^0, F_{in} and they are shown on Table 3.4:

Initial Filling Ratio	$f_p^0 = 1.2 f_p^* = 0.7367$
Initial interface Position	$l^0 = 0.4331$ m
Initial input Flow	$F_{in} = 324/3600$ kg/s

TABLE 3.4: Initial conditions for the extrusion process simulation with constant viscosity and variable input flow.(Source: Personal collection).

Taking into account that the extruder length is $L = 2$ m, in this case initially, the positions $x_1 = 0.5$ m, $x_2 = 1$ m and $x_3 = 1.5$ m belongs to the *FFZ*. Fig. 3.4 shows the evolution of the filling ratio for the simulation period of 1200 s. Recall that in this case the initial position of the interface is $l^0 = 0.4331$ m.
Note that the filling ratio changes accordingly to the variation of the input flow. For example, regarding to the filling ratio evolution at $x_2 = 1$ m the following behaviour can be described :

- At the beginning, this position belongs to the *FFZ*. Then, the filling ratio decreases at approximately $t_1 = 190$ s to an equilibrium position of $f_p(x_2, t_1) = 0.49112$ which corresponds to the equilibrium for an input flow of $F_{in} = 216/3600$ kg/s.
- At around $t_2 = 600$ s the filling ratio increases accordingly to the change of the input flow, i.e. $F_{in} = 270/3600$ kg/s, and reaches an equilibrium point of $f_p(x_2, t_2) = 0.6139$.

Also comparing the filling ratio evolution to the interface position on Fig. 3.5 it is possible to validate the coupling between these two variables. For instance, in the case of the filling ratio f_p at $x_1 = 0.5$ m the value changes from its initial condition ($f_p(x_1, t_0) = 1$ at $t_0 = 0$ s) and decreases to its second state at $t_1 = 50$ s to a value of $f_p(x_1, t_1) = 0.49112$. The same behaviour can be found on the interface position evolution where it is shown that it becomes higher than 0.5 m after approximately 50 s.
In addition, note that the interface position does not change on the first 50 s of simulation because it corresponds to the equilibrium point of $l(t) = 0.4331$ m. After 50 s, when the input flow changes, the interface position increases to reach its steady state of $l(t) = 1.46$ m. Finally at 600 s when the input flow changes again, the interface position

decreases in order to reach its final state at $l(t) = 1.1095$ m

On the other hand Fig. 3.6 shows the melt temperature evolution. Note that the temperature reaches its steady state value depending on the changes on the input flow, although the behaviour is not so noticeable as in the case of the filling ratio or the interface position.This is particularly due to the fact that the influence of the input flow on the temperature of the melt due to the heat produced by the friction of the material with the barrel and the screw can be considered to be as small if it is compared to the heat exchange between the barrel and the melt.

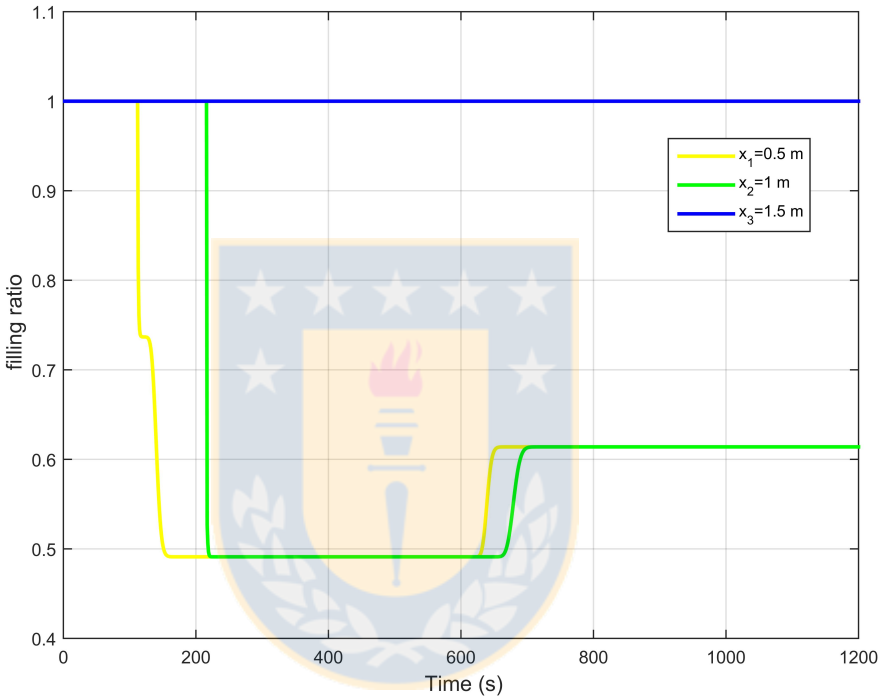

FIGURE 3.4: Filling ratio dynamics for constant viscosity and variable input flow. (Source: Personal collection).

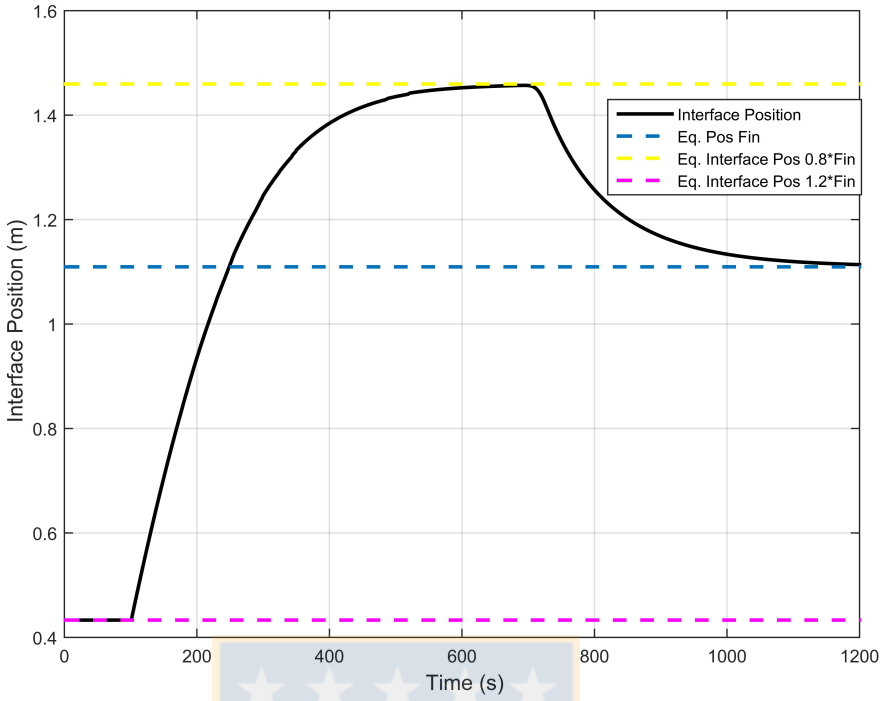

FIGURE 3.5: Interface position dynamics for constant viscosity and variable input flow. (Source: Personal collection).

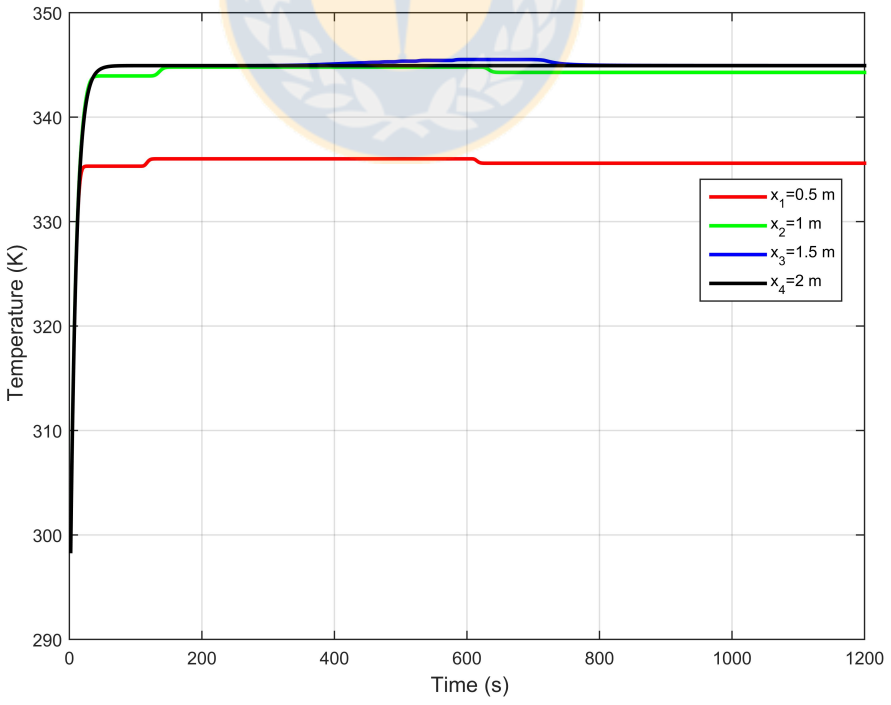

FIGURE 3.6: Temperature dynamics for constant viscosity and variable input flow. (Source: Personal collection).

3.2.4 Dynamic simulation with constant viscosity and variable screw speed

In this case a variable screw speed $N(t)$ and a constant input flow of $F_{in} = 324/3600$ kg/s were used in order to test the behaviour of the process within the following operational conditions:

- Initial operation starting from a theoretical equilibrium of the interface and the filling ratio using a screw speed of $N(t) = 250$ rpm.
- After 50 s of operation up to 600 s, the screw speed increases to $N(t) = 300$ rpm.
- After 600 s of operation up to 1200 s, the screw speed increases again up to $N(t) = 350$ rpm in order to empty the extruder.
- After 1200 s up to 2000 s, the screw speed changes to its original value $N(t) = 250$ rpm in order to fill up the extruder.

A spatial discretization N_d of 200 elements and a simulation time of 2000 s were used. Summarizing, the initial conditions defined for the filing ratio, the interface position and the input flow along the extruder are f_p^0, l^0, F_{in} and they are shown on Table 3.5:

Initial Filling Ratio	$f_p^0 = 1.2 f_p^* = 0.7367$
Initial interface Position	$l^0 = 0.4331$ m
Initial input Flow	$F_{in} = 324/3600$ kg/s

TABLE 3.5: Initial conditions for the extrusion process simulation with constant viscosity and variable screw speed. (Source: Personal collection).

In this case the positions of the extruder $x_1 = 0.5$ m, $x_2 = 1$ m and $x_3 = 1.5$ m are analyzed. At the beginning, those positions belongs to the *FFZ*. Fig. 3.7 shows the evolution of the filling ratio during the simulation period of 2000 s. In this case the filling ratio changes accordingly to every variation of the screw speed in a similar way than the changes generated by the variation of the input flow. That means, the dynamics of the filling ratio depends on the screw speed and the input flow. Recalling the filling ratio evolution at $x_2 = 1$ m the following behaviour can be described:

- At the beginning this position belongs to the *FFZ*. Then, the filling ratio decreases at approximately $t_1 = 253$ s to an equilibrium position of $f_p(x_2, t_1) = 0.6139$ which corresponds to the equilibrium at a screw speed of $N(t_1) = 300$ rpm.

- At around $t_2 = 600$ s the filling ratio decreases accordingly to an increment of the screw speed, i.e., $N(t_2) = 350/60$rpm, and reaches an equilibrium point of $f_p(x_2, t_2) = 0.5262$.

- At approximately $t_3 = 1200$ s the filling ratio returns to its initial position, i.e. to the *FFZ* because of a decrease of the screw speed to an initial value of $N(t_3) = 250$ rpm.

In this case, the evolution of the filling ratio relates to the evolution of the interface position as it is shown on Fig. 3.8 and 3.9 . For instance, at approximately 50 s, the interface position moves from its initial position $l^0 = 0.433$ m to another equilibrium point at $l(t) = 1.1095$ m due to the changes on the screw speed from $N(t_0) = 250$ rpm to $N(t_1) = 300$ rpm.
After 600 s, the interface position changes again due to the variation of the screw speed and reaches an equilibrium point of $l(t) = 1.3780$ m with $N(t_2) = 350$ rpm. Finally, the interface position decreases to its initial value after 1200 s of simulation due to a decrease on the screw speed of $N(t_3) = 250$ rpm.

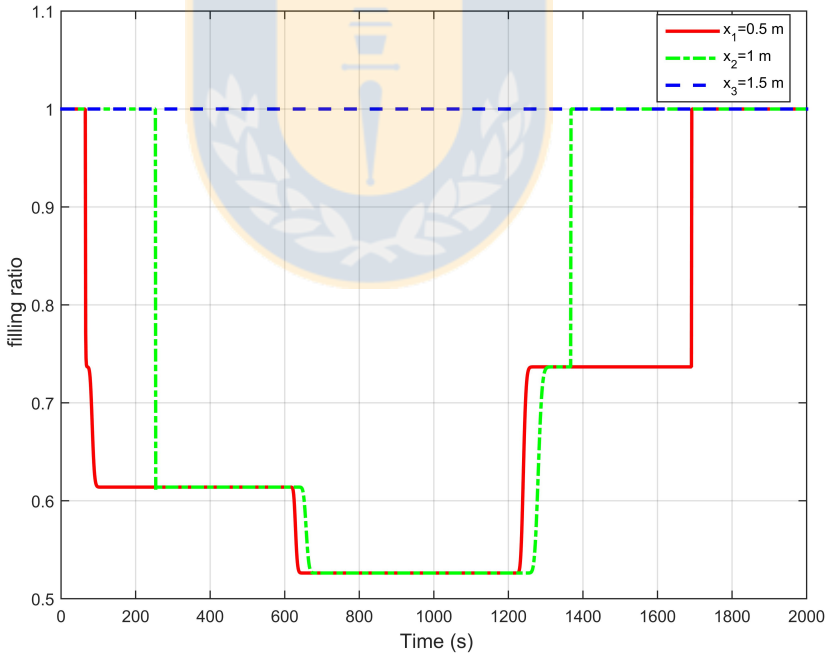

FIGURE 3.7: Filling ratio evolution for constant viscosity and variable screw speed. (Source: Personal collection).

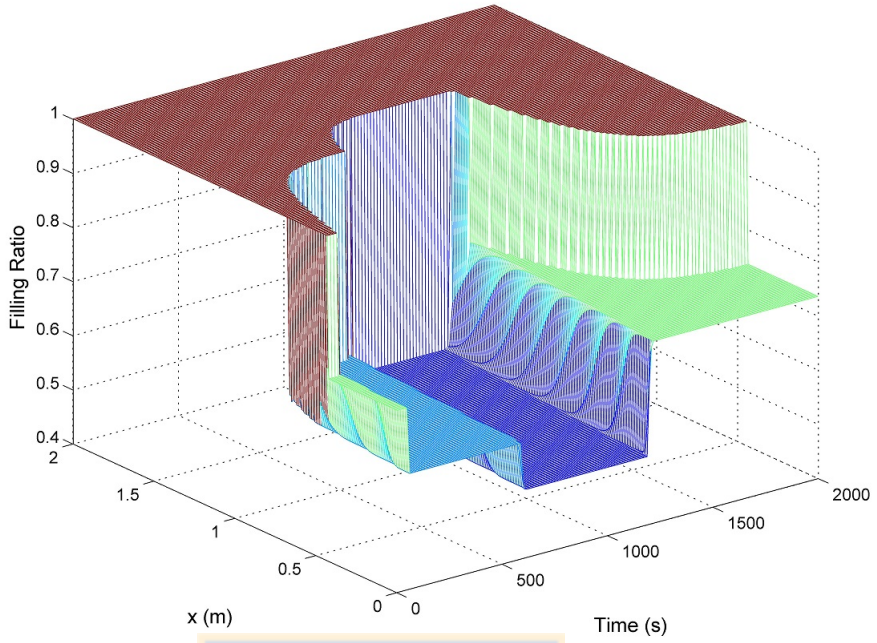

FIGURE 3.8: Filling ratio and moving interface evolution for constant viscosity and variable screw speed. (Source: Personal collection).

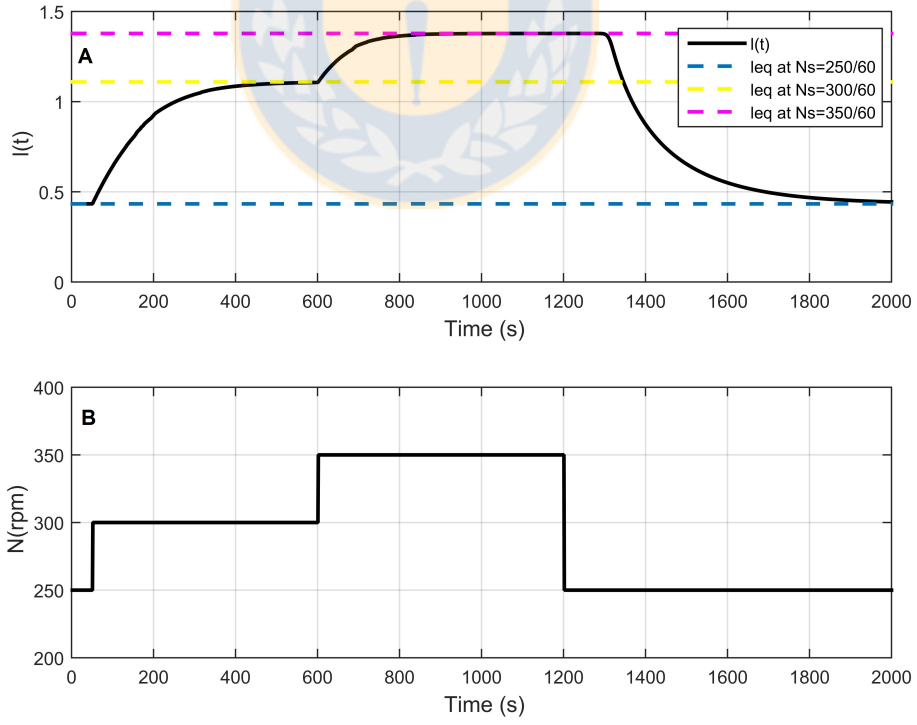

FIGURE 3.9: Dynamic simulations with constant viscosity: (A)Interface position evolution and (B) Screw speed. (Source: Personal collection).

The evolution of the melt temperature is shown in Fig. 3.10. Note that in this case, the changes on the screw speed are reflected on the melt temperature behaviour. The melt temperature increases and decreases accordingly to the screw speed changes. For instance, for a position of $x_2 = 1$ m at approximately $t_2 = 600$ s the melt temperature increases from $T(x_2, t_1) = 352.6$ K to $T(x_2, t_2) = 361.4$ K due to an increase of the screw speed from $N(t_1) = 300$ rpm to $N(t_2) = 350$ rpm. After $t_3 = 1200$ s of simulation, the melt temperature decreases to a final value of $T(x_2, t_3) = 345.1$ K due to a decrease of the screw speed $N(t_3) = 250$ rpm.

This is particularly due to the fact that the influence of the screw speed on the melt temperature is higher than the influence of the input flow. In fact, if the screw speed is slow, the energy transferred to the melt is mainly form the barrel heating. If the screw speed is high, shear heating provided by the screw rotation becomes the main heating source [28]. Then it is possible to conclude that, the melt temperature highly depends on the barrel temperature, the input temperature and the screw speed.

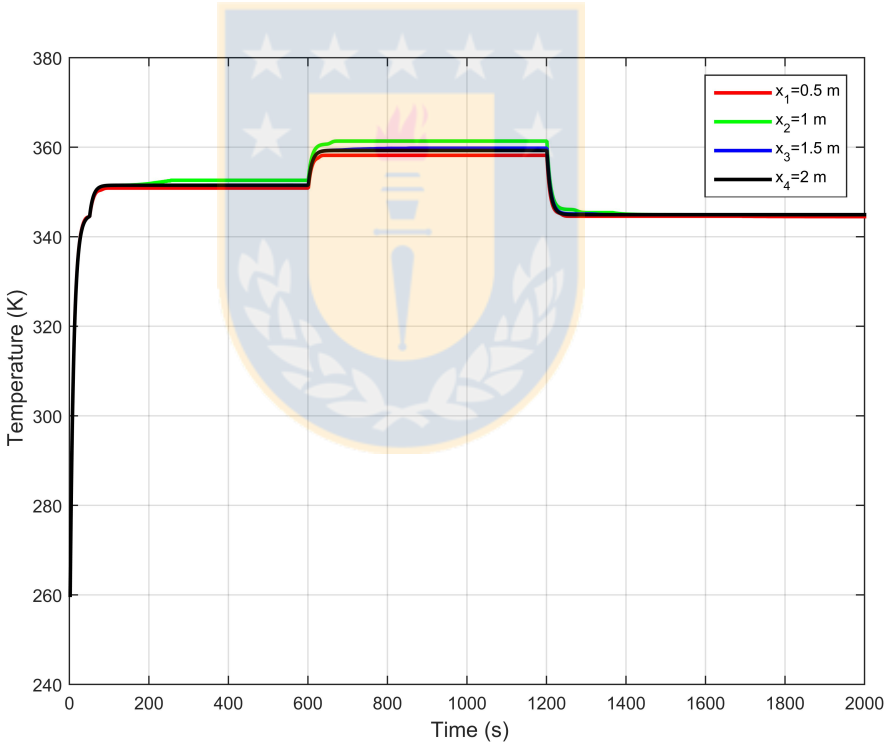

FIGURE 3.10: Temperature evolution for constant viscosity and variable screw speed. (Source: Personal collection).

3.3 Extrusion process model with variable viscosity

3.3.1 Description of the simulated model

In this section, simulation tests for the mass and energy balance equations of the extrusion process model with variable viscosity are presented. In order to test the behaviour of the discretized model, the following simulations were made:

- Test No.1: variable feed rate F_{in} with constant screw speed $N(t) = N_0$
- Test No.2: variable screw speed $N(t)$ with constant feed rate F_{in}

The simulations used are based on the equations shown in Section (2.4.1) and the discretization process explained in Section (2.4.2)with variable viscosity. In both cases a power-law model for viscosity is used [24]. In this model, the viscosity is highly dependent on the temperature of the melt as it is shown by the following equations:

$$\eta_p(T_p(x,t)) = \eta_p^0 e^{-\beta_T(T_p(x,t)-T_0)} \text{ (t,x)} \in (\mathbb{R}^+, [0, l(t)[, \tag{3.23}$$

$$\eta_f(T_f(x,t)) = \eta_f^0 e^{-\beta_T(T_f(x,t)-T_0)} \text{ (t,x)} \in (\mathbb{R}^+, [l(t), L]. \tag{3.24}$$

where, $\eta(T(x,t))$ is the viscosity as a function of the melt temperature, β_T is a temperature shift factor in the expression that relates viscosity to temperature and η_0 is the viscosity at a reference temperature T_0. The values of β_T for polymers are usually in the range of $0.01 - 0.04/°C$, but occasionally they may reach $0.1/°C$ or more for some materials [38]. Table 3.6 shows the input variables used in the simulation process, most of the data are obtained from Diagne [17].

Initial screw speed	$N_0 = 250[rpm]$
Barrel temperature	$T_b = 330[K]$
Input temperature	$T_{in} = 320[K]$
Extruder length	$L = 2[m]$
Initial feed rate	$F_{in} = 270/3600[kg/s]$
Initial filling ratio	$f_p^{in} = \dfrac{F_{in}}{\rho_0 V_{eff} N_0} = 0.6139$

TABLE 3.6: Input values used on the simulation process for variable viscosity. (Amended from [17]). (Source: Personal collection).

In addition, the following screw and thermodynamical parameters were used on the simulation process which are detailed on Table 3.7 and 3.8 respectively.

External diameter	$D = L/15 = 0.133[m]$
Internal diameter	$D_s = 0.001[m]$
Screw pitch	$\xi = 30 \times 10^{-}4[m]$
Effective surface	$S_{eff} = \frac{\pi}{4}(D^2 - D_s^2) = 0.01396[m^2]$
Effective volume	$V_{eff} = S_{eff}\xi = 4.188 \times 10^{-}5[m^3]$

TABLE 3.7: Screw parameters used on the simulation process for variable viscosity. (Source: Personal collection).

Thermal exchange coefficient	$\alpha = 10.41 \times 10^1[J/(m^2Ks)]$
Material density	$\rho_0 = 1400/2[kg/m^3]$
Exchange surface	$S_{exc} = \pi D^2 L[m^2]$
Initial viscosity	$\eta_0 = 173.4[Pa.s]$
Heat capacity	$C_p = 3.6 \times 10^3[J/(kgK)]$

TABLE 3.8: Thermodynamical parameters used on the simulation process for variable viscosity. (Source: Personal collection).

3.3.2 Equilibrium Points Computation

Recalling the extrusion process model and the boundary conditions shown in Section 2.4.1, we shall compute the equilibrium points using $\partial/\partial t = 0$ for the filling ratio, the temperature and the moving interface:

3.3.2.1 Filling Ratio

By using the mass balance equation from (2.10) the following expression in steady state can be proposed:

$$-\xi N_0 \frac{\partial f_p(x)}{\partial x} = 0, \tag{3.25}$$

then,

$$\frac{\partial f_p(x)}{\partial x} = 0, \tag{3.26}$$

that is,

$$f_p^* = \kappa, \tag{3.27}$$

with κ as a constant,

3.3.2.2 Moving Interface

Assuming $dl(t)/dt = 0$ we have the following expression in steady state:

$$\frac{F_d^* - \rho_0 N_0 V_{eff} f_p^*}{\rho_0 S_{eff}(1 - f_p^*)} = 0, \tag{3.28}$$

then, solving for the filling ratio we can have an equilibrium value for the given parameters as it follows:

$$f_p^{in} = f_p^* = \frac{F_{in}}{\rho_0 N_0 V_{eff}} = \kappa = 0.6139, \tag{3.29}$$

That means, the steady state of the filling ratio is the same that in the case of constant viscosity. However, if we recall the position of the interface from equation (2.37), finding an analytical solution for the steady state equation is not possible because of the total viscosity term, $\int_{l(t)}^{L} \eta(T_f(x,t))dx$, included in equation (2.42).

3.3.2.3 Temperature of the Melt

3.3.2.3.1 Temperature at the *PFZ*:

By assuming $\partial T_p(x,t)/\partial t = 0$ on the energy balance of the PFZ from equation (2.16), then we have on steady state:

$$-\xi N_0 \frac{\partial T_p^*(x)}{\partial x} + \Omega_p(f_p^*, N^*, T_b^*, T_p^*, \eta(T_p^*(x))) = 0, \tag{3.30}$$

where,

$$\Omega_p(f_p^*, N^*, T_b^*, T_p^*, \eta(T_p^*(x))) = \frac{\mu\eta(T_p(x))N^{*2}}{f_p^*\rho_0 V_{eff} C_p} + \frac{S_{exc}\alpha}{\rho_0 V_{eff} C_p}(T_b^* - T_p^*(x)), \tag{3.31}$$

with T_p^* as temperature at the equilibrium is given by. Then,

$$-\xi N^* \frac{\partial T_p^*(x)}{\partial x} + \frac{\mu\eta(T_p^*(x))N^{*2}}{f_p^*\rho_0 V_{eff} C_p} + \frac{S_{exc}\alpha}{\rho_0 V_{eff} C_p}(T_b^* - T_p^*(x)) = 0, \tag{3.32}$$

redistributing terms,

$$\frac{\partial T_p^*(x)}{\partial x} = \frac{\mu\eta(T_p^*(x))N^*}{\xi f_p^*\rho_0 V_{eff} C_p} + \frac{S_{exc}\alpha}{\xi N^*\rho_0 V_{eff} C_p}(T_b^* - T_p^*(x)), \tag{3.33}$$

Therefore, T_p^* is the solution of the first-order nonlinear equation (3.33).

3.3.2.3.2 Temperature at the *FFZ* By assuming $\partial T_f(x,t)/\partial t = 0$ on the energy balance of the FFZ from equation (2.21), then we have on steady state:

$$-\frac{F_d^*\xi}{\rho_0 V_{eff}}\frac{\partial T_f^*(x)}{\partial x} + \Omega_f(N^*, T_b^*, T_f^*, \eta(T_f^*(x))) = 0, \tag{3.34}$$

where,

$$\Omega_f(N^*, T_b^*, T_f^*, \eta(T_f^*(x))) = \frac{\mu\eta(T_f^*(x))N^{*2}}{\rho_0 V_{eff} C_p} + \frac{S_{exc}\alpha}{\rho_0 V_{eff} C_p}(T_b^* - T_f^*(x)), \tag{3.35}$$

then,

$$-\frac{F_d^*\xi}{\rho_0 V_{eff}}\frac{\partial T_f^*(x)}{\partial x} + \frac{\mu\eta(T_f^*(x))N^{*2}}{\rho_0 V_{eff} C_p} + \frac{S_{exc}\alpha}{\rho_0 V_{eff} C_p}(T_b^* - T_f^*(x)) = 0, \tag{3.36}$$

redistributing terms,

$$\frac{\partial T_f^*(x)}{\partial x} = -\frac{S_{exc}\alpha}{F_d^*\xi C_p}T_f^*(x) + \frac{\mu\eta(T_f^*(x))N^{*2} + S_{exc}\alpha T_b^*}{F_d^*\xi C_p}, \tag{3.37}$$

where $F_d^* = F_{in}^*$.Therefore, T_f^* is the solution of the first-order nonlinear equation (3.37). On the other hand, the equilibrium for the flow at the die should also satisfy the equation of pressure continuity at the interface; i.e. equation (2.46),

$$F_{in}^* = \frac{K_d\rho_0 V_{eff} N^* \int_{l^*}^{L}\eta(T_f^*(x))dx}{B\rho_0\eta_d^* + K_d\int_{l^*}^{L}\eta(T_f^*(x)))dx}. \tag{3.38}$$

Finding an analytical solution to the first-order nonlinear equation (3.37) since the term F_{in} depends on the total viscosity term $\int_{l(t)}^{L}\eta(T_f(x,t))dx$. However, with a given N^* and F_{in}^*, it is possible to find a l^* so that equations (3.33), (3.37) and (3.38) are satisfied. In order to compute the steady state values of the interface position an optimization problem can be proposed. This matter is analyzed in detail in Section 4.3 for the application of the proposed model to an industrial type twin screw extruder.

3.3.3 Dynamic simulation with non-constant viscosity and variable input flow

In this case a variable input flow was used in order to test three important operational conditions:

- Initial operation starting from a theoretical equilibrium of the filling ratio using an input flow of $F_{in} = 324/3600$ kg/s.

- After 50 s of operation up to 600 s, the input flow decreases to $F_{in} = 216/3600$ kg/s in order to empty the extruder.
- After 600 s of operation up to 1200 s, the input flow changes to its original value $F_{in} = 270/3600$ kg/s in order to fill up the extruder.

A spatial discretization N_d of 200 meshes and a simulation time of 1200 s were used. Summarizing, the initial conditions defined for the filing ratio, the interface position and the input flow along the extruder are f_p^0, l^0, F_{in} and they are shown on Table 3.9:

Initial Filling ratio	$f_p^0 = 1.2 f_p^* = 0.7367$
Initial interface position	$l^0 = 0.4331$ m
Initial input flow	$F_{in} = 324/3600$ kg/s

TABLE 3.9: Initial conditions for the extrusion process simulation with non-constant viscosity and variable input flow. (Source: Personal collection).

Taking into account that the extruder length is $L = 2$ m, in this case initially, the positions $x_1 = 0.5$ m, $x_2 = 1$ m and $x_3 = 1.5$ m belongs to the *FFZ*. Fig. 3.11 shows the evolution of the filling ratio for the simulation period of 1200 s. Recall that in this case the initial position of the interface is $l^0 = 0.4331$ m. Note that the filling ratio changes accordingly to every variation of the input flow.

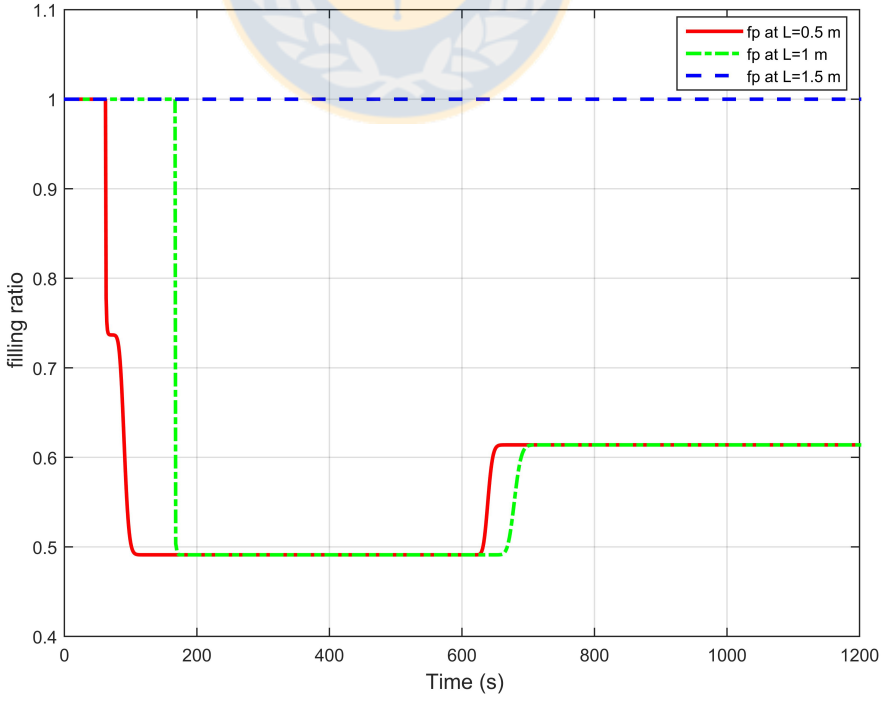

FIGURE 3.11: Filling ratio dynamics for non-constant viscosity and variable input flow. (Source: Personal collection).

For instance, recalling the filling ratio evolution at $x_2 = 1$ m the following behaviour can be described:

- At the beginning this position belongs to the *FFZ*. Then, the filling ratio decreases at approximately $t_1 = 190$ s to an equilibrium position of $f_p(x_2, t_1) = 0.49112$ which corresponds to the steady state for an input flow of $F_{in} = 216/3600$ kg/s.
- At around $t_2 = 600$ s the filling ratio increases accordingly to the change of the input flow, i.e. $F_{in} = 270/3600$ kg/s, and reaches an equilibrium point of $f_p(x_2, t_2) = 0.6139$.

The behaviour of the filling ratio in this case is the same as in the case of constant viscosity. In addition, comparing the filling ratio evolution with the interface position on Fig. 3.12 it is possible to validate the coupling between those two variables. For instance, in the case of f_p at $x_1 = 0.5$ m the value changes from its initial condition ($f_p = 1$) and decreases to its second state at approximately $t_1 = 50$ s to a value of $f_p(x_1, t_1) = 0.49112$. The same behaviour can be found at the interface position where it is shown that it becomes bigger than 0.5 m after approximately 50 s.

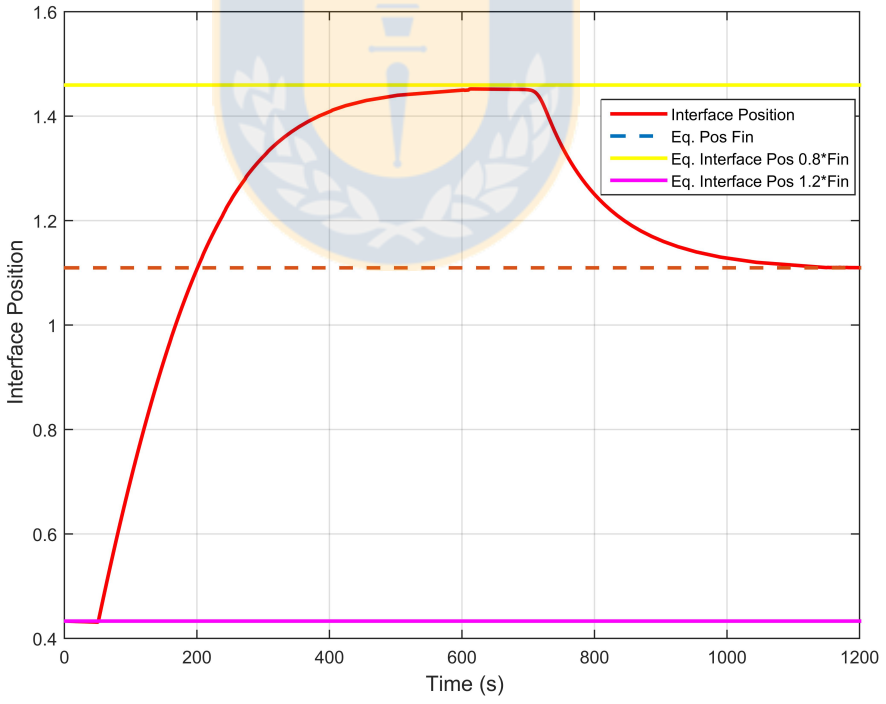

FIGURE 3.12: Interface position dynamicsfor non-constant viscosity and variable input flow. (Source: Personal collection).

In this case the plotted equilibrium points are obtained only for constant viscosity. However, it is possible to note that the equilibrium points of the moving interface are slightly

different from those obtained for the case of constant viscosity. This is particularly due to the influence of the viscosity on the model.

Regarding to the melt temperature, its evolution can be found on Fig. 3.13 A. Note that the temperature reaches steady state value depending on the changes of the input flow, although the behaviour is similar to the case of constant viscosity. This is particularly due to the fact, that with constant screw speed the viscosity influence on the temperature is not very noticeable. This can be shown with the behaviour of the viscosity on the Fig. 3.13 B. Note that the viscosity reaches the steady state very fast (approximately 20 s) and it is highly dependable of the temperature dynamics.

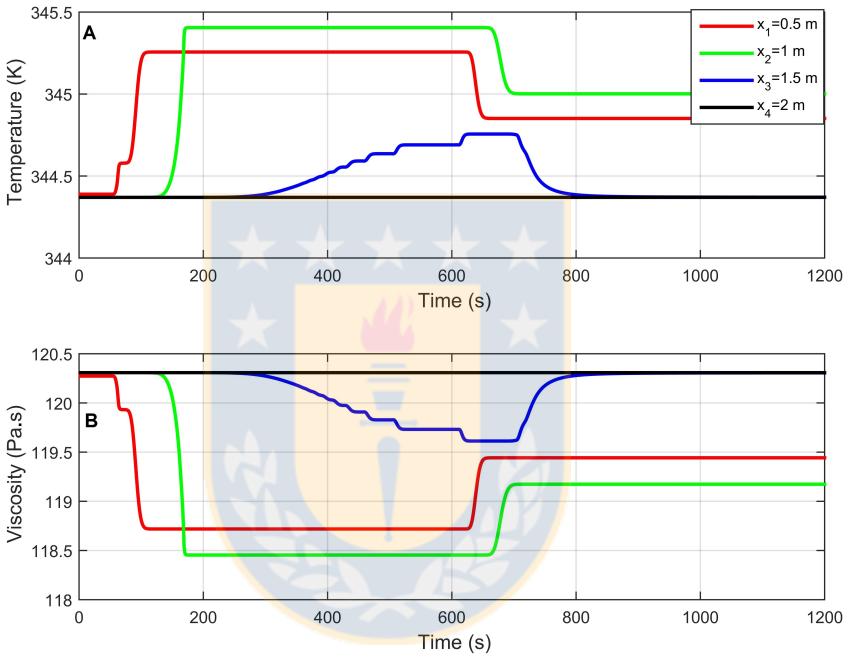

FIGURE 3.13: Dynamic simulations for non-constant viscosity: (A) Melt temperature and (B) Viscosity. (Source: Personal collection).

3.3.4 Dynamic simulation with non-constant viscosity and variable screw speed

In this case a variable screw speed $N(t)$ and a constant input flow of $F_{in} = 324/3600$ kg/s were used in order to test the behaviour of the process within the following operational conditions:

- Initial operation starting from a theoretical equilibrium of the filling ratio using a screw speed of $N(t) = 250$ rpm

- After 50 s of operation up to 600 s, the screw speed increases to $N(t) = 300$ rpm in order to empty the extruder
- After 600 s of operation up to 1200 s, the screw speed increases again up to $N(t) = 350$ rpm in order to empty the extruder
- After 1200 s up to 2000 s, the screw speed changes to its original value $N(t) = 250$ rpm in order to fill up the extruder

A spatial discretization N_d of 200 elements and a simulation time of 2000 s were used. Summarizing, the initial conditions defined for the filing ratio, the interface position and the input flow along the extruder are f_p^0, l^0, F_{in} and are shown on Table 3.10:

Initial Filling ratio	$f_p^0 = 1.2 f_p^* = 0.7367$
Initial interface position	$l^0 = 0.4331$ m
Initial input flow	$F_{in} = 324/3600$ kg/s

TABLE 3.10: Initial conditions for the extrusion process simulation with non-constant viscosity and variable screw speed. (Source: Personal collection).

In this case the positions of the extruder $x_1 = 0.5$ m, $x_2 = 1$ m and $x_3 = 1.5$ m are analyzed. At the beginning, those positions belongs to the *FFZ*. Fig. 3.14 shows the evolution of the filling ratio during the simulation period of 2000 s. In this case the filling ratio changes accordingly to every variation of the screw speed in a similar way than the case of constant viscosity. Recalling the filling ratio evolution at $x_2 = 1$ m the following behaviour can be described:

- At the beginning this position belongs to the *FFZ*. Then, the filling ratio decreases at approximately $t_1 = 253$ s to an equilibrium position of $f_p(x_2, t_1) = 0.6139$ which corresponds to the equilibrium for an screw speed of $N(t_1) = 300$ rpm.
- At around $t_2 = 600$ s the filling ratio decreases accordingly to an increment of the screw speed, i.e, $N(t_2) = 350/60$ kg/s, and reaches an equilibrium point of $f_p(x_2, t_2) = 0.5262$.
- At approximately $t_3 = 1200$ s the filling ratio returns to its initial position, i.e, to the *FFZ* because of a decrease of the screw speed to an initial value of $N(t_3) = 250$ rpm.

In this case, the evolution of the filling ratio relates to the interface position dynamics as it is shown on Fig. 3.15. However, as in the case of constant screw speed, it is possible

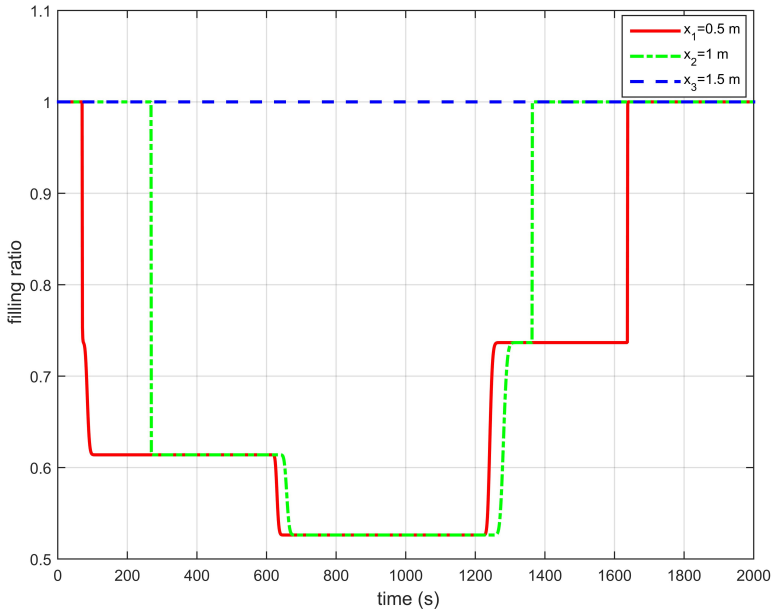

FIGURE 3.14: Filling ratio dynamics for non-constant viscosity and variable screw speed. (Source: Personal collection).

to note that the equilibrium points of the interface position are slightly different from those obtained for constant viscosity.

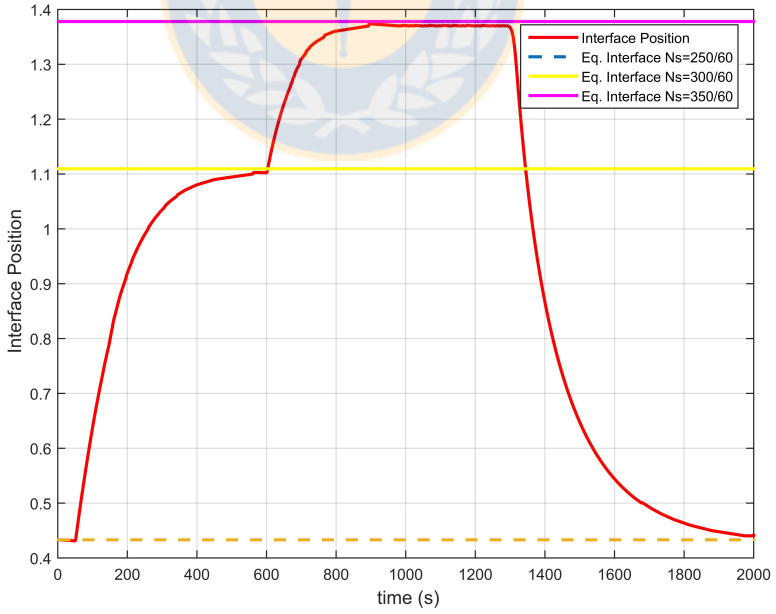

FIGURE 3.15: Interface position dynamics for non-constant viscosity and variable screw speed. (Source: Personal collection).

The evolution of the melt temperature is shown in Figure 3.16 A. Note that the changes

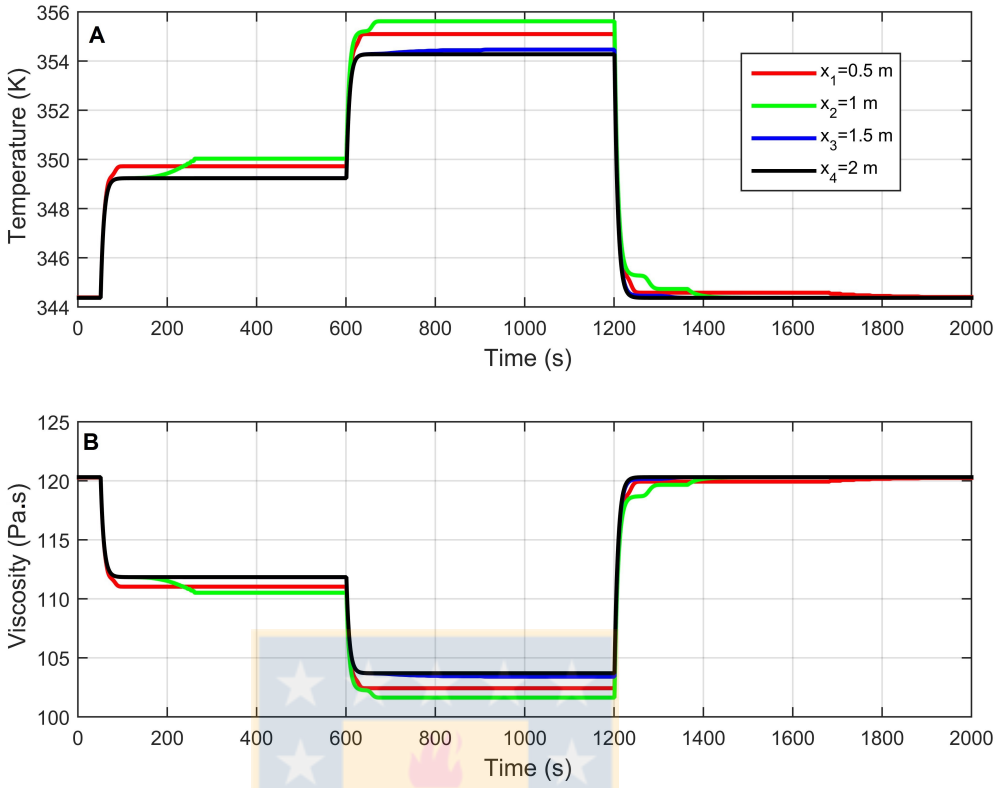

FIGURE 3.16: Dynamic simulations for non-constant viscosity: (A) Melt temperature and (B) Viscosity. (Source: Personal collection).

on the screw speed are reflected on the melt temperature behaviour. This is due to the fact that the influence of the screw speed on the melt temperature is higher than the influence of the input flow [25]. In fact, if the screw speed is slow, the energy transferred to the melt is mainly from the barrel heating. If the screw speed is high, shear heating provided by the screw rotation becomes the main heating source [28]. The behaviour of the viscosity is shown in the Fig. 3.16 B. Note that the viscosity changes accordingly to the variations on the temperature and the screw speed. Finally, the evolution of the die pressure on the extruder is presented in Fig. 3.17. Note that according to the changes on the screw speed there exist some transient phenomena on the pressure. Those peaks where observed by Poulesquen [39] and are related to a transient rise on the pressure at the die due to the variation on the screw speed.

3.4 Summary

In this chapter, the analysis of the bi-zone model of the extrusion process with variable screw-speed and variable input flow was presented. Two different conditions for viscosity

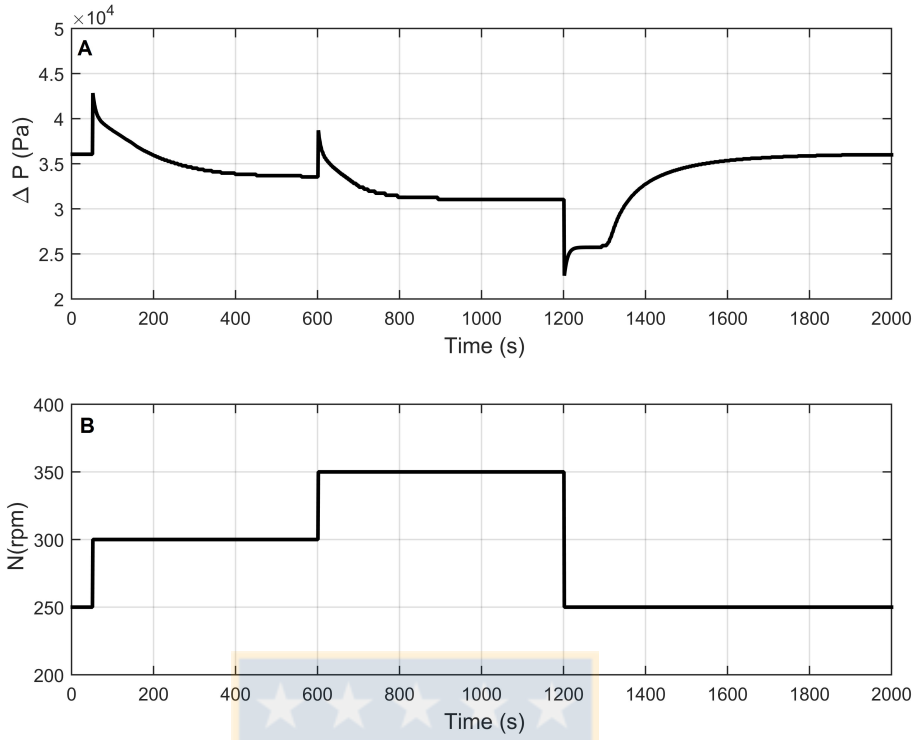

FIGURE 3.17: Dynamic simulations: (A)Die pressure dynamics for non-constant viscosity and (B) variable screw speed. (Source: Personal collection).

were tested: constant and variable viscosity. The equilibrium points were computed for both cases. The main difficulty in such system arises from the definition of the coupling condition between the *PFZ* and the *FFZ*. Open loop simulations where carried out in order to illustrate the behaviour of the model. The results show the dynamics of the moving interface, filling ratio and temperature along the process with physical coherence. Also, trough the simulations it was possible to conclude that the temperature dynamics depends entirely on the viscosity model. Therefore, for the experimental validation of the model and subsequent applications for control purposes this should be considered in detail. A proper viscosity model should be used depending on the properties of the material. However, the interface position and the filling ratio dynamics are very similar in both cases proving that the constant viscosity model could be adapted for control problems because of its simplicity. In the next chapter, the bi-zone model is adapted to an industrial twin screw extruder. The extrusion of Polypropylene *(PP)* has been taken into account with the Cross-WLF model of viscosity. The data obtained from simulations will be compared with experimental tests.

Chapter 4

Validation and experimental results

4.1 Introduction

Modern extruders are constructed in a modular way, allowing to compose different geometrical configurations in order to process different type of material upon several operational conditions. However, the bi-zone model presented in Chapter 2 is highly simplified in terms of the geometry of the extruder. This is an advantage from the modelling point of view, since fewer parameters should be identified in a validation stage. However, this simplicity needs to be addressed carefully since some parameters that may be most sensitive should be accurately identified in order to adapt the model to an industrial process with given operational conditions. Therefore, it is necessary to collect all the information regarding the geometrical properties and thermal parameters of the extruder in which the experimental data will be gathered. In this chapter, the twin-screw extruder used in this study is explained with detail, together with the description of the material used for experimental tests. The by-zone model is adapted with the available data of the equipment and a proper viscosity model for the material. In addition, the steady state of the extrusion process is analyzed in order to validate the model with the description of an optimization problem presented in the case of the melt temperature equilibrium. Additional tests regarding to the conservativeness of the finite volume method are also presented in this chapter. Experimental data is obtained directly through the extruder monitoring system and a data acquisition interface for additional sensing devices. Finally, dynamic simulations for variable screw speed are presented at the end of this chapter together with a quantitative analysis of the results.

4.2 Materials and methods

4.2.1 Material

A polypropylene homo-polymer (PP, PPH7060, Total Petrochemicals, France) with a specific density of 900 kg/m^3 was chosen. The viscosity of the matter on both *PFZ* and *FFZ* was simulated using the Cross-WLF model. This model provides a representation of viscosity over a wide range of processing conditions [29]:

$$\eta(T) = \frac{\eta_0(T)}{1 + \left(\frac{\eta_0(T)\gamma}{\tau}\right)^{1-n}}. \tag{4.1}$$

The zero shear viscosity η_0 is modeled with the WLF (Williams-Landel-Ferry) equation

$$\eta_0(T) = D_1 \exp\left[-\frac{A_1(T - D_2)}{A_2 + T - D_2}\right]. \tag{4.2}$$

In addition the shear rate γ is defined as:

$$\gamma = \frac{\pi D N(t)}{H}. \tag{4.3}$$

Some parameters of the Cross-WLF model for viscosity are shown in Table 4.1 and are obtained from [40], [41] and [42]:

Material density	$\rho_0 = 900[kg/m^3]$
Heat capacity	$C_p = 1860[J/(kgK)]$
Exchange surface	$S_{exc} = \pi D^2 L[m^2]$
Viscosity WLF parameter	$D_1 = 564[Pa/s]$
Temperature WLF parameter	$D_2 = 493[K]$
Power law index	$n = 0.251$
Temperature dependency 1	$A_1 = 2803.3$
Temperature dependency 2	$A_2 = 165097.1$
Critical shear stress	$\tau = \left(\frac{4n}{3n+1}\right)^{\frac{n}{(1-n)}}$

TABLE 4.1: Some thermal properties used for Polypropylene. (Amended from [40], [41] and [42]).

4.2.2 Twin screw extruder

A ZSE 18-Leistritz twin screw extruder was used for experimental tests. The screw profile used in this work is described in Fig. 4.3. In this case the screws are composed of

33 different sections which include direct flow and kneading block elements. No reverse flow elements were used in this work. The barrel diameter is 18 mm, the centerline is 15 mm, and the L/D ratio is 60 [43]. This extruder is capable of handling different screw speeds up to 1200 rpm. The throughput can be also varied from 1.5 to 22 $kg.h^{-1}$. This extruder is equipped with melt temperature and pressure sensors at the die, and two additional thermo-couples at positions 50D and 40D as it is shown on Fig. 4.1 and Fig. 4.2. The pellets were introduced through the main hopper and the barrel temperature T_b was set at 200°C along the screw profile. Some geometrical parameters are summarized in Table 4.2. Although some of the geometrical information of the screw sections can be obtained from the manufacturer's data sheet, there exist different data that is not usually available (i.e geometrical details of the mixing blocks, flight angles of the screws,etc). Therefore, the computed screw pitch has been simplified to an equivalent value equal to the mean value of the different type of screw sections used on the experiments as it follows:

$$\xi = \frac{\sum_{i=1}^{m} x_i \xi_i}{\sum_{i=1}^{m} x_i} \tag{4.4}$$

with, m the number of screw elements, x_i and ξ_i the length and the pitch of the element i respectively.

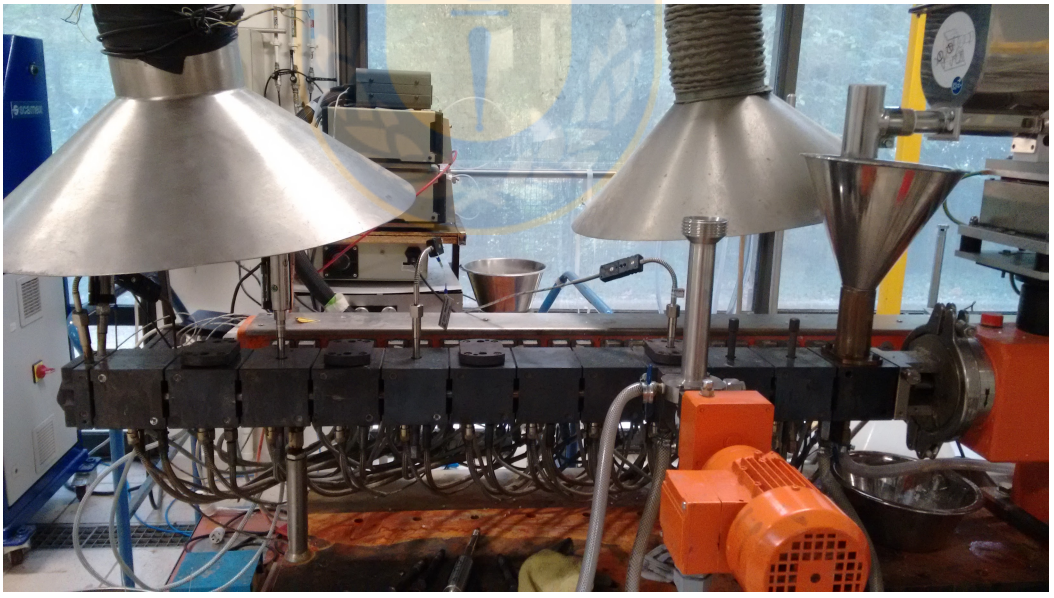

FIGURE 4.1: Twin-screw extruder used in this study. (Courtesy of Ingénierie des Matériaux Polymères/IMP Lyon).

In addition Table 4.3 provides some input values used in both the experimental tests as in the open-loop simulations.

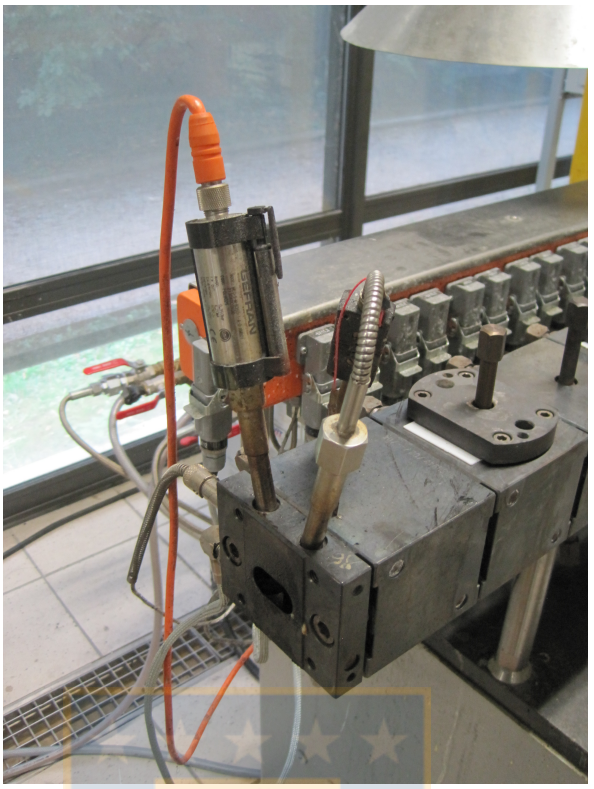

FIGURE 4.2: Melt temperature and pressure sensing at the die. Courtesy of Ingénierie des Matériaux Polymères/IMP Lyon.

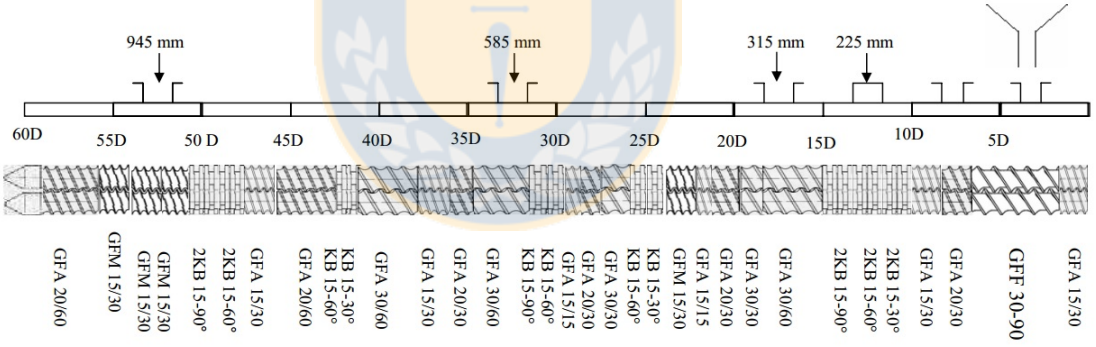

FIGURE 4.3: Screw profiles used in the study. (Courtesy of Ingénierie des Matériaux Polymères/IMP Lyon).

4.3 Steady state of the twin-screw extrusion model

As it was discussed in Section 3.3.2 the solution of the steady state model of the twin-screw extrusion process requires an iterative method because of the nonlinearity of the bi-zone model. A steady state expression of the filling ratio can be obtained from equation (2.10) and the boundary conditions (2.51) :

$$f_p^* = \frac{F_{in}^*}{\rho_0 N^* V_{eff}}, \tag{4.5}$$

Thermal conductivity	$\alpha = 800[J/m^2sK]$
Screw diameter	$D_s = L/60 = 0.0175[m]$
External diameter	$D = 0.0118[m]$
Screw pitch	$\xi = 0.023 \times 10^-4[m]$
Effective surface	$S_{eff} = \frac{\pi}{4}(D^2 - D_s^2) = 7.6246 \times 10^-6[m^2]$
Effective volume	$V_{eff} = S_{eff}\xi = 1.7537 \times 10^-7[m^3]$
Die radius	$R_d = 0.001[m]$
Die length	$L_d = 0.03[m]$
Die conductance	$K_d = 3.9843 \times 10^{-11}[m^3]$
Pressure flow coefficient	$B = 3.76938 \times 10^{-10}[m^4]$

TABLE 4.2: Some screw parameters used on the simulation process. (Source: Personal collection).

Initial screw speed	$N_0 = 500[rpm]$
Barrel temperature	$T_b = 473[K]$
Input temperature	$T_{in} = 293[K]$
Extruder length	$L = 1.05[m]$
Feed rate	$F_{in} = 5/3600[kg/s]$
Channel depth	$H = D/2 - D_s/2 = 2.5 \times 10^-4[m]$

TABLE 4.3: Some input values used on the simulation process. (Source: Personal collection).

In addition, expressions for temperature can be written from equations (2.16) for *PFZ* and from (2.21) for *FFZ* as follows:

$$\frac{dT_p^*(x)}{dx} = \frac{\mu\eta(T_p^*(x))N^*}{f_p^*\rho_0 V_{eff} C_p \xi} + \frac{S_{exc}\alpha}{\rho_0 V_{eff} C_p \xi N^*}(T_b^* - T_p^*(x)) \quad x \in [0, l^*[\,, \tag{4.6}$$

$$\frac{dT_f^*(x)}{dx} = \frac{\mu\eta(T_f^*(x))N^{*2}}{\xi F_d^* C_p} + \frac{S_{exc}\alpha}{\xi F_d^* C_p}(T_b^* - T_f^*(x)) \quad x \in]l^*, L] \tag{4.7}$$

where $F_d^* = F_{in}^*$. On the other hand, the equilibrium for the flow at the die should also satisfy the equation of pressure continuity at the interface; i.e. equation (2.46),

$$F_{in}^* = \frac{K_d \rho_0 V_{eff} N^* \int_{l^*}^{L} \eta(T_f^*(x))dx}{B\rho_0 \eta_d^* + K_d \int_{l^*}^{L} \eta(T_f^*(x)))dx}. \tag{4.8}$$

It is important to note that first-order ordinary differential equations (4.6) and (4.7) are coupled through F_{in} and η with l^* as the equilibrium of the interface position. Therefore finding an analytical solution is not possible. Moreover, for a given N^* and F_{in}^*, it is possible to find an l^* so that equations (4.6), (4.7) and (4.8) are satisfied. In order to compute the steady state values of the interface position the following optimization

problem can be formulated :

$$\begin{aligned} &\min_{l} I(l) \\ &\text{subject to} \\ &\text{(4.6), (4.7) and (4.8).} \end{aligned} \tag{4.9}$$

where $I(l) = \left(\frac{F_d^* - F_{in}^*}{F_{in}^*}\right)^2$ is defined as the quadratic error function. The cost function has been chosen taking into account that, on steady state the following equality is given: $F_d^* = F_{in}^*$.

The quadratic error $I(l)$ is plotted for different screw speeds in Fig. 4.4. Note that, this function is unimodal, hence the optimization problem has only one optimal solution. Efficient unidimensional search algorithms can be applied to obtain the solution with a desired tolerance. This approach for computing the steady state does not require the use of back iterations as proposed by [23]. The equilibrium points were computed using a

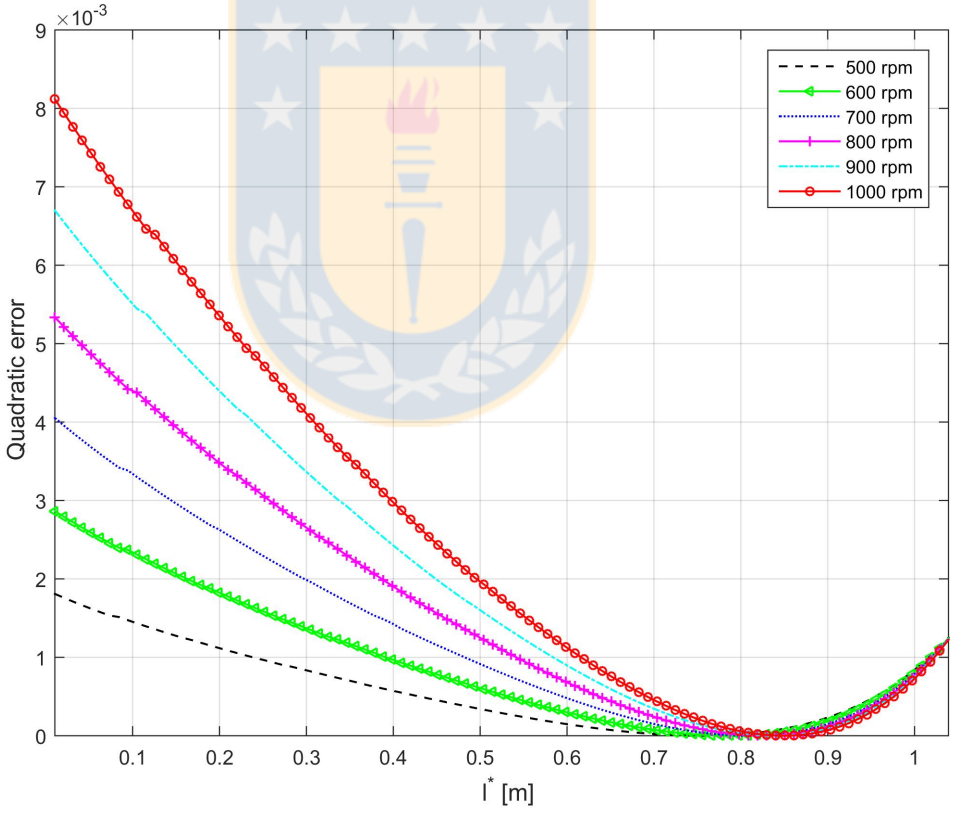

FIGURE 4.4: Quadratic error versus interface position for different screw speed. (Source: Personal collection).

golden search algorithm for different screw speed values, from 500 rpm to 1150 rpm and a constant input flow of 5 kgh. The results are summarized in Fig. 4.5. For instance, at 500 rpm the equilibrium of the interface is about $l^* = 0.751$ m. Meanwhile at a higher

screw speed, i.e. 1150 rpm, the interface moves to $l^* = 0.859$ m.

On the other hand, Fig. 4.6 shows the steady state melt temperature distribution on

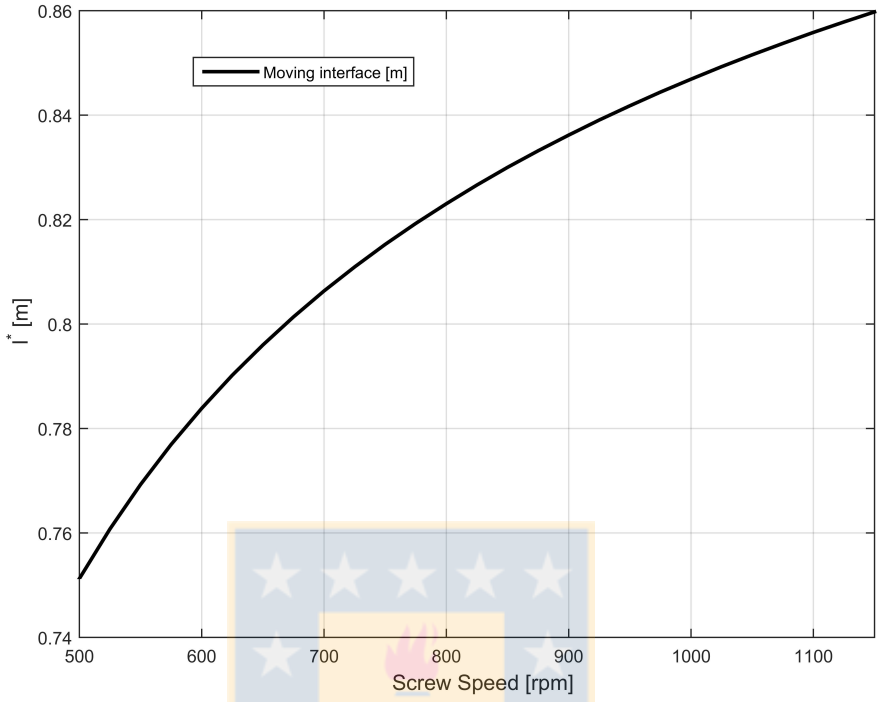

FIGURE 4.5: Interface position as a function of the screw speed. (Source: Personal collection).

the extruder for different screw speed values. For each curve, the equilibrium interface is located at the inflexion point marked into a circle dot. For example, at 500 rpm the position of the interface is $l^* = 0.751$ m with a temperature of $T(l^*) = 468$ K. In addition, it is worth to point out that closer to the die, i.e. $x = 1.05$ m, the steady state temperature is higher when the screw speed increases. This behavior is explained in detail together with the experimental results in Section 4.5.

4.4 Conservativeness and the finite volume method

Finite volume methods are well know for being locally conservative because they are based on a "balance" approach: a local balance is written on each discretization cell or control volume; hence, an integral formulation of the fluxes over the boundary of the control volume is then obtained by the divergence formula [44]. In order to show the conservativeness of the discretized model a small simulation test for constant screw speed of 500 rpm and variable input flow was made using the parameters for the extrusion

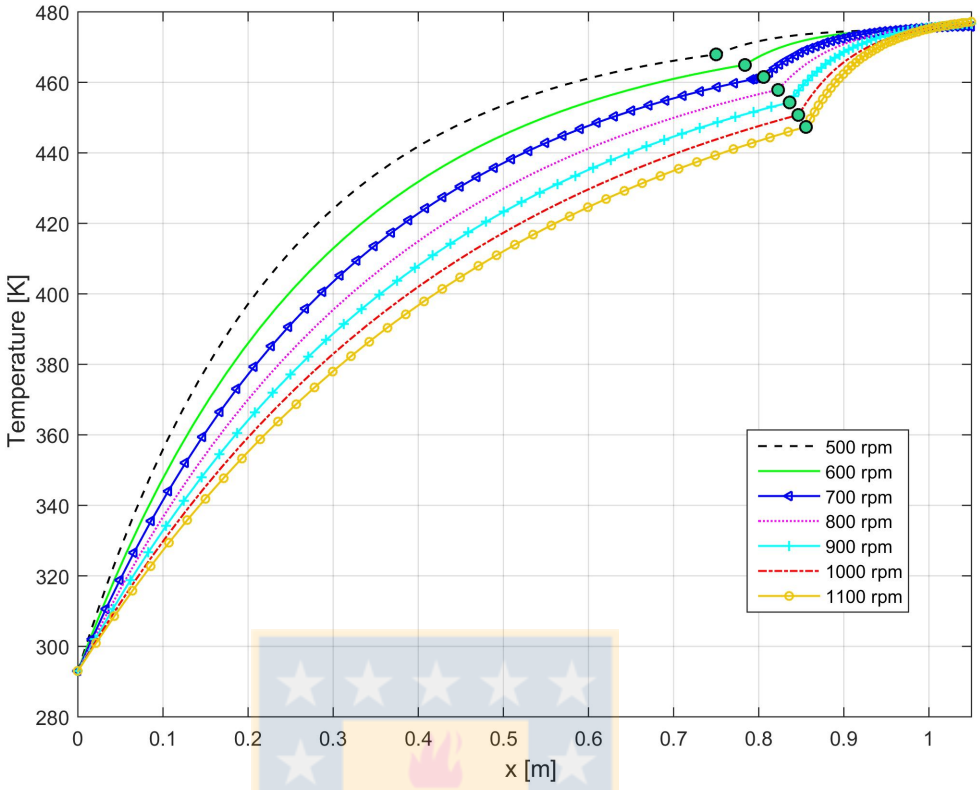

FIGURE 4.6: Melt temperature distribution for different screw speed values. (Source: Personal collection).

model that are shown in Section 4.2 using the following operational conditions:

$$F_{in}(t) = \begin{cases} 5/3600 \text{ kg/s } 0 < t \leq 50 \text{ s} \\ 8/3600 \text{ kg/s } 50 < t \leq 100 \text{ s} \\ 5/3600 \text{ kg/s } 100 < t \leq 150 \text{ s} \end{cases} \tag{4.10}$$

The total input mass $M_0 = \sum_{t=0}^{t} F_{in}(t) = 0.2486$ is calculated and compared against the total output mass $M_d = \sum_{t=0}^{t=} F_d(t) = 0.2490$. The results obtained, are almost identical and the difference $(3.6249 \times 10^{-}4)$ lies on the fact that the computed output mass depends on the estimated parameters of the model. Therefore, it is possible to say that the discretized model for the extrusion process is conservative.

4.5 Dynamic simulation and experimental Results

In order to illustrate the behavior of the proposed model, experimental data was obtained and compared against simulation tests with variable screw speed $N(t)$ and constant feed

rate F_{in} within the following operational conditions:

$$N(t) = \begin{cases} 500 \text{ rpm } 0 < t \leq 300 \text{ s} \\ 1150 \text{ rpm } 300 < t \leq 600 \text{ s} \\ 800 \text{ rpm } 600 < t \leq 900 \text{ s} \end{cases} \tag{4.11}$$

Time integration is performed with $Ode113$ routine of $Matlab^{®}$. A spatial discretization N_d of 100 elements and a simulation time of 900 s were used with a sampling time of 1 s. However, the sampling time of the experimental data was 6 s due to some hardware limitations of the extruder monitoring system. Unfortunately, this monitoring system only provides filtered values of the measured temperatures. Summarizing the initial conditions defined for the filling ratio, the interface position and the input flow along the extruder are $f_p^0 = 0.28877$, $l^0 = 0.751$ m and $F_{in} = 5/3600$ kg/s.

Fig. 4.7 shows the evolution of the interface position compared to the screw speed. It is worth to point out that the interface position changes with every change on the screw speed. For instance, at 300 s, the interface moves from its initial position $l^0 = 0.751$ m to another equilibrium point at $l = 0.859$ m. On the other hand, increasing the screw speed with constant feed rate means that the amount of matter accumulated into the extruder is lower because the polymer is transported through the machine in less time. Moreover, it is clear from the simulated data, that the dynamic of the interface position is directly proportional to the screw speed.

Fig. 4.8 shows the superposition of the experimental data (dotted line) and simulated data (continuous line) of the pressure and temperature at the die. Note that, according to the changes on the screw speed, there exists some transient phenomena on the pressure (Fig. 4.8b). Those peaks observed are related to a transient rise on the pressure at the die due to the variation on the screw speed [20]. However, during the initial 300 s of operation the measured pressure is higher than the predicted values from the simulations. This, could be related to the simplifications made on the geometry of the screw sections. From equation (2.18) it is clear that the pressure highly depends on the interface position and this variable is strictly related to the geometry of the extruder.

The die melt temperature dynamics is also shown in Fig 4.8c. Note that the simulated model gives a reasonable estimate of the temperature. If the screw speed is high the melt temperature increases, otherwise it decreases. This influence of the screw speed on the melt temperature is due to the fact that the shear heating provided by the screw rotation becomes the main heating source when the screw speed is high[45]. On the other hand, if the screw speed is slow, most of the energy transferred to the melt comes from the heating system in the barrel. In the experiments the melt temperature was measured using a fixed thermocouple directly at the die. Although this method is simple to adapt to most industrial extruders, in some cases, for instance at high screw speed,

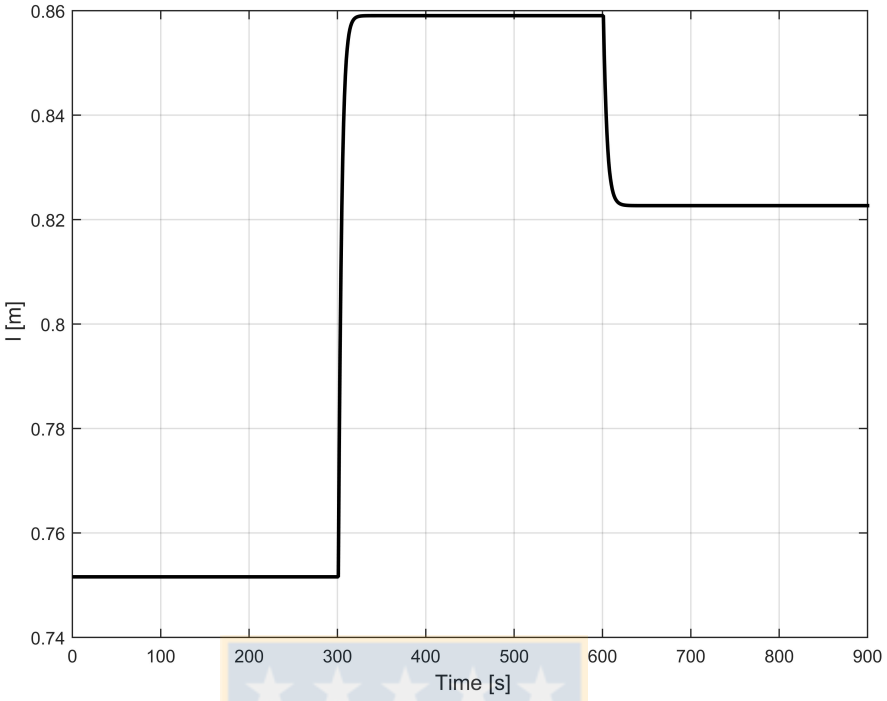

FIGURE 4.7: Simulated interface position dynamics with screw speed as control input. (Source: Personal collection).

measurements are not entirely precise because the melt cannot be in contact with the thermocouple at all times [46]. This behaviour could be the main reason of the sudden increase or decrease of the measured temperature from 300 to 900 s. Therefore, further research on the adaptation of a different sensing technique for the temperature at the die could be done.

Moreover, there is a qualitative agreement between the simulated data and the experimental results. The main difference lies on the fact that some geometrical parameters of the screws should be accurately identified. The geometry of the screws and the die in twin screw extruders is highly complex. For instance, the screw pitch ξ is not uniform along the extruder which means that further research on the identification of the equivalent geometry of the extrusion process should be implemented.In addition, it is important to consider as a future work the use of identification techniques to estimate some of the parameters based on experimental data in order to have a good quantitative agreement between the simulated and real behavior.

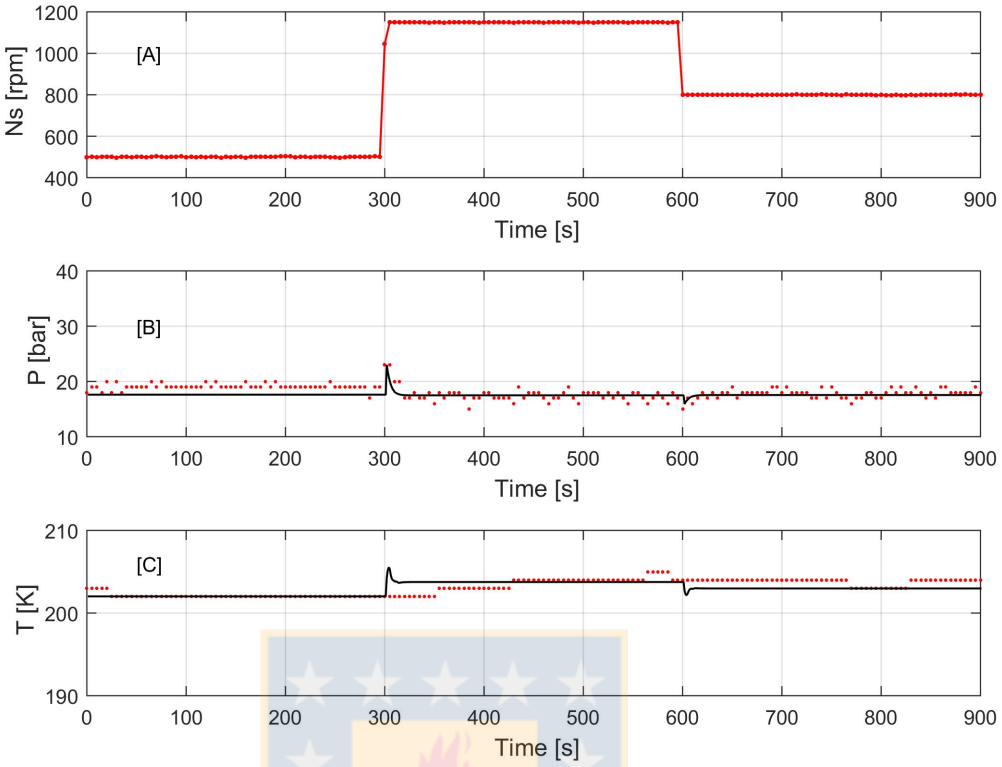

FIGURE 4.8: Experimental test results:(a) Screw speed (b) Die pressure (c) Die melt temperature. The dotted line and continuous line represents experimental values and simulated values respectively. (Source: Personal collection).

4.6 Summary

In this chapter, the bi-zone model adapted to an industrial twin-screw extruder is presented. Simulation and experimental tests performed for the extrusion of Polypropylene *(PP)* are analyzed. The results shows that there is a right qualitative agreement between the experimental and simulation results. Future work considers the development of a systematic approach for the identification of the equivalent geometry and a viscosity model of the extrusion process. Improving the instrumentation of the extruder in order to obtain raw temperature measurements will be considered. Also, the addition of more pressure sensors in the extruder will be taken into account in order to give a rough estimation of the moving interface position. Experiments using different operational conditions, such as the addition of a tracer on the process for resident time distribution tests could be considered. The next chapter will be devoted to the development of control strategies for the extrusion process. In this case an energy based controller is proposed with screw speed as the control input and temperature as control objective.

Chapter 5

Energy-based approach to modelling and control

5.1 Introduction

The task of controlling the extrusion process is complex due to strong interactions that exist between a large number of factors such as material properties (rheology, thermal conductivity, etc), geometrical factors (screw design, screw wear, etc) and operating conditions (screw speed, barrel temperature, flow rate, etc). There also exists several modelling challenges such as moving interfaces and complex screw geometries.
It is because of these reasons that the design of efficient controllers still remains a hard task at the industrial level [30]. Most of the proposed control oriented models of extruders available in literature are related with some black box linear model identification around some operating conditions in which different classical methods were applied such as Predictive Control [17], [2], [18],[47], [48] and Linearized Multivariable Control [20], [49], [31]. Also, modern control methodologies such as fuzzy logic can also be found in literature. For instance, Abeykoon [50] proposed a novel model-based control approach to control the polymer extrusion process incorporating a melt temperature profile prediction soft sensor and fuzzy logic. On the other hand, it is worth to point out the works by Diagne [30], who presented a feedback stabilization of a food extrusion process described by 1D PDE's defined on coupled time-varying spatial domains. The extrusion process model used in [30] is similar to the one presented in this work, despite the assumptions of constant viscosity and the use of a controller for the barrel temperature in order to limit the action of some source terms in the energy balance during the stabilization of the melt temperature. However, this last assumption cannot be used for industrial applications since the barrel temperature is usually kept as fixed depending

on the processing conditions in order to avoid problems related to the product quality. Although these control methodologies are very useful, they do not take into account entirely the behaviour of the real system due to the limitations on linearization and stability issues in the case of predictive control [51]. It is because of these reasons that this topic has been under constant interest in the last years [6], [52], [45].

In this chapter we address the problem of the stabilization of the moving interface, the filling ratio and the melt temperature to desired set-points in the extrusion process bi-zone model. An energy-based controller is derived using internal energy as a storage function and controlled variable with the screw speed as control input.

The stabilization problems for hyperbolic systems, similar to the bi-zone model presented in this work, have been widely studied in literature. A first approach,related to the analysis of the classical solutions along the characteristics was presented by Greenberg and Li [53] who worked in the case of second-order systems of conservations laws. In addition, Li [54] also presented a similar approach, but in the case more general situations on nth order systems. Another approach based on Lyapunov techniques was introduced by Coron et al. [55], [56] were a strict Lyapunov function in terms of Riemann invariants was constructed and its time derivative can be made negative by choosing properly the boundary conditions. In addition, it is worth to point out the developments presented by Johansen and Storaa [57] in which a energy-based control of the outlet temperature of a distributed solar collector field is studied. In this work, an energy-based controller is derived using internal energy as a storage function and controlled variable were a quadratic Lyapunov function is formulated or the distributed parameter model.

This chapter is organized as follows: In section 5.2 the entropy balance of the extrusion process is presented by using the Gibb's equation and assuming a local thermodynamic equilibrium in the extruder. This entropy balance can be used in future works as the basis of control design based on the balance equation of an availability function which is derived from the entropy balance equation. For instance, [58], [59] studied the use of the entropy balance as a candidate function for a passivity based approach formulation of the process. Further applications on process systems have been proposed showing the utility of those methodologies [60], [61], [62].

On the other hand, in Section 5.3 we address the problem of the stabilization of the moving interface, the filling ratio and the melt temperature to desired set-points in the extrusion process bi-zone model. First, the total energy balance of the extrusion process is presented in order to suggest a model-base control of the melt temperature for the bi-zone model. An energy-based controller is derived using internal energy as a storage function and controlled variable with the screw speed as control input. The stability of the controller is proved through the use of Lyapunov stability theorem. Finally, the practical usefulness of the method is illustrated by some closed-loop simulations of the experimentally verified model of the extrusion process.

5.2 Entropy Balance of the extrusion process

5.2.1 Partially Filled Zone

5.2.1.1 Internal Energy Balance of the *PFZ*

The first law of thermodynamics states that the variation of the energy per unit of time for a closed system is equal to the power of the external forces plus the external heat exchanged between the system and its environment. Defining $u(x,t)$ as the internal energy per unit of volume and $h(x,t)$ as the enthalpy, we obtain the following relation:

$$u(x,t) = h(x,t) - P(x,t), \tag{5.1}$$

where, $P(x,t)$ is the extruder pressure. The variation of internal energy $u(x,t)$ per unit of volume depends on the enthalpy inflow and outflow $F(x,t)$ and the viscous dissipation $Q_c(x,t)$ and convective heat from the barrel to the mass ϕ_e as source terms. Then, an expression of the energy balance at the *PFZ* with transport velocity $\xi N(t)$ is given by the following relation:

$$\begin{aligned}\rho_0 S_{eff}\frac{\partial u_p(x,t) f_p(x,t)}{\partial t} = &-\rho_0 S_{eff}\xi N(t)\frac{\partial u_p(x,t) f_p(x,t)}{\partial x} \\ &+(Q_c^p(x,t) + \phi_e^p(x,t))S_{eff} f_p(x,t),\end{aligned} \tag{5.2}$$

with,

$$\begin{aligned}Q_c^p(x,t) &= \frac{\mu\eta(T_p(x,t))N^2(t)}{f_p(x,t)V_{eff}}, \\ \phi_e^p(x,t) &= \frac{S_{exc}\alpha(T_b(x,t) - T_p(x,t))}{V_{eff}},\end{aligned} \tag{5.3}$$

then,

$$\begin{aligned}\rho_0 S_{eff} f_p(x,t)\frac{\partial u_p(x,t)}{\partial t} + \rho_0 S_{eff} u_p(x,t)\frac{\partial f_p(x,t)}{\partial t} = &-\rho_0 S_{eff}\xi N(t) f_p(x,t)\frac{\partial u_p(x,t)}{\partial x} \\ -\rho_0 S_{eff}\xi N(t) u_p(x,t)\frac{\partial f_p(x,t)}{\partial x} &+ (Q_c^p(x,t) + \phi_e^p(x,t))S_{eff} f_p(x,t).\end{aligned} \tag{5.4}$$

Recalling the mass balance at the partially filled zone:

$$\frac{\partial f_p(x,t)}{\partial t} = -\xi N(t)\frac{\partial f_p(x,t)}{\partial x}, \tag{5.5}$$

then, replacing in equation (5.4):

$$\begin{aligned}\rho_0 S_{eff} f_p(x,t)\frac{\partial u_p(x,t)}{\partial t} &= -\rho_0 S_{eff}\xi N(t) f_p(x,t)\frac{\partial u_p(x,t)}{\partial x} \\ &+(Q_c^p(x,t)+\phi_e^p(x,t))S_{eff} f_p(x,t),\end{aligned} \tag{5.6}$$

simplifying,

$$\frac{\partial u_p(x,t)}{\partial t} = -\xi N(t)\frac{\partial u_p(x,t)}{\partial x} + \frac{Q_c^p(x,t)}{\rho_0} + \frac{\phi_e^p(x,t)}{\rho_0} \tag{5.7}$$

5.2.1.2 Entropy Balance at the *PFZ*

Assuming a local thermodynamic equilibrium it is possible to write Gibbs' Relation as it follows:

$$dU = TdS - PdV + \sum_{i=1}^{n}\mu_i dM_{mi} \tag{5.8}$$

where M_{mi} is the molar mass of each material on the extruder and μ_i is the chemical potential of each material.
Then, assuming the following quantities per volume unit at the *PFZ*:

$$\begin{aligned}u_p(x,t) = \frac{U_p(x,t)}{V_{eff}}, s_p(x,t) = \frac{S_p(x,t)}{V_{eff}}, c_{ip}(x,t) = \frac{M_{mip}(x,t)}{V_{eff}}, \\ v_p(x,t) = \frac{V_0(x,t)}{V_{eff}} = f_p(x,t),\end{aligned} \tag{5.9}$$

then,

$$du_p(x,t)V_{eff} = T_p(x,t)ds_p(x,t)V_{eff} - P(x,t)dv_p(x,t)V_{eff} + \sum_{i=1}^{n}\mu_i(x,t)dc_{ip}(x,t)V_{eff}, \tag{5.10}$$

distributing terms,

$$\begin{aligned}V_{eff}du_p(x,t) + u_p(x,t)dV_{eff} &= T_p(x,t)V_{eff}ds_p(x,t) + T_p(x,t)s_p(x,t)dV_{eff} \\ -P(x,t)V_{eff}dv_p(x,t) - P(x,t)v_p(x,t)dV_{eff} &+ \sum_{i=1}^{n}\mu_i(x,t)c_{ip}(x,t)dV_{eff} \\ &+ \sum_{i=1}^{n}\mu_i(x,t)V_{eff}dc_{ip}(x,t),\end{aligned} \tag{5.11}$$

then,

$$\begin{aligned} V_{eff}du_p(x,t) = V_{eff}\left(T_p(x,t)ds_p(x,t) - P(x,t)dv_p + \sum_{i=1}^{n}\mu_i(x,t)dc_{ip}(x,t)\right) \\ +dV_{eff}\left(T_p(x,t)s_p(x,t) - P(x,t)v_p(x,t) + \sum_{i=1}^{n}\mu_i c_{ip}(x,t) - u_p(x,t)\right), \end{aligned} \tag{5.12}$$

simplifying in order to obtain,

$$du_p(x,t) = T_p(x,t)ds_p(x,t) - P(x,t)dv_p(x,t) + \sum_{i=1}^{n}\mu_i(x,t)dc_{ip}(x,t). \tag{5.13}$$

Remark 5.1. The derivative that represents the variation of a scalar Eulerian field, such as a velocity component, chemical concentration or temperature following a fluid particle is called the *substantial* or *material derivative* [63]. That means, is a derivative taken along a path moving with a given velocity and it is made from a *temporal term* and a *convective term* as it follows:

$$\frac{D\bullet}{Dt} = \frac{\partial\bullet}{\partial t} + \xi N(t)\frac{\partial\bullet}{\partial x}. \tag{5.14}$$

The last term represents the transport of a property in the fluid due to its macroscopic motion.

Now, the equation (5.13) can be written in the form of the material derivatives as follows,

$$\frac{Du_p(x,t)}{Dt} = T_p(x,t)\frac{Ds_p(x,t)}{Dt} - P(x,t)\frac{Dv_p(x,t)}{Dt} + \sum_{i=1}^{n}\mu_i(x,t)\frac{Dc_{ip}(x,t)}{Dt}, \tag{5.15}$$

then,

$$\begin{aligned} \frac{\partial u_p(x,t)}{\partial t} + \xi N(t)\frac{\partial u_p(x,t)}{\partial x} = T_p(x,t)\frac{\partial s_p(x,t)}{\partial t} + \xi N(t)T_p(x,t)\frac{\partial s_p(x,t)}{\partial x} \\ -P(x,t)\frac{\partial v_p(x,t)}{\partial t} - P(x,t)\xi N(t)\frac{\partial v_p(x,t)}{\partial x} + \sum_{i=1}^{n}\mu_i(x,t)\frac{\partial c_{ip}(x,t)}{\partial t} \\ + \sum_{i=1}^{n}\xi N(t)\mu_i(x,t)\frac{\partial c_{ip}(x,t)}{\partial x}, \end{aligned} \tag{5.16}$$

taking into account that $v_p(x,t) = f_p(x,t)$:

$$\begin{aligned}\frac{\partial u_p(x,t)}{\partial t} + \xi N(t)\frac{\partial u_p(x,t)}{\partial x} = T_p(x,t)\frac{\partial s_p(x,t)}{\partial t} + \xi N(t)T_p(x,t)\frac{\partial s_p(x,t)}{\partial x} \\ -P(x,t)\frac{\partial f_p(x,t)}{\partial t} - P(x,t)\xi N(t)\frac{\partial f_p(x,t)}{\partial x} + \sum_{i=1}^{n}\mu_i(x,t)\frac{\partial c_{ip}(x,t)}{\partial t} \\ + \sum_{i=1}^{n}\xi N(t)\mu_i(x,t)\frac{\partial c_{ip}(x,t)}{\partial x},\end{aligned} \tag{5.17}$$

simplifying in order to have,

$$\begin{aligned}\frac{\partial u_p(x,t)}{\partial t} + \xi N(t)\frac{\partial u_p(x,t)}{\partial x} = T_p(x,t)\frac{\partial s_p(x,t)}{\partial t} + \xi N(t)T_p(x,t)\frac{\partial s_p(x,t)}{\partial x} \\ + \sum_{i=1}^{n}\left[\mu_i(x,t)\frac{\partial c_{ip}(x,t)}{\partial t} + \xi N(t)\mu_i(x,t)\frac{\partial c_{ip}(x,t)}{\partial x}\right].\end{aligned} \tag{5.18}$$

Taking into account the concentration balance at the *PFZ*:

$$\frac{\partial c_{ip}(x,t)}{\partial t} = -\xi N(t)\frac{\partial c_{ip}(x,t)}{\partial x}. \tag{5.19}$$

Rearranging terms in order to obtain the entropy balance,

$$T_p(x,t)\frac{\partial s_p(x,t)}{\partial t} = -\xi N(t)T_p(x,t)\frac{\partial s_p(x,t)}{\partial x} + \frac{\partial u_p(x,t)}{\partial t} + \xi N(t)\frac{\partial u_p(x,t)}{\partial x}, \tag{5.20}$$

taking into account the local energy balance from equation (5.7) and replacing it into equation (5.20),

$$\begin{aligned}T_p(x,t)\frac{\partial s_p(x,t)}{\partial t} = -\xi N(t)T_p(x,t)\frac{\partial s_p(x,t)}{\partial x} - \xi N(t)\frac{\partial u_p(x,t)}{\partial x} + \frac{Q_c^p(x,t)}{\rho_0} \\ + \frac{\phi_e^p(x,t)}{\rho_0} + \xi N(t)\frac{\partial u_p(x,t)}{\partial x},\end{aligned} \tag{5.21}$$

simplifying,

$$\frac{\partial s_p(x,t)}{\partial t} = -\xi N(t)\frac{\partial s_p(x,t)}{\partial x} + \frac{1}{T_p(x,t)\rho_0}(Q_c^p(x,t) + \phi_e^p(x,t)). \tag{5.22}$$

Now, adding and subtracting a new source term related to the entropy flux outside of the melt, i.e $\phi_e^p(x,t)/T_b(x,t)\rho_0$, in order to obtain the entropy balance at the *PFZ*,

$$\frac{\partial s_p(x,t)}{\partial t} = -\xi N(t)\frac{\partial s_p(x,t)}{\partial x} + \frac{\phi_e^p(x,t)}{T_b(x,t)\rho_0} + \sigma_p(x,t), \tag{5.23}$$

where,

$$\sigma_p(x,t) = \frac{1}{T_p(x,t)\rho_0}(Q_c^p(x,t) + \phi_e^p(x,t)) - \frac{\phi_e^p(x,t)}{T_b(x,t)\rho_0}, \tag{5.24}$$

Recalling the definition of $Q_c^p(x,t)$ and $\phi_e^p(x,t)$ from equation (5.3) it is possible to note that $Q_c^p(x,t) > 0$. In addition, the terms $\frac{\phi_e^p(x,t)}{T_p(x,t)\rho_0}$ and $-\frac{\phi_e^p(x,t)}{T_b(x,t)\rho_0}$ are always positive or zero. Then, analyzing equation (5.24) it is possible to conclude that the source term $\sigma_p(x,t)$ is always positive or zero. It worth to point out that, $\sigma_p(x,t)$ is usually referred to as entropy-production rate of the process. From the second law of the thermodynamics, we know that in irreversible processes entropy is not conserved, so we actually expect that $\sigma_p(x,t) \geq 0$ [64].

5.2.2 Fully Filled Zone

5.2.2.1 Internal Energy Balance of the *FFZ*

Recall, that in the *FFZ*, the thermal phenomena are identical to those which occur in the *FFZ*. However, the heat transport velocity is given by equation (5.25).

$$v(t) = \frac{1}{S_{eff}} \frac{F_d(t)}{\rho_0} = \frac{\xi F_d(t)}{\rho_0 V_{eff}}. \tag{5.25}$$

Viscous dissipation and heat exchange have to be considered as source terms. The viscous heat generation is much important in this zone due to the mixing effect. The local energy balance can be made in a similar way than for the *PFZ*,

$$\rho_0 S_{eff} \frac{\partial u_f(x,t) f_f(x,t)}{\partial_t} = -F_d(t) \frac{\partial u_f(x,t) f_p(x,t)}{\partial x} + (Q_c^f(x,t) + \phi_e^f(x,t)) S_{eff} f_f(x,t). \tag{5.26}$$

with,

$$\begin{aligned} Q_c^f(x,t) &= \frac{\mu \eta(T_f(x,t)) N^2(t)}{f_f(x,t) V_{eff}}, \\ \phi_e^f(x,t) &= \frac{S_{exc} \alpha (T_b(x,t) - T_f(x,t))}{V_{eff}}, \end{aligned} \tag{5.27}$$

Taking into account that, in the *FFZ*, f_f is equal to one and using the internal energy relation from equation (5.1):

$$\rho_0 S_{eff} \frac{\partial u_f(x,t)}{\partial t} = -F_d(t) \frac{\partial u_f(x,t)}{\partial x} + (Q_c^f(x,t) + \phi_e^f(x,t) S_{eff}, \tag{5.28}$$

distributing terms,

$$\frac{\partial u_f(x,t)}{\partial t} = -\frac{F_d(t)\xi}{\rho_0 V_{eff}} \frac{\partial u_f(x,t)}{\partial x} + \frac{1}{\rho_0}(Q_c^f(x,t) + \phi_e^f(x,t)), \tag{5.29}$$

5.2.2.2 Entropy Balance at the *FFZ*

Recalling the Gibbs' Relation with variable pressure as it follows:

$$dU = TdS - PdV + \sum_{i=1}^{n} \mu_i dM_{mi} \tag{5.30}$$

Then, assuming the following quantities per volume unit:

$$u_f(x,t) = \frac{U_f(x,t)}{V_{eff}}, s_f(x,t) = \frac{S_f(x,t)}{V_{eff}}, c_{if}(x,t) = \frac{M_{mi}(x,t)}{V_{eff}}, v_f(x,t) = \frac{V_0(x,t)}{V_{eff}} = 1, \tag{5.31}$$

then,

$$du_f(x,t)V_{eff} = T(x,t)ds_f(x,t)V_{eff} - P(x,t)dv_f(x,t)V_{eff} + \sum_{i=1}^{n} \mu_i(x,t)dc_{if}(x,t)V_{eff}, \tag{5.32}$$

distributing terms,

$$\begin{aligned} V_{eff}du_f(x,t) + u_f(x,t)dV_{eff} &= T_f(x,t)V_{eff}ds_f(x,t) + T_f(x,t)s_f(x,t)dV_{eff} \\ -P(x,t)V_{eff}dv_f(x,t) &+ \sum_{i=1}^{n} \left[\mu_i(x,t)c_{if}(x,t)dV_{eff} + \mu_i(x,t)V_{eff}dc_{if}(x,t)\right], \end{aligned} \tag{5.33}$$

then,

$$\begin{aligned} V_{eff}du_f(x,t) = &\left(T_f(x,t)ds_f(x,t) - P(x,t)dv_f(x,t) + \sum_{i=1}^{n} \mu_i(x,t)dc_{if}(x,t)\right)V_{eff} \\ &+ \left(T_f(x,t)s_f(x,t) - P(x,t)v_f(x,t) + \sum_{i=1}^{n} \mu_i(x,t)c_{if}(x,t) - u_f(x,t)\right)dV_{eff} \end{aligned} \tag{5.34}$$

simplifying,

$$du_f(x,t) = T_f(x,t)ds_f(x,t) - P(x,t)dv_f(x,t) + \sum_{i=1}^{n} \mu_i(x,t)dc_{if}(x,t), \tag{5.35}$$

and, finally taking into account that $v_f(x,t) = \frac{V_f(x,t)}{V_{eff}} = 1$,

$$du_f(x,t) = T_f(x,t)ds_f(x,t) + \sum_{i=1}^{n} \mu_i(x,t)dc_{if}(x,t). \tag{5.36}$$

Now, equation (5.36) can be written in the form of the material derivatives as it follows,

$$\frac{Du_f(x,t)}{Dt} = T_f(x,t)\frac{Ds_f(x,t)}{Dt} + \sum_{i=1}^{n}\mu_i(x,t)\frac{Dc_{if}(x,t)}{Dt} \tag{5.37}$$

where, $\frac{D\bullet}{Dt} = \frac{\partial\bullet}{\partial t} + \frac{F_d(t)\xi}{\rho_0 V_{eff}}\frac{\partial\bullet}{\partial x}$, then:

$$\begin{aligned}\frac{\partial u_f(x,t)}{\partial t} + \frac{F_d(t)\xi}{\rho_0 V_{eff}}\frac{\partial u_f(x,t)}{\partial x} &= T_f(x,t)\frac{\partial s_f(x,t)}{\partial t} + T_f(x,t)\frac{F_d(t)\xi}{\rho_0 V_{eff}}\frac{\partial s_f(x,t)}{\partial x} \\ &+ \sum_{i=1}^{n}\mu_i(x,t)\frac{\partial c_{if}(x,t)}{\partial t} + \sum_{i=1}^{n}\mu_i(x,t)\frac{F_d(t)\xi}{\rho_0 V_{eff}}\frac{\partial c_{if}(x,t)}{\partial x}.\end{aligned} \tag{5.38}$$

Recalling the local energy balance from equation (5.29) and replacing it into equation (5.38):

$$\begin{aligned}\frac{\partial s_f(x,t)}{\partial t} &= -\frac{F_d(t)\xi}{\rho_0 V_{eff}}\frac{\partial s_f(x,t)}{\partial x} + \frac{1}{T_f(x,t)}\left(\frac{Q_c^f(x,t)+\phi_e^f(x,t)}{\rho_0}\right) \\ &-\frac{1}{T_f(x,t)}\sum_{i=1}^{n}\left(\mu_i(x,t)\frac{\partial c_{if}(x,t)}{\partial t} + \frac{\mu_i(x,t)F_d(t)\xi}{\rho_0 V_{eff}}\frac{\partial c_{if}(x,t)}{\partial x}\right),\end{aligned} \tag{5.39}$$

Recalling the concentration balance at the *FFZ*:

$$\frac{\partial c_{if}(x,t)}{\partial t} = -\frac{\xi F_d(t)}{\rho_0 V_{eff}}\frac{\partial c_{if}(x,t)}{\partial x}, \tag{5.40}$$

then,

$$\frac{\partial s_f(x,t)}{\partial t} = -\frac{F_d(t)\xi}{\rho_0 V_{eff}}\frac{\partial s_f(x,t)}{\partial x} + \frac{1}{T_f(x,t)}\left(\frac{Q_c^f(x,t)+\phi_e^f(x,t)}{\rho_0}\right), \tag{5.41}$$

Now, adding and subtracting a new source term related to the entropy flux outside of the melt, i.e $\phi_e^f(x,t)/(T_b(x,t)\rho_0)$, in order to obtain the entropy balance at the fully filled zone.

$$\frac{\partial s_f(x,t)}{\partial t} = -\frac{F_d(t)\xi}{\rho_0 V_{eff}}\frac{\partial s_f(x,t)}{\partial x} + \frac{\phi_e^f(x,t)}{T_b(x,t)\rho_0} + \sigma_f(x,t) \tag{5.42}$$

where

$$\sigma_f(x,t) = \frac{1}{T_f(x,t)}\left(\frac{Q_c^f(x,t)+\phi_e^f(x,t)}{\rho_0}\right) - \frac{\phi_e^f(x,t)}{T_b(x,t)\rho_0}. \tag{5.43}$$

Recalling the definition of $Q_c^f(x,t)$ and $\phi_e^p(x,t)$ from equation (5.27) it is possible to note that $Q_c^f(x,t) > 0$. In addition, the terms $\frac{\phi_e^f(x,t)}{T_f(x,t)\rho_0}$ and $-\frac{\phi_e^f(x,t)}{T_b(x,t)\rho_0}$ are always positive or zero. Then, analyzing equation (5.43) it is possible to conclude that the source term $\sigma_f(x,t)$ is always positive or zero. Analogously, as in the case of the *PFZ*, the source term $\sigma_f(x,t)$ referred to as entropy-production rate of the process and according to the

second law of the thermodynamics, we expect that $\sigma_f(x,t) \geq 0$.
As stated in the introduction of this chapter, in this work we suggest a control law based on the balance equation ot the internal energy of the extrusion process. Therefore, the entropy balance of the extrusion process model found in this section could be the basis of control design based on the balance equation of an availability function which is derived from the entropy balance equation and can be applied for future works. Developments on the design of a control law using the entropy balance equation can be found in the works by Hoang [65] and Ruszkowski [66].

5.3 Energy-based control of the extrusion process

In this section, we shall suggest a control law based on the balance equation of the internal energy of the extrusion process. The objective is to control the melt temperature in the extruder to a specific set-point profile. The screw speed $0 \leq N(t) < N_{max}$ is the control input. The upper constraint N_{max} is due to the maximum speed of the extrusion process; this limitation is related to the electric motor capacity, screw design and maximum pressure of the system. The internal energy of the extrusion process is simplified for control purposes by assuming a constant melt viscosity, i.e. η_p and η_f are constants. This assumption is necessary to the control design in order to simplify the control law. Let us recall that assuming a variable viscosity imposes another term with temperature dependency to the balance equation of the internal energy. It is worth to point out that this simplification is made just for designing the controller and the original model is used to simulate the plant. Also, as $N(t)$ is defined as control input, then the input flow F_{in} is assumed as time-invariant. Finally, a simulation test is presented at the end of this section in order to show the capabilities of the controller to follow the set-point temperature.

5.3.1 Total energy balance of the extrusion process

Recalling the energy balance equations of the extrusion process by-zone model with constant viscosity and assuming the filling ratio as invariant only at the viscous dissipation part :
-For the PFZ:

$$\frac{\partial T_p(x,t)}{\partial t} = -\xi N(t)\frac{\partial T_p(x,t)}{\partial x} + \frac{\mu \eta_{pt} N^2(t)}{\rho_0 V_{eff} C_p} + \frac{S_{exc}\alpha}{\rho_0 V_{eff} C_p}(T_b - T_p(x,t)). \tag{5.44}$$

where $\eta_{pt} = \eta_p / f_p^*$ and f_p^* as the equilibrium of the filling ratio.
-For the FFZ:

$$\frac{\partial T_f(x,t)}{\partial t} = -\frac{F_d(t,l(t))\xi}{\rho_0 V_{eff}} \frac{\partial T_f(x,t)}{\partial x} + \frac{\mu \eta_f N^2(t)}{\rho_0 V_{eff} C_p} + \frac{S_{exc}\alpha}{\rho_0 V_{eff} C_p}(T_b - T_f(x,t)). \tag{5.45}$$

Recalling the color function that represents both the *PFZ* and *FFZ* as it follows:

$$k(x,l(t)) = \begin{cases} 1 & \text{if } x \in [0, l(t)[\\ 0 & \text{if } x \in [l(t), L] \end{cases} \text{ and } \overline{k}(x,l(t)) = \begin{cases} 0 & \text{if } x \in [0, l(t)[\\ 1 & \text{if } x \in [l(t), L]. \end{cases} \tag{5.46}$$

Omitting x in k and $\overline{k}$ for simplicity. Then, the temperature and the filling ratio can be expressed as:

$$T(x,t) = k(l(t))T_p(x,t) + \overline{k}(l(t))T_f(x,t). \tag{5.47}$$

$$f(x,t) = k(l(t))f_p(x,t) + \overline{k}(l(t))f_f(x,t). \tag{5.48}$$

Defining the internal energy for the extruder as $U = \int_0^L C_p \rho_0 S_{eff} f(x,t) T(x,t) dx$:

$$\frac{dU(t)}{dt} = \int_0^L C_p \rho_0 S_{eff} \frac{\partial}{\partial t}[f(x,t)T(x,t)]dx, \tag{5.49}$$

Then,

$$\frac{dU(t)}{dt} = \int_0^L C_p \rho_0 S_{eff} \frac{\partial}{\partial t}[k(l(t))f_p(x,t)T_p(x,t) + \overline{k}(l(t))T_f(x,t)]dx, \tag{5.50}$$

distributing,

$$\begin{aligned} \frac{dU(t)}{dt} = C_p \rho_0 S_{eff} \int_0^L & f_p(x,t)T_p(x,t)\frac{\partial k(l(t))}{\partial t} + k(l(t))T_p(x,t)\frac{\partial f_p(x,t)}{\partial t} \\ & + k(l(t))f_p(x,t)\frac{\partial T_p(x,t)}{\partial t} + \overline{k}(l(t))\frac{\partial T_f(x,t)}{\partial t} + T_f(x,t)\frac{\partial \overline{k}(l(t))}{\partial t}dx, \end{aligned} \tag{5.51}$$

From (5.44) and (5.45) it is possible to have:

$$\begin{aligned} \frac{dU(t)}{dt} = C_p \rho_0 S_{eff} \int_0^L & f_p(x,t)T_p(x,t)\frac{\partial k(l(t))}{\partial t} - \xi N(t) k(l(t))T_p(x,t)\frac{\partial f_p(x,t)}{\partial x} \\ & + k(l(t))f_p(x,t)\left[-\xi N(t)\frac{\partial T_p(x,t)}{\partial x} + \Omega(f_p, T_p, N, T_b)\right] \\ & + \overline{k}(l(t))\left[-\frac{F_d(t,l(t))\xi}{\rho_0 V_{eff}}\frac{\partial T_f(x,t)}{\partial x} + \Omega(f_f, T_f, N, T_b)\right] + T_f(x,t)\frac{\partial \overline{k}(l(t))}{\partial t}dx, \end{aligned} \tag{5.52}$$

then,

$$\begin{aligned}\frac{dU(t)}{dt} = C_p\rho_0 S_{eff}\int_0^L f_p(x,t)T_p(x,t)\frac{\partial k(l(t))}{\partial t} - \xi N(t)k(l(t))T_p(x,t)\frac{\partial f_p(x,t)}{\partial x}\\ +k(l(t))f_p(x,t)\Big[-\xi N(t)\frac{\partial T_p(x,t)}{\partial x} + \frac{\mu\eta_{pt}N^2(t)}{\rho_0 V_{eff}C_p} + \frac{S_{exc}\alpha}{\rho_0 V_{eff}C_p}(T_b - T_p(x,t))\Big]\\ +\overline{k}(l(t))\Big[-\frac{F_d(t,l(t))\xi}{\rho_0 V_{eff}}\frac{\partial T_f(x,t)}{\partial x} + \frac{\mu\eta_f N^2(t)}{\rho_0 V_{eff}C_p}\\ +\frac{S_{exc}\alpha}{\rho_0 V_{eff}C_p}(T_b - T_f(x,t))\Big] + T_f(x,t)\frac{\partial\overline{k}(l(t))}{\partial t}dx.\end{aligned} \tag{5.53}$$

Distributing terms,

$$\begin{aligned}\frac{dU(t)}{dt} = C_p\rho_0 S_{eff}\int_0^L \frac{\mu N^2(t)}{\rho_0 V_{eff}C_p}\Big[\eta_{pt}f_p(x,t)k(l(t)) + \eta_f\overline{k}(l(t))\Big]\\ -\Big[\xi N(t)k(l(t))T_p(x,t)\frac{\partial f_p(x,t)}{\partial x} + \xi N(t)k(l(t))f_p(x,t)\frac{\partial T_p(x,t)}{\partial x}\\ +\overline{k}(l(t))\frac{F_d(t,l(t))}{\rho_0 S_{eff}}\frac{\partial T_f(x,t)}{\partial x}\Big] + \Big[\frac{k(l(t))f_p(x,t)S_{exc}\alpha}{\rho_0 V_{eff}C_p}(T_b - T_p(x,t))\\ +\frac{\overline{k}(l(t))S_{exc}\alpha}{\rho_0 V_{eff}C_p}(T_b - T_f(x,t)) + f_p(x,t)T_p(x,t)\frac{\partial k(l(t))}{\partial t} - T_f(x,t)\frac{\partial k(l(t))}{\partial t}\Big]dx,\end{aligned} \tag{5.54}$$

then rearranging items,

$$\begin{aligned}\frac{dU(t)}{dt} = N^2(t)\int_0^L \frac{\mu}{\xi}\Big[\eta_{pt}f_p(x,t)k(l(t)) + \eta_f\overline{k}(l(t))\Big]dx\\ -N(t)\int_0^L C_p\rho_0 V_{eff}k(l(t))\Big[T_p(x,t)\frac{\partial f_p(x,t)}{\partial x} + f_p(x,t)\frac{\partial T_p(x,t)}{\partial x}\Big]dx\\ +\int_0^L \overline{k}(l(t))C_p F_d(t,l(t))\frac{\partial T_f(x,t)}{\partial x}dx + \frac{S_{exc}\alpha}{\xi}\int_0^L\Bigg[k(l(t))f_p(x,t)(T_b - T_p(x,t))\\ +\overline{k}(l(t))(T_b - T_f(x,t)) + C_p\rho_0 S_{eff}\Big[f_p(x,t)T_p(x,t)\frac{\partial k(l(t))}{\partial t} - T_f(x,t)\frac{\partial k(l(t))}{\partial t}\Big]\Bigg]dx,\end{aligned} \tag{5.55}$$

The last term in the equation above is zero due to assumption of continuity of temperature at the interface. Recalling the definition of the flow at the die for constant viscosity as:

$$F_d(l(t),t) = \frac{K_d\rho_0 V_{eff}N(t)(L - l(t))}{B\rho_0 + K_d(L - l(t))} \tag{5.56}$$

then, it is possible to define $F_n(l(t),t) = F_d(l(t),t)/N(t)$. Therefore, the total energy balance could be written as:

$$\begin{aligned}\frac{dU(t)}{dt} = N^2(t)\int_0^L \frac{\mu}{\xi}\Big[\eta_{pt} f_p(x,t)k(l(t)) + \eta_f \overline{k}(l(t))\Big]dx - N(t)\int_0^L C_p\rho_0 V_{eff}k(l(t))\Big[T_p(x,t)\frac{\partial f_p(x,t)}{\partial x} \\ + f_p(x,t)\frac{\partial T_p(x,t)}{\partial x} + \overline{k}(l(t))C_p F_n(t,l(t))\frac{\partial T_f(x,t)}{\partial x}\Big]dx \\ + \frac{S_{exc}\alpha}{\xi}\int_0^L \Big[k(l(t))f_p(x,t)(T_b - T_p(x,t)) + \overline{k}(l(t))(T_b - T_f(x,t))\Big]dx,\end{aligned} \tag{5.57}$$

integrating terms when possible,

$$\begin{aligned}\frac{dU(t)}{dt} = N^2(t)\int_0^L \frac{\mu}{\xi}\Big[\eta_{pt} f_p(x,t)k(l(t)) + \eta_f \overline{k}(l(t))\Big]dx \\ -N(t)\Big[C_p\rho_0 V_{eff}\Big[T_p(l(t),t)f_p(l(t),t) - T_p(0,t)f_p(0,t)\Big] \\ + C_p F_n(t,l(t))\Big[T_f(L,t) - T_f(l(t),t)\Big]\Big] \\ + \frac{S_{exc}\alpha}{\xi}\int_0^L \Big[k(l(t))f_p(x,t)(T_b - T_p(x,t)) + \overline{k}(l(t))(T_b - T_f(x,t))\Big]dx,\end{aligned} \tag{5.58}$$

Equation (5.58) can be written in the form:

$$\frac{dU(t)}{dt} = \mathcal{A}(t)N^2(t) + \mathcal{B}(t)N(t) + \mathcal{C}(t), \tag{5.59}$$

where,

$$\begin{aligned}\mathcal{A}(t) &= \frac{\mu}{\xi}\int_0^L \Big[\eta_{pt} f_p(x,t)k(l(t)) + \eta_f \overline{k}(l(t))\Big]dx \\ \mathcal{B}(t) &= -C_p\rho_0 V_{eff}\Big[T_p(l(t),t)f_p(l(t),t) - T_p(0,t)f_p(0,t)\Big] \\ &\quad -C_p F_n(t,l(t))\Big[T_f(L,t) - T_f(l(t),t)\Big] \\ \mathcal{C}(t) &= \frac{S_{exc}\alpha}{\xi}\int_0^L \Big[k(l(t))f_p(x,t)(T_b - T_p(x,t)) + \overline{k}(l(t))(T_b - T_f(x,t))\Big]dx\end{aligned} \tag{5.60}$$

Analyzing each coefficient from equation (5.60) we have that $\mathcal{A}(t)$ is always positive. In addition, the first term in $\mathcal{B}(t)$ is negative if and only if $T_p(l(t),t)f_p(l(t),t) > T_p(0,t)f_p(0,t)$. Analogously, the second term in $\mathcal{B}(t)$ is negative if and only if $T_f(L,t) > T_f(l(t),t)$. Finally, regarding to $\mathcal{C}(t)$ it is possible to note that it is related to the difference of temperature between the barrel and the melt in the extruder.

5.3.2 Model Based Control

A control strategy with guaranteed global stability that explicitly utilizes total energy balance equation (5.59) is designed. Assuming the internal energy associated with a set point profile $T^*(x)$ with constant input flow $F_{in} = F_d(l^*) = \rho_0 V_{eff} f_p^* N^*$:

$$U^*(t) = \int_0^L C_p \rho_0 S_{eff} f^*(x) T^*(x) dx, \tag{5.61}$$

where,

$$T^*(x) = k(l^*) T_p^*(x) + \overline{k}(l^*) T_f^*(x), \tag{5.62}$$

$$f^*(x,t) = k(l^*) f_p^*(x) + \overline{k}(l^*) f_f^*(x). \tag{5.63}$$

The main idea of the controller is to choose $N(t)$ based on (5.59) in order to explicitly assign a desired linear closed loop dynamic response $U(t)$, with the consequence that $T(x,t) = T^*(x)$ as $t \to \infty$. It is worth to point out that the suggested control requires the computation of the internal energy which in turn requires the knowledge of the temperature and the filling ratio inside the extruder.
Let $N(t)$ be defined as the control input:

$$N(t) = \frac{-\mathcal{B}(t) \pm \sqrt{\mathcal{B}^2(t) - 4\mathcal{A}(t)(\mathcal{C}(t) + \gamma(t))}}{2\mathcal{A}(t)} \tag{5.64}$$

with,

$$\gamma = K_p \left(e(t) + T_d \frac{de(t)}{dt} + \frac{1}{T_i} \int_0^t e(\tau) d\tau \right), \tag{5.65}$$

and

$$e(t) = U(t) - U^*(t) = \int_0^L C_p \rho_0 S_{eff} (f(x,t) T(x,t) - f^*(x) T^*(x)) dx, \tag{5.66}$$

where $K_p, T_i > 0, T_d \geq 0$, and assume $T(L,t) > T(0,t)$ for all t. Then, combining equations (5.59) and (5.65) we have:

$$\frac{dU(t)}{dt} = -\gamma(t), \tag{5.67}$$

then,

$$\frac{dU(t)}{dt} = -K_p \left(e(t) + T_d \frac{de(t)}{dt} + \frac{1}{T_i} \int_0^t e(\tau) d\tau \right), \tag{5.68}$$

and

$$\frac{dU(t)}{dt} = K_p(U^*(t) - U(t)) + K_p T_d\left(\frac{dU^*(t)}{dt} - \frac{dU(t)}{dt}\right) + \frac{K_p}{T_i}\int_0^t (U^*(\tau) - U(\tau))d\tau. \quad (5.69)$$

By applying Laplace transformation of this linear second order ordinary differential equation we have:

$$U(s)\Big(s^2(1 + K_p T_d) + K_p s + K_p/T_i\Big) = U^*(s)\Big(K_p T_d s^2 + K_p s + K_p/T_i\Big). \quad (5.70)$$

Since $U^*(t)$ is time-invariant, it follows from (5.70) that $U(t) \to U^*(t)$ as $t \to \infty$. Stability of (5.70) follows from the Hurwitz' criterion since all coefficients fo the left-hand side polynomial are positive.

On the other hand, there exists a minimum admissible value of the screw speed N_{min} which guarantees the existence of a solution of the quadratic equation (5.64):

$$N_{min}(t) = \frac{-\mathcal{B}}{2\mathcal{A}}. \quad (5.71)$$

then, using equation (5.60)

$$N_{min}(t) = \frac{C_p \rho_0 V_{eff}[T_p(l(t),t) f_p(l(t),t) - T_p(0,t) f_p(0,t)] + C_p F_n(t, l(t))[T_f(L,t) - T_f(l(t),t)]}{\frac{2\mu}{\xi}\int_0^L \Big[\eta_{pt} f_p(x,t) k(l(t)) + \eta_f \overline{k}(l(t))\Big] dx}. \quad (5.72)$$

It is physically coherent to say that the screw speed in the extruder should be always greater than zero then N_{min} should be greater than zero too. Therefore, analyzing each term individually in equation (5.72) we have that N_{min} is positive only when $T_p(l(t),t) f_p(l(t),t) > T_p(0,t) f_p(0,t)$ and $T_f(L,t) > T_f(l(t),t)$. This imposes a restriction on the controller that should be taken into account during the implementation stage. This means, an exact solution for equation (5.64) exists if and only if $N(t) > N_{min}(t)$ for all t with $T_p(l(t),t) f_p(l(t),t) > T_p(0,t) f_p(0,t)$ and $T_f(L,t) > T_f(l(t),t)$.

5.3.3 Stability analysis through a Lyapunov candidate function

Let us recall the suggested control law that was presented in the previous section from equations (5.64), (5.65) and (5.66). It is important to note that the bi-zone model of the extrusion process is composed of a system of transport equations coupled through a moving interface. Therefore, the main difficulty in the stability analysis arises from the moving domains $[0, l(t)[$ and $]l(t), L]$. In this section, the stability analysis of the

proposed control law is presented through the use of different Lyapunov candidate functions. First, we prove the stability of the closed loop for the filling ratio and the moving interface. Finally, after stabilizing $f_p(x,t)$ and $l(t)$, we turn to stabilize the temperature for both the PFZ and the PFZ.

5.3.3.1 Stabilization of $f_p(x,t)$

Recalling, the dynamics of the filling ratio as it follows:

$$\frac{\partial f_p(x,t)}{\partial t} = -\xi N(t)\frac{\partial f_p(x,t)}{\partial x}. \tag{5.73}$$

Defining the following Lyapunov candidate function for filling ratio:

$$V_{fp}(t) = 1/2\int_0^{l(t)} (f_p(x,t) - f^*(x))^2 dx. \tag{5.74}$$

with $f^*(x) = k(l^*)f_p^*(x) + \overline{k}(l^*)f_f^*(x)$. Then, the time derivative of $V_{fp}(t)$ is:

$$\dot{V}_{fp}(t) = \int_0^{l(t)} \Big[f_p(x,t) - f_p^*(x)\Big]\frac{\partial f_p(x,t)}{\partial t}dx + \Big[f_p(l(t),t) - f_p^*(l(t))\Big]^2\frac{dl(t)}{dt}. \tag{5.75}$$

Let us recall the moving interface and the filling ratio from equations (2.37) and (5.73), replacing in equation (5.75):

$$\begin{aligned}\dot{V}_{fp}(t) = -\xi N(t)\int_0^{l(t)} \Big(f_p(x,t) - f_p^*(x)\Big)\frac{\partial f_p(x,t)}{\partial x}dx \\ + \frac{(f_p(l(t),t) - f_p^*(l(t)))^2}{(1 - f_p(l(t),t))}\Big[\frac{F_d(l(t),t)}{\rho_0 S_{eff}} - \xi N(t) f_p(l(t),t)\Big],\end{aligned} \tag{5.76}$$

adding and subtracting $\xi N^*\dfrac{\partial f_p(x,t)}{\partial x}$ inside the integral

$$\begin{aligned}\dot{V}_{fp}(t) = \int_0^{l(t)} \Big(f_p(x,t) - f_p^*(x)\Big)\Big[-(\xi N(t) - \xi N^*)\frac{\partial f_p(x,t)}{\partial x} - \xi N^*\frac{\partial f_p(x,t)}{\partial x}\Big]dx \\ + \frac{(f_p(l(t),t) - f_p^*(l(t)))^2}{(1 - f_p(l(t),t))}\Big[\frac{F_d(l(t),t)}{\rho_0 S_{eff}} - \xi N(t) f_p(l(t),t)\Big],\end{aligned} \tag{5.77}$$

adding and subtracting $\xi N^* \dfrac{\partial f_p^*(x)}{\partial x}$ inside the integral

$$\begin{aligned}\dot{V}_{fp}(t) = \int_0^{l(t)} \Big(f_p(x,t) - f_p^*(x)\Big) \Bigg[&- (\xi N(t) - \xi N^*) \frac{\partial f_p(x,t)}{\partial x} \\ &- \xi N^* \Big[\frac{\partial f_p(x,t)}{\partial x} - \frac{\partial f_p^*(x)}{\partial x}\Big] - \xi N^* \frac{\partial f_p^*(x)}{\partial x}\Bigg] dx \\ &+ \frac{(f_p(l(t),t) - f_p^*(l(t)))^2}{(1 - f_p(l(t),t))} \Big[\frac{F_d(l(t),t)}{\rho_0 S_{eff}} - \xi N(t) f_p(l(t),t)\Big],\end{aligned} \tag{5.78}$$

Distributing and taking into account that $\dfrac{\partial f_p^*(x)}{\partial x} = 0$,

$$\begin{aligned}\dot{V}_{fp}(t) = &-[\xi N(t) - \xi N^*] \int_0^{l(t)} \Big(f_p(x,t) - f_p^*(x)\Big) \frac{\partial f_p(x,t)}{\partial x} dx \\ &- \xi N^* \int_0^{l(t)} \Big(f_p(x,t) - f_p^*(x)\Big) \Big(\frac{\partial f_p(x,t)}{\partial x} - \frac{\partial f_p^*(x)}{\partial x}\Big) dx \\ &+ \frac{(f_p(l(t),t) - f_p^*(l(t)))^2}{(1 - f_p(l(t),t))} \Big[\frac{F_d(l(t),t)}{\rho_0 S_{eff}} - \xi N(t) f_p(l(t),t)\Big].\end{aligned} \tag{5.79}$$

Integrating the second term of equation (5.79)

$$\begin{aligned}\dot{V}_{fp}(t) = &-[\xi N(t) - \xi N^*] \int_0^{l(t)} \Big(f_p(x,t) - f_p^*(x)\Big) \frac{\partial f_p(x,t)}{\partial x} dx \\ &- \xi N^* [f_p(l(t),t) - f_p^*(l(t))]^2 + \xi N^* [f_p(0,t) - f_p^*(0)]^2 \\ &+ \frac{(f_p(l(t),t) - f_p^*(l(t)))^2}{(1 - f_p(l(t),t))} \Big[\frac{F_d(l(t),t)}{\rho_0 S_{eff}} - \xi N(t) f_p(l(t),t)\Big],\end{aligned} \tag{5.80}$$

Taking into account the definition of $F_d(l(t),t)$ with constant viscosity from equation (5.56), then:

$$\begin{aligned}\dot{V}_{fp}(t) = &-[\xi N(t) - \xi N^*] \int_0^{l(t)} \Big(f_p(x,t) - f_p^*(x)\Big) \frac{\partial f_p(x,t)}{\partial x} dx \\ &- \xi N^* [f_p(l(t),t) - f_p^*(l(t))]^2 + \xi N^* [f_p(0,t) - f_p^*(0)]^2 \\ &+ \frac{\xi N(t)(f_p(l(t),t) - f_p^*(l(t)))^2}{(1 - f_p(l(t),t))} \Big[\frac{K_d(L - l(t))}{B\rho_0 + K_d(L - l(t))} - f_p(l(t),t)\Big],\end{aligned} \tag{5.81}$$

Since $l(t)$ is bounded between 0 and L it is possible to have the following:

$$\begin{aligned}\dot{V}_{fp}(t) \leq &-[\xi N(t) - \xi N^*] \int_0^{l(t)} \Big(f_p(x,t) - f_p^*(x)\Big) \frac{\partial f_p(x,t)}{\partial x} dx \\ &- \xi N^* [f_p(l(t),t) - f_p^*(l(t))]^2 + \xi N^* [f_p(0,t) - f_p^*(0)]^2 \\ &- \frac{\xi N(t)(f_p(l(t),t) - f_p^*(l(t)))^2}{(1 - f_p(l(t),t))} f_p(l(t),t),\end{aligned} \tag{5.82}$$

then, recalling the boundary conditions from equation (2.51) and taking into account the assumption of constant input flow, i.e. $F_{in} = F_{in}^*$ we have:

$$\begin{aligned}\dot{V}_{fp}(t) \leq -[\xi N(t) - \xi N^*] \int_0^{l(t)} \Big(f_p(x,t) - f_p^*(x)\Big) \frac{\partial f_p(x,t)}{\partial x} dx \\ -\xi N^* [f_p(l(t),t) - f_p^*(l(t))]^2 + \xi N^* [\frac{F_{in}}{\rho_0 N(t) V_{eff}} - \frac{F_{in}}{\rho_0 N^* V_{eff}}]^2 \\ -\frac{\xi N(t)(f_p(l(t),t) - f_p^*(l(t)))^2}{(1 - f_p(l(t),t))} f_p(l(t),t).\end{aligned} \tag{5.83}$$

Distributing,

$$\begin{aligned}\dot{V}_{fp}(t) \leq -[\xi N(t) - \xi N^*] \int_0^{l(t)} \Big(f_p(x,t) - f_p^*(x)\Big) \frac{\partial f_p(x,t)}{\partial x} dx \\ -\xi N^* [f_p(l(t),t) - f_p^*(l(t))]^2 - \frac{\xi N^* F_{in}^2}{(\rho_0 V_{eff})^2} \Big[\frac{N(t) - N^*}{N^* N(t)}\Big]^2 \\ -\frac{\xi N(t)(f_p(l(t),t) - f_p^*(l(t)))^2}{(1 - f_p(l(t),t))} f_p(l(t),t).\end{aligned} \tag{5.84}$$

and finally

$$\begin{aligned}\dot{V}_{fp}(t) \leq -\xi N^* [f_p(l(t),t) - f_p^*(l(t))]^2 - \frac{\xi N^* F_{in}^2}{(\rho_0 V_{eff})^2} \Big[\frac{N(t) - N^*}{N^* N(t)}\Big]^2 \\ -\frac{\xi N(t)(f_p(l(t),t) - f_p^*(l(t)))^2}{(1 - f_p(l(t),t))} f_p(l(t),t) + \Delta_{fp},\end{aligned} \tag{5.85}$$

with,

$$\Delta_{fp} = -[\xi N(t) - \xi N^*] \int_0^{l(t)} \Big(f_p(x,t) - f_p^*(x)\Big) \frac{\partial f_p(x,t)}{\partial x} dx. \tag{5.86}$$

Due to the asymptotic convergence of $N(t)$, it is straightforward to see that $\Delta_{fp}(t)$ from equation (5.86) has asymptotic convergence as $t \to \infty$. Analogously, taking into count the asymptotic convergence of $N(t)$ it is possible to say that the second term of the equation (5.85) has also asymptotic convergence as $t \to \infty$. In addition, the first term of equation (5.85) is negative since ξ and N^* are always positive. A similar analysis can be made for the third term of (5.85) which is also negative since $0 \leq f_p(l(t),t) < 1$ for all t. Integrating equation (5.85), the limit of the right hand side of

$$V_{fp}(t) \leq V_{fp}(0) + \int_0^t \Delta_{fp}(t) dt \tag{5.87}$$

exists and is uniformly bounded and uniformly continuous. Then it follows that $f_p(l(t),t)$ is bounded and $\dot{V}_{fp}$ is uniformly bounded. Then, from Barbalat's lemma it follows that $\dot{V}_{fp} \to 0$ as $t \to \infty$. Since $\Delta_{fp}(t) \to 0$ as $t \to \infty$, it follows from equation (5.85) that

$f_p(l(t),t) \to f_p^*(l(t))$.

5.3.3.2 Stabilization of $l(t)$

Recalling, the dynamics of the moving interface as it follows:

$$\frac{dl(t)}{dt} = \frac{F_d(l(t),t) - \rho_0 V_{eff} N(t) f_p(l(t),t)}{\rho_0 S_{eff}(1 - f_p(l(t),t))}. \tag{5.88}$$

Defining a Lyapunov candidate function for the interface position:

$$V_0(t) = 1/2(l(t) - l^*)^2. \tag{5.89}$$

The time derivative of $V_0(t)$ is

$$\dot{V_0}(t) = (l(t) - l^*)\frac{dl(t)}{dt}. \tag{5.90}$$

then,

$$\dot{V_0}(t) = (l(t) - l^*)\left[\frac{F_d(l(t),t) - \rho_0 V_{eff} N(t) f_p(l(t),t)}{\rho_0 S_{eff}(1 - f_p(l(t),t))}\right], \tag{5.91}$$

distributing terms,

$$\dot{V_0}(t) = (l(t) - l^*)\left[\frac{F_d(l(t),t)}{\rho_0 S_{eff}(1 - f_p(l(t),t))} - \xi N(t)\frac{f_p(l(t),t)}{(1 - f_p(l(t),t))}\right], \tag{5.92}$$

then

$$\dot{V_0}(t) = \frac{(l(t) - l^*)}{(1 - f_p(l(t),t))}\left[\frac{F_d(l(t),t)}{\rho_0 S_{eff}} - \xi N(t) f_p(l(t),t)\right], \tag{5.93}$$

adding and subtracting $\xi N(t) f_p^* \left[\frac{(l(t) - l^*)}{(1 - f_p(l(t),t))}\right]$ in order to have

$$\dot{V_0}(t) = \frac{(l(t) - l^*)}{(1 - f_p(l(t),t))}\left[\frac{F_d(l(t),t)}{\rho_0 S_{eff}} - \xi N(t) f_p(l(t),t) + \xi N(t) f_p^* - \xi N(t) f_p^*\right], \tag{5.94}$$

then,

$$\dot{V_0}(t) = \frac{(l(t) - l^*)}{(1 - f_p(l(t),t))}\left[\frac{F_d(l(t),t)}{\rho_0 S_{eff}} - \xi N(t)[f_p(l(t),t) - f_p^*] - \xi N(t) f_p^*\right], \tag{5.95}$$

taking into account the definition of $f_p^* = \frac{F_d(l^*)}{\rho_0 V_{eff} N^*}$,

$$\dot{V_0}(t) = \frac{(l(t) - l^*)}{(1 - f_p(l(t),t))}\left[-\xi N(t)[f_p(l(t),t) - f_p^*] + \frac{F_d(l(t),t)}{\rho_0 S_{eff}} - \xi N(t)\frac{F_d(l^*)}{\rho_0 V_{eff} N^*}\right], \tag{5.96}$$

Taking into account the definition of F_d from equation (5.56):

$$\dot{V}_0(t) = \frac{(l(t)-l^*)}{(1-f_p(l(t),t))}\Bigg[-\xi N(t)[f_p(l(t),t)-f_p^*] + \xi N(t)\frac{K_d(L-l(t))}{B\rho_0+K_d(L-l(t))} - \xi N(t)\frac{K_d(L-l^*)}{B\rho_0+K_d(L-l^*)}\Bigg], \tag{5.97}$$

distributing,

$$\dot{V}_0(t) = \frac{(l(t)-l^*)}{(1-f_p(l(t),t))}\Bigg[-\xi N(t)[f_p(l(t),t)-f_p^*] \frac{[B\rho_0+K_d(L-l^*)][\xi K_d N(t)(L-l(t))]-[B\rho_0+K_d(L-l(t))][\xi K_d N(t)(L-l^*)]}{[B\rho_0+K_d(L-l(t))][B\rho_0+K_d(L-l^*)]}\Bigg], \tag{5.98}$$

then,

$$\dot{V}_0(t) = \frac{(l(t)-l^*)}{(1-f_p(l(t),t))}\Bigg[-\xi N(t)[f_p(l(t),t)-f_p^*] - \frac{\xi B\rho_0 K_d N(t)(l(t)-l^*)}{[B\rho_0+K_d(L-l(t))][B\rho_0+K_d(L-l^*)]}\Bigg]. \tag{5.99}$$

Distributing terms,

$$\dot{V}_0(t) = -\xi N(t)(l(t)-l^*)^2\frac{B\rho_0 K_d}{[1-f_p(l(t),t)][B\rho_0+K_d(L-l(t))][B\rho_0+K_d(L-l^*)]} - \xi N(t)(f_p(l(t),t)-f_p^*)\frac{(l(t)-l^*)}{(1-f_p(l(t),t))}, \tag{5.100}$$

finally

$$\dot{V}_0(t) = -\xi N(t)\kappa(t)(l(t)-l^*)^2 - \xi N(t)\zeta(t)(l(t)-l^*), \tag{5.101}$$

with,

$$\kappa(t) = \frac{B\rho_0 K_d}{[1-f_p(l(t),t)][B\rho_0+K_d(L-l(t))][B\rho_0+K_d(L-l^*)]} \qquad \zeta(t) = \frac{f_p(l(t),t)-f_p^*}{(1-f_p(l(t),t))}. \tag{5.102}$$

Analyzing equation (5.101) it is clear that $\kappa(t) > 0$ for all t since $0 \leq f_p(x,t) < 1$ and $0 \leq l \leq L$. Also, note that parameters K_d, B and ρ_0 are always positive, therefore the first term of $\dot{V}_0(t)$ is negative for all t. On the other hand, analyzing equation (5.102) it

follows that, due to the asymptotic convergence of $f_p(l(t),t)$, then $\zeta(t)$ tends to zero as $t \to \infty$. Therefore, it is possible to say that $\dot{V}_0$ tend to zero as $t \to \infty$. Then it follows that $l(t) \to l^*$ as $t \to \infty$.

5.3.3.3 Stabilization of $T(x,t)$

In this case we define a Lyapunov-like functional for the system defined by equation (5.57):

$$V(t) = 1/2 \int_0^L [T(x,t) - T^*(x)]^2 dx. \tag{5.103}$$

The time derivative of V is

$$\dot{V}(t) = \int_0^L [T(x,t) - T^*(x)] \frac{\partial T(x,t)}{\partial t} dx \tag{5.104}$$

then, with the characteristic functions it is possible to have:

$$\begin{aligned} \dot{V} = \int_0^L \Big[& k(l(t))T_p(x,t) + \overline{k}(l(t))T_f(x,t) - k(l^*)T_p^*(x) - \overline{k}(l^*)T_f^*(x) \Big] \\ & \Big[\dot{l}(t)\delta(x-l(t))T_p(x,t) - \dot{l}(t)\delta(x-l(t))T_f(x,t) + k(l(t))\frac{\partial T_p(x,t)}{\partial t} \\ & + \overline{k}(l(t))\frac{\partial T_f(x,t)}{\partial t} \Big] dx \end{aligned} \tag{5.105}$$

where, $\dot{l}(t)\delta(x-l(t))T_p(x,t) - \dot{l}(t)\delta(x-l(t))T_f(x,t) = 0$ because of the interface conditions, i.e $T_p(l^-,t) = T_f(l^+,t)$,then:

$$\begin{aligned} \dot{V} = \int_0^L \Big[& k(l(t))T_p(x,t) + \overline{k}(l(t))T_f(x,t) - k(l^*)T_p^*(x) - \overline{k}(l^*)T_f^*(x) \Big] \\ & \Big[+ k(l(t))\frac{\partial T_p(x,t)}{\partial t} + \overline{k}(l(t))\frac{\partial T_f(x,t)}{\partial t} \Big] dx. \end{aligned} \tag{5.106}$$

In order to simplify the analysis $\dot{V}$ can be divided into $\dot{V}_p$, $\dot{V}_f$ and $\dot{V}_i$ as it follows:

$$\begin{aligned} \dot{V}_p &= \textstyle\int_0^L k(l(t))T_p(x,t)\frac{\partial T_p(x,t)}{\partial t} - k(l^*)k(l(t))T_p^*(x)\frac{\partial T_p(x,t)}{\partial t} dx \\ \dot{V}_f &= \textstyle\int_0^L \overline{k}(l(t))T_f(x,t)\frac{\partial T_f(x,t)}{\partial t} - \overline{k}(l^*)\overline{k}(l(t))T_f^*(x)\frac{\partial T_f(x,t)}{\partial t} dx \\ \dot{V}_i &= -\textstyle\int_0^L k(l(t))\overline{k}(l^*)T_f^*(x)\frac{\partial T_p(x,t)}{\partial t} + k(l^*)\overline{k}(l(t))T_p^*(x)\frac{\partial T_f(x,t)}{\partial t} dx. \end{aligned} \tag{5.107}$$

Analyzing equation (5.107), $\dot{V}_p$ is related to the temperature at the PFZ, $\dot{V}_f$ is related with the temperature at the FFZ and finally $\dot{V}_i$ deals with the relationship between the temperature at the PFZ and the FFZ. On the other hand, let us recall that: $k(l^*)k(l(t)) = k(\min(l(t),l^*))$, $\overline{k}(l^*)\overline{k}(l(t)) = 1 - k(l^M(t))$ with $l^M(t) = \max(l(t),l^*)$ and $l_m(t) = \min(l(t),l^*)$. By analyzing the stability of each term from equation (5.107) it

is possible prove the stability of V. First, we develop each term from equation (5.107) and finally, at the end of this section, a stability analysis of V is presented.

5.3.3.3.1 Analysis of $\dot{V}_p$

Analyzing $\dot{V}_p$ which belongs to the *PFZ*:

$$\dot{V}_p = \int_0^L [k(l(t))T_p(x,t) - k(l_m)T_p^*(x)] \frac{\partial T_p(x,t)}{\partial t} dx. \tag{5.108}$$

Replacing $\frac{\partial T_p(x,t)}{\partial t}$ from equation (5.44):

$$\dot{V}_p = \int_0^L \left[k(l(t))T_p(x,t) - k(l_m)T_p^*(x) \right] \left[-\xi N(t) \frac{\partial T_p(x,t)}{\partial x} + \Omega(f_p, T_p, N, T_b) \right] dx. \tag{5.109}$$

Adding and subtracting $\xi N^* \frac{\partial T_p(x,t)}{\partial x}$ in the right term,

$$\begin{aligned} \dot{V}_p = \int_0^L \left[k(l(t))T_p(x,t) - k(l_m)T_p^*(x) \right] \Bigg[& -\xi N(t) \frac{\partial T_p(x,t)}{\partial x} + \xi N^* \frac{\partial T_p(x,t)}{\partial x} \\ & -\xi N^* \frac{\partial T_p(x,t)}{\partial x} + \Omega(f_p, T_p, N, T_b) \Bigg] dx. \end{aligned} \tag{5.110}$$

Rearranging terms,

$$\begin{aligned} \dot{V}_p = \int_0^L \left[k(l(t))T_p(x,t) - k(l_m)T_p^*(x) \right] \Bigg[& -(\xi N(t) - \xi N^*) \frac{\partial T_p(x,t)}{\partial x} \\ & -\xi N^* \frac{\partial T_p(x,t)}{\partial x} + \Omega(f_p, T_p, N, T_b) \Bigg] dx, \end{aligned} \tag{5.111}$$

adding and subtracting $\xi N^* \frac{\partial T_p^*(x)}{\partial x}$ in the right term

$$\begin{aligned} \dot{V}_p = \int_0^L \left[k(l(t))T_p(x,t) - k(l_m)T_p^*(x) \right] \Bigg[& -(\xi N(t) - \xi N^*) \frac{\partial T_p(x,t)}{\partial x} \\ & -\xi N^* \left[\frac{\partial T_p(x,t)}{\partial x} - \frac{\partial T_p^*(x)}{\partial x} \right] - \xi N^* \frac{\partial T_p^*(x)}{\partial x} + \Omega(f_p, T_p, N, T_b) \Bigg] dx. \end{aligned} \tag{5.112}$$

From steady state, it is possible to have:

$$\frac{\partial T_p^*(x)}{\partial x} = \frac{1}{\xi N^*} \Omega(f_p^*, T_p^*, N^*, T_b^*), \tag{5.113}$$

then,

$$\dot{V}_p = \int_0^L \Big[k(l(t))T_p(x,t) - k(l_m)T_p^*(x)\Big]\Bigg[- (\xi N(t) - \xi N^*)\frac{\partial T_p(x,t)}{\partial x} \\ -\xi N^*\Big[\frac{\partial T_p(x,t)}{\partial x} - \frac{\partial T_p^*(x)}{\partial x}\Big] + \Omega(f_p, T_p, N, T_b) - \Omega(f_p^*, T_p^*, N^*, T_b^*)\Bigg]dx. \tag{5.114}$$

Taking into account the definition of Ω from equation (2.53) with constant viscosity, and recalling the assumption of the filling ratio as time-invariant only at the viscous dissipation part,

$$\dot{V}_p = \int_0^L \Bigg[k(l(t))T_p(x,t) - k(l_m)T_p^*(x)\Bigg]\Bigg[- [\xi N(t) - \xi N^*]\frac{\partial T_p(x,t)}{\partial x} \\ -\xi N^*\Big[\frac{\partial T_p(x,t)}{\partial x} - \frac{\partial T_p^*(x)}{\partial x}\Big] + \beta_1[N^2(t) - N^{*2}] - \beta_2[T_p(x,t) - T_p^*(x)]\Bigg]dx. \tag{5.115}$$

with,

$$\beta_1 = \frac{\mu\eta_{pt}}{\rho_0 V_{eff} C_p}. \tag{5.116}$$

$$\beta_2 = \frac{S_{exc}\alpha}{\rho_0 V_{eff} C_p}, \tag{5.117}$$

It is worth to point out that β_1 and β_2 are both time-invariant and always positive. Then, distributing equation (5.115) we have:

$$\begin{aligned}\dot{V}_p = &-\Big[\xi N(t) - \xi N^*\Big]\int_0^L \Big[k(l(t))T_p(x,t) - k(l_m)T_p^*(x)\Big]\frac{\partial T_p(x,t)}{\partial x}dx \\ &-\xi N^*\int_0^L \Big[k(l(t))T_p(x,t) - k(l_m)T_p^*(x)\Big]\Big[\frac{\partial T_p(x,t)}{\partial x} - \frac{\partial T_p^*(x)}{\partial x}\Big]dx \\ &+\beta_1\Big[N^2(t) - N^{*2}\Big]\int_0^L \Big[k(l(t))T_p(x,t) - k(l_m)T_p^*(x)\Big]dx \\ &-\beta_2\int_0^L \Big[k(l(t))T_p(x,t) - k(l_m)T_p^*(x)\Big]\Big[T_p(x,t) - T_p^*(x)\Big]dx.\end{aligned} \tag{5.118}$$

Then, two different cases could be considered $l(t) \leq l^*$ and $l(t) > l^*$. That means $\dot{V_{p1}}$ and $\dot{V_{p2}}$ respectively:

i. When $l(t) \leq l^*$, it is possible to write $\dot{V_{p1}}$ as it follows:

$$\begin{aligned}\dot{V_{p1}} = &-[\xi N(t) - \xi N^*] \int_0^{l(t)} \Big[T_p(x,t) - T_p^*(x)\Big] \frac{\partial T_p(x,t)}{\partial x} dx \\ &-\xi N^* \int_0^{l(t)} \Big[T_p(x,t) - T_p^*(x)\Big] \Big[\frac{\partial T_p(x,t)}{\partial x} - \frac{\partial T_p^*(x)}{\partial x}\Big] dx \\ +\beta_1[N^2(t) - N^{*2}] &\int_0^{l(t)} \Big[T_p(x,t) - T_p^*(x)\Big] dx - \beta_2 \int_0^{l(t)} \Big[T_p(x,t) - T_p^*(x)\Big]^2 dx.\end{aligned} \tag{5.119}$$

And finally, integrating the second term of equation (5.119) and distributing in order to have:

$$\begin{aligned}\dot{V_{p1}} = &-\xi N^*[T_p(l(t),t) - T_p^*(l(t))]^2 + \xi N^*[T_p(0,t) - T_p^*(0)]^2 \\ &-\beta_2 \int_0^{l(t)} [T_p(x,t) - T_p^*(x)]^2 dx + \Delta_{p1}(t),\end{aligned} \tag{5.120}$$

where,

$$\begin{aligned}\Delta_{p1}(t) = &-[\xi N(t) - \xi N^*] \int_0^{l(t)} \Big[T_p(x,t) - T_p^*(x)\Big] \frac{\partial T_p(x,t)}{\partial x} dx \\ &+\beta_1[N^2(t) - N^{*2}] \int_0^{l(t)} [T_p(x,t) - T_p^*(x)] dx\end{aligned} \tag{5.121}$$

The first and third terms in equation (5.120) are always negative since β_1, ξ and N^* are always positive. Recalling, $\Delta_{p1}(t)$ from equation (5.121) it is worth to point out that it is related to the difference between the input screw speed $N(t)$ and the set-point screw speed N^*. Further details regarding the stability of T will be discussed in detail at the end of this section.

ii. When $l(t) > l^*$, then $k(l^*)k(l(t)) = k(min(l(t), l^*)) = l^*$. Therefore $\dot{V_{p2}}$ can be written as follows:

$$\begin{aligned}\dot{V_{p2}} = &-[\xi N(t) - \xi N^*] \int_0^{L} \Big[k(l(t))T_p(x,t) - k(l^*)T_p^*(x)\Big] \frac{\partial T_p(x,t)}{\partial x} dx \\ &-\xi N^* \int_0^{L} \Big[k(l(t))T_p(x,t) - k(l^*)T_p^*(x)\Big] \Big[\frac{\partial T_p(x,t)}{\partial x} - \frac{\partial T_p^*(x)}{\partial x}\Big] dx \\ &+\beta_1[N^2(t) - N^{*2}] \int_0^{L} \Big[k(l(t))T_p(x,t) - k(l^*)T_p^*(x)\Big] dx \\ &-\beta_2 \int_0^{L} \Big[k(l(t))T_p(x,t) - k(l^*)T_p^*(x)\Big] \Big[T_p(x,t) - T_p^*(x)\Big] dx,\end{aligned} \tag{5.122}$$

distributing,

$$\begin{aligned}\dot{V_{p2}} = &-\xi N^* \int_0^{l^*} \Big[T_p(x,t) - T_p^*(x)\Big]\Big[\frac{\partial T_p(x,t)}{\partial x} - \frac{\partial T_p^*(x)}{\partial x}\Big]dx \\ &-[\xi N(t) - \xi N^*] \int_0^{l^*} \Big[T_p(x,t) - T_p^*(x)\Big]\frac{\partial T_p(x,t)}{\partial x}dx \\ -\xi N(t) &\int_{l^*}^{l(t)} T_p(x,t)\frac{\partial T_p(x,t)}{\partial x}dx + \xi N^* \int_{l^*}^{l(t)} T_p(x,t)\frac{\partial T_p^*(x)}{\partial x}dx \\ &+\beta_1[N^2(t) - N^{*2}] \int_0^{l^*} \Big[T_p(x,t) - T_p^*(x)\Big]dx \\ +\beta_1[N^2(t) - N^{*2}] &\int_{l^*}^{l(t)} T_p(x,t)dx - \beta_2 \int_0^{l^*} \Big[T_p(x,t) - T_p^*(x)\Big]^2 dx \\ &-\beta_2 \int_{l^*}^{l(t)} T_p(x,t)\Big[T_p(x,t) - T_p^*(x)\Big]dx,\end{aligned} \tag{5.123}$$

Integrating the first term in equation (5.123) we have ,

$$\begin{aligned}\dot{V_{p2}} = &-\xi N^* \Big[T_p(l^*,t) - T_p^*(l^*)\Big]^2 + \xi N^* \Big[T_p(0,t) - T_p^*(0)\Big]^2 \\ &-[\xi N(t) - \xi N^*] \int_0^{l^*} \Big[T_p(x,t) - T_p^*(x)\Big]\frac{\partial T_p(x,t)}{\partial x}dx \\ -\xi N(t) &\int_{l^*}^{l(t)} T_p(x,t)\frac{\partial T_p(x,t)}{\partial x}dx + \xi N^* \int_{l^*}^{l(t)} T_p(x,t)\frac{\partial T_p^*(x)}{\partial x}dx \\ &+\beta_1[N^2(t) - N^{*2}] \int_0^{l^*} \Big[T_p(x,t) - T_p^*(x)\Big]dx \\ +\beta_1[N^2(t) - N^{*2}] &\int_{l^*}^{l(t)} T_p(x,t)dx - \beta_2 \int_0^{l^*} \Big[T_p(x,t) - T_p^*(x)\Big]^2 dx \\ &-\beta_2 \int_{l^*}^{l(t)} T_p(x,t)\Big[T_p(x,t) - T_p^*(x)\Big]dx,\end{aligned} \tag{5.124}$$

adding and subtracting $\xi N^* T_p(x,t)\frac{\partial T_p(x,t)}{\partial x}$ in the fourth term from equation (5.124)

$$\begin{aligned}\dot{V_{p2}} = &-\xi N^* \Big[T_p(l^*,t) - T_p^*(l^*)\Big]^2 + \xi N^* \Big[T_p(0,t) - T_p^*(0)\Big]^2 \\ &-\Big[\xi N(t) - \xi N^*\Big] \int_0^{l^*} \Big[T_p(x,t) - T_p^*(x)\Big]\frac{\partial T_p(x,t)}{\partial x}dx \\ -\Big[\xi N(t) - \xi N^*\Big] &\int_{l^*}^{l(t)} T_p(x,t)\frac{\partial T_p(x,t)}{\partial x}dx - \xi N^* \int_{l^*}^{l(t)} T_p(x,t)\Big[\frac{\partial T_p(x,t)}{\partial x} - \frac{\partial T_p^*(x)}{\partial x}\Big]dx \\ &-\beta_2 \int_0^{l^*} \Big[T_p(x,t) - T_p^*(x)\Big]^2 dx - \beta_2 \int_{l^*}^{l(t)} T_p(x,t)\Big[T_p(x,t) - T_p^*(x)\Big]dx \\ &+\beta_1[N^2(t) - N^{*2}] \int_{l^*}^{l(t)} T_p(x,t)dx + \beta_1[N^2(t) - N^{*2}] \int_0^{l^*} \Big[T_p(x,t) - T_p^*(x)\Big]dx\end{aligned} \tag{5.125}$$

And, finally:

$$\begin{aligned}\dot{V}_{p2} = -\xi N^*[T_p(l^*,t) - T_p^*(l^*)]^2 + \xi N^*[T_p(0,t) - T_p^*(0)]^2 \\ -\xi N^* \int_{l^*}^{l(t)} T_p(x,t)\Big[\frac{\partial T_p(x,t)}{\partial x} - \frac{\partial T_p^*(x)}{\partial x}\Big]dx - \beta_2 \int_0^{l^*} \Big[T_p(x,t) - T_p^*(x)\Big]^2 dx \\ -\beta_2 \int_{l^*}^{l(t)} T_p(x,t)\Big[T_p(x,t) - T_p^*(x)\Big]dx + \Delta_{p2}(t),\end{aligned} \tag{5.126}$$

where,

$$\begin{aligned}\Delta_{p2}(t) = -\Big[\xi N(t) - \xi N^*\Big] \int_0^{l^*} \Big[T_p(x,t) - T_p^*(x)\Big]\frac{\partial T_p(x,t)}{\partial x}dx \\ -\Big[\xi N(t) - \xi N^*\Big] \int_{l^*}^{l(t)} T_p(x,t)\frac{\partial T_p(x,t)}{\partial x}dx \\ +\beta_1[N^2(t) - N^{*2}] \int_{l^*}^{l(t)} T_p(x,t)dx + \beta_1[N^2(t) - N^{*2}] \int_0^{l^*} \Big[T_p(x,t) - T_p^*(x)\Big]dx.\end{aligned} \tag{5.127}$$

The first and fourth terms in equation (5.126) are always negative since β_1, ξ and N^* are always positive. Recalling, $\Delta_{p2}(t)$ from equation (5.127) it is worth to point out that it is related to the difference between the input screw speed $N(t)$ and the set-point screw speed N^*. As stated before, further details regarding the stability of T will be discussed in detail at the end of this section.

5.3.3.3.2 Analysis of $\dot{V}_f$

Analyzing $\dot{V}_f$ which belongs to the *FFZ*:

$$\dot{V}_f = \int_0^L [\overline{k}(l(t))T_f(x,t) - \overline{k}(l^M(t))T_f^*(x)]\frac{\partial T_f(x,t)}{\partial t}dx \tag{5.128}$$

Replacing $\frac{\partial T_f(x,t)}{\partial t}$ from equation (5.45):

$$\begin{aligned}\dot{V}_f = \int_0^L \Big[\overline{k}(l(t))T_f(x,t) - \overline{k}(l^M(t))T_f^*(x)\Big]\Big[- \frac{F_d(t,l(t))\xi}{\rho_0 V_{eff}}\frac{\partial T_f(x,t)}{\partial x} \\ +\Omega(f_f, T_f, N, T_b)\Big]dx,\end{aligned} \tag{5.129}$$

adding and subtracting $\frac{F_d^*(l^*)\xi}{\rho_0 V_{eff}}\frac{\partial T_f(x,t)}{\partial x}$

$$\dot{V}_f = \int_0^L \left[\overline{k}(l(t))T_f(x,t) - \overline{k}(l^M(t))T_f^*(x)\right] \left[-\left[\frac{F_d(t,l(t))\xi}{\rho_0 V_{eff}} - \frac{F_d^*(l^*)\xi}{\rho_0 V_{eff}}\right]\frac{\partial T_f(x,t)}{\partial x} - \frac{F_d^*(l^*)\xi}{\rho_0 V_{eff}}\frac{\partial T_f(x,t)}{\partial x} + \Omega(f_f, T_f, N, T_b)\right] dx, \tag{5.130}$$

adding and subtracting $\frac{F_d^*(l^*)\xi}{\rho_0 V_{eff}}\frac{\partial T_f^*(x)}{\partial x}$ in the right term from equation (5.130):

$$\dot{V}_f = \int_0^L \left[\overline{k}(l(t))T_f(x,t) - \overline{k}(l^M(t))T_f^*(x)\right] \Big[-\nu_1[F_d(t,l(t)) - F_d^*(l^*)]\frac{\partial T_f(x,t)}{\partial x} - \nu_1 F_d^*(l^*)\Big[\frac{\partial T_f(x,t)}{\partial x} - \frac{\partial T_f^*(x)}{\partial x}\Big] - \nu_1 F_d^*(l^*)\frac{\partial T_f^*(x)}{\partial x} + \Omega(f_f, T_f, N, T_b)\Big] dx. \tag{5.131}$$

with,

$$\nu_1 = \frac{\xi}{\rho_0 V_{eff}}. \tag{5.132}$$

From the steady state, it is possible to have:

$$\frac{\partial T_f^*(x)}{\partial x} = \frac{\rho_0 V_{eff}}{F_d^*(l^*)\xi}\Omega(f_f^*, T_f^*, N^*, T_b^*). \tag{5.133}$$

Then,

$$\dot{V}_f = \int_0^L \left[\overline{k}(l(t))T_f(x,t) - \overline{k}(l^M(t))T_f^*(x)\right] \Big[-\nu_1[F_d(t,l(t)) - F_d^*(l^*)]\frac{\partial T_f(x,t)}{\partial x} - \nu_1 F_d^*(l^*)\Big[\frac{\partial T_f(x,t)}{\partial x} - \frac{\partial T_f^*(x)}{\partial x}\Big] - \Omega(f_f^*, T_f^*, N^*, T_b^*) + \Omega(f_f, T_f, N, T_b)\Big] dx. \tag{5.134}$$

Taking into account the definition of Ω_f from equation(2.55) with constant viscosity and $T_b(x,t) = T_b^*(x)$,

$$\dot{V}_f = \int_0^L \left[\overline{k}(l(t))T_f(x,t) - \overline{k}(l^M(t))T_f^*(x)\right] \Big[-\nu_1[F_d(t,l(t))F_d^*(l^*)]\frac{\partial T_f(x,t)}{\partial x} - \nu_1 F_d^*(l^*)\Big[\frac{\partial T_f(x,t)}{\partial x} - \frac{\partial T_f^*(x)}{\partial x}\Big] + \beta_3[N^2(t) - N^{*2}] - \beta_2(T_f(x,t) - T_f^*(x))\Big] dx, \tag{5.135}$$

with,

$$\beta_3 = \frac{\mu\eta_f}{\rho_0 V_{eff} C_p}. \tag{5.136}$$

Then, distributing equation (5.135),

$$\begin{aligned}\dot{V}_f = &-\nu_1[F_d(t,l(t)) - F_d^*(l^*)]\int_0^L \Big[\overline{k}(l(t))T_f(x,t) - \overline{k}(l^M(t))T_f^*(x)\Big]\frac{\partial T_f(x,t)}{\partial x}dx \\ &-\nu_1 F_d^*(l^*)\int_0^L \Big[\overline{k}(l(t))T_f(x,t) - \overline{k}(l^M(t))T_f^*(x)\Big]\Big[\frac{\partial T_f(x,t)}{\partial x} - \frac{\partial T_f^*(x)}{\partial x}\Big]dx \\ &+\beta_3[N^2(t) - N^{*2}]\int_0^L \Big[\overline{k}(l(t))T_f(x,t) - \overline{k}(l^M(t))T_f^*(x)\Big]dx \\ &-\beta_2\int_0^L \Big[\overline{k}(l(t))T_f(x,t) - \overline{k}(l^M(t))T_f^*(x)\Big]\Big[T_f(x,t) - T_f^*(x)\Big]dx.\end{aligned} \tag{5.137}$$

Then, two different cases should be considered $l(t) \geq l^*$ and $l(t) < l^*$. That means $\dot{V_{f1}}$ and $\dot{V_{f2}}$ respectively:

i. When $l(t) \geq l^*$, it is possible to write $\dot{V_{f1}}$ as it follows:

$$\begin{aligned}\dot{V_{f1}} = &-\nu_1 F_d^*(l^*)\int_{l(t)}^L [T_f(x,t) - T_f^*(x)]\Big[\frac{\partial T_f(x,t)}{\partial x} - \frac{\partial T_f^*(x)}{\partial x}\Big]dx \\ &-\nu_1[F_d(t,l(t)) - F_d^*(l^*)]\int_{l(t)}^L [T_f(x,t) - T_f^*(x)]\frac{\partial T_f(x,t)}{\partial x}dx \\ &+\beta_3[N^2(t) - N^{*2}]\int_{l(t)}^L [T_f(x,t) - T_f^*(x)]dx - \beta_2\int_{l(t)}^L [T_f(x,t) - T_f^*(x)]^2 dx.\end{aligned} \tag{5.138}$$

Integrating when possible

$$\begin{aligned}\dot{V_{f1}} = &-\nu_1 F_d^*(l^*)[T_f(L,t) - T_f^*(L)]^2 + \nu_1 F_d^*(l^*)[T_f(l(t),t) - T_f^*(l(t))]^2 \\ &-\nu_1[F_d(t,l(t)) - F_d^*(l^*)]\int_{l(t)}^L [T_f(x,t) - T_f^*(x)]\frac{\partial T_f(x,t)}{\partial x}dx \\ &+\beta_3[N^2(t) - N^{*2}]\int_{l(t)}^L [T_f(x,t) - T_f^*(x)]dx - \beta_2\int_{l(t)}^L [T_f(x,t) - T_f^*(x)]^2 dx.\end{aligned} \tag{5.139}$$

And, finally:

$$\begin{aligned}\dot{V_{f1}} = &-\nu_1 F_d^*(l^*)[T_f(L,t) - T_f^*(L)]^2 + \nu_1 F_d^*(l^*)[T_f(l(t),t) - T_f^*(l(t))]^2 \\ &-\beta_2\int_{l(t)}^L \Big[T_f(x,t) - T_f^*(x)\Big]^2 dx + \Delta_{f1}(t),\end{aligned} \tag{5.140}$$

where,

$$\Delta_{f1}(t) = -\nu_1[F_d(t,l(t)) - F_d^*(l^*)]\int_{l(t)}^{L}[T_f(x,t) - T_f^*(x)]\frac{\partial T_f(x,t)}{\partial x}dx + \beta_3[N^2(t) - N^{*2}]\int_{l(t)}^{L}[T_f(x,t) - T_f^*(x)]dx. \tag{5.141}$$

By analyzing equation (5.140) it is clear that the first term is always negative since ν_1 is always positive. In addition, the third term in equation (5.140) is always negative since β_2 is always positive. Recalling $\Delta_{f1}(t)$ from equation (5.141), then it is possible to note that it is related to the difference between the input screw speed $N(t)$ and the set-point screw speed N^*. Also note that the term $[F_d(t,l(t)) - F_d^*(l^*)]$ is related to the difference of the estimated interface position $l(t)$ and the set-point value of the interface l^*.

ii. On the other hand, when $l(t) < l^*$, then $l^M(t) = max(l(t), l^*) = l^*$. Therefore $\dot{V_{f2}}$ can be written as follows:

$$\begin{aligned}\dot{V_{f2}} = &-\nu_1[F_d(t,l(t)) - F_d^*(l^*)]\int_0^L[\overline{k}(l(t))T_f(x,t) - \overline{k}(l^*)T_f^*(x)]\frac{\partial T_f(x,t)}{\partial x}dx \\ &-\nu_1 F_d^*(l^*)\int_0^L[\overline{k}(l(t))T_f(x,t) - \overline{k}(l^*)T_f^*(x)]\Big[\frac{\partial T_f(x,t)}{\partial x} - \frac{\partial T_f^*(x)}{\partial x}\Big]dx \\ &+\beta_3\int_0^L[\overline{k}(l(t))T_f(x,t) - \overline{k}(l^*)T_f^*(x)][N^2(t) - N^{*2}]dx \\ &-\beta_2\int_0^L[\overline{k}(l(t))T_f(x,t) - \overline{k}(l^*)T_f^*(x)][T_f(x,t) - T_f^*(x)]dx,\end{aligned} \tag{5.142}$$

distributing

$$\begin{aligned}\dot{V_{f2}} = &-\nu_1 F_d^*(l^*)\int_{l(t)}^{L}[T_f(x,t) - T_f^*(x)]\Big[\frac{\partial T_f(x,t)}{\partial x} - \frac{\partial T_f^*(x)}{\partial x}\partial x\Big]dx \\ &-\nu_1[F_d(t,l(t)) - F_d^*(l^*)]\int_{l(t)}^{L}[T_f(x,t) - T_f^*(x)]\frac{\partial T_f(x,t)}{\partial x}dx \\ &+\nu_1 F_d^*(l^*)\int_{l(t)}^{l^*}T_f(x,t)\frac{\partial T_f^*(x)}{\partial x}dx - \nu_1 F_d(t,l(t))\int_{l(t)}^{l^*}T_f(x,t)\frac{\partial T_f(x,t)}{\partial x}dx \\ &+\beta_3[N^2(t) - N^{*2}]\int_{l^*}^{L}[T_f(x,t) - T_f^*(x)]dx + \beta_3[N^2(t) - N^{*2}]\int_{l(t)}^{l^*}(T_f(x,t)dx \\ &-\beta_2\int_{l^*}^{L}[T_f(x,t) - T_f^*(x)]^2dx - \beta_2\int_{l^*}^{L}[T_f(x,t) - T_f^*(x)]T_f(x,t)dx.\end{aligned} \tag{5.143}$$

By integrating the first term from equation (5.143) we have:

$$\begin{aligned}\dot{V_{f2}} = &-\nu_1 F_d^*(l^*)[T_f(L,t) - T_f^*(L)]^2 + \nu_1 F_d^*(l^*)[T_f(l^*,t) - T_f^*(l^*)]^2 \\ &-\nu_1[F_d(t,l(t)) - F_d^*(l^*)]\int_{l(t)}^{L}[T_f(x,t) - T_f^*(x)]\frac{\partial T_f(x,t)}{\partial x}dx \\ &+\nu_1 F_d^*(l^*)\int_{l(t)}^{l^*} T_f(x,t)\frac{\partial T_f^*(x)}{\partial x}dx - \nu_1 F_d(t,l(t))\int_{l(t)}^{l^*} T_f(x,t)\frac{\partial T_f(x,t)}{\partial x}dx \\ &+\beta_3[N^2(t) - N^{*2}]\int_{l^*}^{L}[(T_f(x,t) - T_f^*(x)]dx + \beta_3[N^2(t) - N^{*2}]\int_{l(t)}^{l^*}(T_f(x,t)dx \\ &-\beta_2\int_{l^*}^{L}[T_f(x,t) - T_f^*(x)]^2dx - \beta_2\int_{l^*}^{L}[T_f(x,t) - T_f^*(x)]T_f(x,t)dx,\end{aligned} \tag{5.144}$$

adding and subtracting $\nu_1 F_d^*(l^*)T_f(x,t)\frac{\partial T_f(x,t)}{\partial x}$:

$$\begin{aligned}\dot{V_{f2}} = &-\nu_1 F_d^*(l^*)[T_f(L,t) - T_f^*(L)]^2 + \nu_1 F_d^*(l^*)[T_f(l^*,t) - T_f^*(l^*)]^2 \\ &-\nu_1[F_d(t,l(t)) - F_d^*(l^*)]\int_{l(t)}^{L}[T_f(x,t) - T_f^*(x)]\frac{\partial T_f(x,t)}{\partial x}dx \\ &-\nu_1[F_d(t,l(t) - F_d^*(l^*)]\int_{l(t)}^{L} T_f(x,t)\frac{\partial T_f(x,t)}{\partial x}dx \\ &-\nu_1 F_d^*(l^*)\int_{l(t)}^{l^*} T_f(x,t)\Big[\frac{\partial T_f(x,t)}{\partial x} - \frac{\partial T_f^*(x)}{\partial x}\Big]dx \\ &+\beta_3[N^2(t) - N^{*2}]\int_{l^*}^{L}[T_f(x,t) - T_f^*(x)]dx + \beta_3[N^2(t) - N^{*2}]\int_{l(t)}^{l^*}(T_f(x,t)dx \\ &-\beta_2\int_{l^*}^{L}[T_f(x,t) - T_f^*(x)]^2dx - \beta_2\int_{l^*}^{L}[T_f(x,t) - T_f^*(x)]T_f(x,t)dx.\end{aligned} \tag{5.145}$$

And, finally:

$$\begin{aligned}\dot{V_{f2}} = &-\nu_1 F_d^*(l^*)[T_f(L,t) - T_f^*(L)]^2 + \nu_1 F_d^*(l^*)[T_f(l^*,t) - T_f^*(l^*)]^2 \\ &-\beta_2\int_{l^*}^{L}[T_f(x,t) - T_f^*(x)]^2dx - \nu_1 F_d^*(l^*)\int_{l(t)}^{l^*} T_f(x,t)\Big[\frac{\partial T_f(x,t)}{\partial x} - \frac{\partial T_f^*(x)}{\partial x}\Big]dx \\ &-\beta_2\int_{l^*}^{L}[T_f(x,t) - T_f^*(x)]T_f(x,t)dx + \Delta_{f2}(t),\end{aligned} \tag{5.146}$$

where,

$$\Delta_{f2}(t) = -\nu_1[F_d(t,l(t)) - F_d^*(l^*)]\int_{l(t)}^{L}[T_f(x,t) - T_f^*(x)]\frac{\partial T_f(x,t)}{\partial x}dx$$
$$-\nu_1[F_d(t,l(t)) - F_d^*(l^*)]\int_{l(t)}^{L}T_f(x,t)\frac{\partial T_f(x,t)}{\partial x}dx$$
$$+\beta_3[N^2(t) - N^{*2}]\int_{l^*}^{L}[(T_f(x,t) - T_f^*(x)]dx + \beta_3[N^2(t) - N^{*2}]\int_{l(t)}^{l^*}T_f(x,t)dx \tag{5.147}$$

By analyzing equation (5.146) it is clear that the first and fourth terms are always negative since ν_1 is always positive. In addition, the third and fifth terms in equation (5.146) are always negative since β_2 is always positive. Recalling $\Delta_{f2}(t)$ from equation (5.147), then it is possible to note that it is related to the difference between the input screw speed $N(t)$ and the set-point screw speed N^*. Also recall that, the term $[F_d(t,l(t)) - F_d^*(l^*)]$ is related to the difference of the estimated interface position $l(t)$ and the set-point value of the interface l^*.

5.3.3.3.3 Analysis of $\dot{V}_i$

Finally, we have for $\dot{V}_i$:

$$\dot{V}_i = -\int_0^L k(l(t))\overline{k}(l^*)T_f^*(x)\tfrac{\partial T_p(x,t)}{\partial t} + k(l^*)\overline{k}(l(t))T_p^*(x)\tfrac{\partial T_f(x,t)}{\partial t}dx. \tag{5.148}$$

Three different cases should be considered: $l(t) = l^*$, $l(t) < l^*$ and $l(t) > l^*$. That means $\dot{V}_{i1}$, $\dot{V}_{i2}$ and $\dot{V}_{i3}$ respectively:

i. When $l(t) = l^*$

$$\dot{V}_{i1} = 0 \tag{5.149}$$

ii. When $l(t) < l^*$

$$\dot{V}_{i2} = -\int_0^L [k(l^*) - k(l(t))]T_p^*(x)\tfrac{\partial T_f(x,t)}{\partial t}dx. \tag{5.150}$$

Then,

$$\dot{V}_{i2} = -\int_{l(t)}^{l^*} T_p^*(x)\tfrac{\partial T_f(x,t)}{\partial t}dx. \tag{5.151}$$

Replacing $\frac{\partial T_f(x,t)}{\partial t}$ from equation (5.45) and taking into account the deffinition of ν_1 from equation (5.132):

$$\dot{V}_{i2} = -\int_{l(t)}^{l^*} T_p^*(x)\Big[-\nu_1 F_d(t,l(t))\frac{\partial T_f(x,t)}{\partial x} + \Omega(f_f, T_f, N, T_b)\Big]dx. \tag{5.152}$$

Adding and subtracting $\nu_1 F_d^*(l^*)\frac{\partial T_f(x,t)}{\partial x}$ to the right term of equation (5.152)

$$\dot{V}_{i2} = -\int_{l(t)}^{l^*} T_p^*(x)\Big[-\nu_1[F_d(t,l(t)) - F_d^*(l^*)]\frac{\partial T_f(x,t)}{\partial x} - \nu_1 F_d^*(l^*)\frac{\partial T_f(x,t)}{\partial x} + \Omega(f_f, T_f, N, T_b)\Big]dx, \tag{5.153}$$

adding and subtracting $\nu_1 F_d^*(l^*)\frac{\partial T_f^*(x)}{\partial x}$ to the right term of equation (5.153)

$$\dot{V}_{i2} = -\int_{l(t)}^{l^*} T_p^*(x)\Big[-\nu_1\Big[F_d(t,l(t)) - F_d^*(l^*)\Big]\frac{\partial T_f(x,t)}{\partial x} - \nu_1 F_d^*(l^*)\Big[\frac{\partial T_f(x,t)}{\partial x} - \frac{\partial T_f^*(x)}{\partial x}\Big] - \nu_1 F_d^*(l^*)\frac{\partial T_f^*(x)}{\partial x} + \Omega(f_f, T_f, N, T_b)\Big]dx, \tag{5.154}$$

From the steady state, it is possible to have:

$$\frac{\partial T_f^*(x)}{\partial x} = \frac{\rho_0 V_{eff}}{F_d^*(l^*)\xi}\Omega(f_f^*, T_f^*, N^*, T_b^*). \tag{5.155}$$

then,

$$\dot{V}_{i2} = -\int_{l(t)}^{l^*} T_p^*(x)\Big[-\nu_1[F_d(t,l(t)) - F_d^*(l^*)]\frac{\partial T_f(x,t)}{\partial x} - \nu_1 F_d^*(l^*)\Big[\frac{\partial T_f(x,t)}{\partial x} - \frac{\partial T_f^*(x)}{\partial x}\Big] - \Omega(f_f^*, T_f^*, N^*, T_b^*) + \Omega(f_f, T_f, N, T_b)\Big]dx, \tag{5.156}$$

Taking into account the definition of Ω_f from equation(2.55) with constant viscosity and $T_b(x,t) = T_b^*(x)$,

$$\dot{V}_{i2} = \int_{l(t)}^{l^*} T_p^*(x)\Big[\nu_1[F_d(t,l(t)) - F_d^*(l^*)]\frac{\partial T_f(x,t)}{\partial x} + \nu_1 F_d^*(l^*)\Big[\frac{\partial T_f(x,t)}{\partial x} - \frac{\partial T_f^*(x)}{\partial x}\Big] - \beta_3[N^2(t) - N^{*2}] + \beta_2[T_f(x,t) - T_f^*(x)]\Big]dx. \tag{5.157}$$

Finally, distributing in order to have:

$$\begin{aligned}\dot{V}_{i2} = \nu_1 F_d^*(l^*)\int_{l(t)}^{l^*} T_p^*(x)\Big[\frac{\partial T_f(x,t)}{\partial x} - \frac{\partial T_f^*(x)}{\partial x}\Big]dx \\ +\beta_2\int_{l(t)}^{l^*} T_p^*(x)[T_f(x,t) - T_f^*(x)]dx + \Delta_{i2}(t).\end{aligned} \tag{5.158}$$

with

$$\begin{aligned}\Delta_{i2}(t) = \nu_1[F_d(t,l(t)) - F_d^*(l^*)] \int_{l(t)}^{l^*} T_p^*(x)\frac{\partial T_f(x,t)}{\partial x}dx \\ -\beta_3[N^2(t) - N^{*2}] \int_{l(t)}^{l^*} T_p^*(x)dx\end{aligned} \tag{5.159}$$

Analyzing equation (5.157)

iii. When $l(t) > l^*$

$$\dot{V_{i3}} = -\int_0^L [k(l(t)) - k(l^*)]T_f^*(x)\tfrac{\partial T_p(x,t)}{\partial t}dx. \tag{5.160}$$

Then,

$$\dot{V_{i3}} = -\int_{l^*}^{l(t)} T_f^*(x)\tfrac{\partial T_p(x,t)}{\partial t}dx. \tag{5.161}$$

Replacing $\frac{\partial T_p(x,t)}{\partial t}$ from equation (5.44):

$$\dot{V_{i3}} = -\int_{l^*}^{l(t)} T_f^*(x)\Big[-\xi N(t)\frac{\partial T_p(x,t)}{\partial x} + \Omega(f_p, T_p, N, T_b)\Big]dx. \tag{5.162}$$

Adding and subtracting $\xi N^* \frac{\partial T_p(x,t)}{\partial x}$ to the right term of equation (5.162):

$$\begin{aligned}\dot{V_{i3}} = -\int_{l^*}^{l(t)} T_f^*(x)\Big[-[\xi N(t) - \xi N^*]\frac{\partial T_p(x,t)}{\partial t} - \xi N^*\frac{\partial T_p(x,t)}{\partial x} \\ +\Omega(f_p, T_p, N, T_b)\Big]dx.\end{aligned} \tag{5.163}$$

Adding and subtracting $\xi N^* \frac{\partial T_p^*(x)}{\partial x}$ to the right term of equation (5.163):

$$\begin{aligned}\dot{V_{i3}} = -\int_{l^*}^{l(t)} T_f^*(x)\Big[-[\xi N(t) - \xi N^*]\frac{\partial T_p(x,t)}{\partial t} - \xi N^*\Big[\frac{\partial T_p(x,t)}{\partial x} - \frac{\partial T_p^*(x)}{\partial x}\Big] \\ -\xi N^*\frac{\partial T_p^*(x)}{\partial x} + \Omega(f_p, T_p, N, T_b)\Big]dx.\end{aligned} \tag{5.164}$$

Taking into account the steady state of the temperature at the *PFZ* and the definition of Ω_p from equation(2.53) with constant viscosity and $T_b(x,t) = T_b^*(x)$,

$$\begin{aligned}\dot{V_{i3}} = -\int_{l^*}^{l(t)} T_f^*(x)\Big[-[\xi N(t) - \xi N^*]\frac{\partial T_p(x,t)}{\partial t} - \xi N^*\Big[\frac{\partial T_p(x,t)}{\partial x} - \frac{\partial T_p^*(x)}{\partial x}\Big] \\ -\beta_2[T_p(x,t) - T_p^*(x)] + \beta_1[N^2(t) - N^{*2}]\Big]dx.\end{aligned} \tag{5.165}$$

Finally, distributing in order to have:

$$\begin{aligned}\dot{V_{i3}} = \xi N^* \int_{l^*}^{l(t)} T_f^*(x)\Big[\frac{\partial T_p(x,t)}{\partial x} - \frac{\partial T_p^*(x)}{\partial x}\Big]dx \\ +\beta_2 \int_{l^*}^{l(t)} T_f^*(x)[T_p(x,t) - T_p^*(x)]dx + \Delta_{i3},\end{aligned} \tag{5.166}$$

with,

$$\Delta_{i3}(t) = [\xi N(t) - \xi N^*] \int_{l^*}^{l(t)} T_f^*(x)\frac{\partial T_p(x,t)}{\partial t}dx - \beta_1[N^2(t) - N^{*2}] \int_{l^*}^{l(t)} T_f^*(x)dx. \tag{5.167}$$

5.3.3.3.4 Summary

Summarizing, it is possible to analyze the results presented in this section for three different cases of the moving interface, i.e. $l(t) = l^*$, $l(t) < l^*$ and $l(t) > l^*$:

- **Case 1:** Where $l(t) = l^*$, therefore $\dot{V}_1 = \dot{V_{p1}} + \dot{V_{f1}} + \dot{V_{i1}}$:

$$\begin{cases} \dot{V_{p1}} = -\xi N^*[T_p(l(t),t) - T_p^*(l(t))]^2 + \xi N^*[T_p(0,t) - T_p^*(0)]^2 \\ -\beta_2 \int_0^{l(t)} [T_p(x,t) - T_p^*(x)]^2 dx + \Delta_{p1}(t) \\ \\ \dot{V_{f1}} = -\nu_1 F_d^*(l^*)[T_f(L,t) - T_f^*(L)]^2 + \nu_1 F_d^*(l^*)[T_f(l(t),t) - T_f^*(l(t))]^2 \\ -\beta_2 \int_{l(t)}^{L} \Big[T_f(x,t) - T_f^*(x)\Big]^2 dx + \Delta_{f1}(t) \\ \\ \dot{V_{i1}} = 0. \end{cases} \tag{5.168}$$

Where,

$$\begin{aligned}\Delta_{p1}(t) = -[\xi N(t) - \xi N^*] \int_0^{l(t)} \Big[T_p(x,t) - T_p^*(x)\Big]\frac{\partial T_p(x,t)}{\partial x}dx \\ +\beta_1[N^2(t) - N^{*2}] \int_0^{l(t)} [T_p(x,t) - T_p^*(x)]dx\end{aligned} \tag{5.169}$$

$$\begin{aligned}\Delta_{f1}(t) = -\nu_1[F_d(t,l(t)) - F_d^*(l^*)] \int_{l(t)}^{L} [T_f(x,t) - T_f^*(x)]\frac{\partial T_f(x,t)}{\partial x}dx \\ +\beta_3[N^2(t) - N^{*2}] \int_{l(t)}^{L} [T_f(x,t) - T_f^*(x)]dx.\end{aligned} \tag{5.170}$$

Due to asymptotic convergence of $U(t)$, f_p and $l(t)$ it is straightforward to see that $\Delta_{p1}(t) \to 0$ and $\Delta_{f1}(t) \to 0$ with asymptotic convergence as $t \to \infty$. Integrating

(5.168), the limit of the right hand side of

$$V_1(t) \leq V_1(0) + \int_0^t \Delta_{p1}(t) + \Delta_{f1}(t)dt \tag{5.171}$$

exists and is uniformly bounded and uniformly continuous. Then it is possible to say that $T_p(l(t),t)$ and $T_f(L,t)$ are bounded and $\dot{V}_1$ is uniformly bounded. Then, from Barbalat's lemma it follows that $\dot{V}_1 \to 0$ as $t \to \infty$.Then it follows from (5.168) that $T_p((l(t),t) \to T_p^*(l(t))$, $T_p((0,t) \to T_p^*(0)$,$T_f((l(t),t) \to T_f^*(l(t))$ and $T_f(L,t) \to T_f^*(L)$ as $t \to \infty$.

- **Case 2:** Where $l(t) < l^*$, therefore $\dot{V}_2 = \dot{V_{p1}} + \dot{V_{f2}} + \dot{V_{i2}}$:

$$\begin{cases} \dot{V_{p1}} = -\xi N^*[T_p(l(t),t) - T_p^*(l(t))]^2 + \xi N^*[T_p(0,t) - T_p^*(0)]^2 \\ -\beta_2 \int_0^{l(t)} [T_p(x,t) - T_p^*(x)]^2 dx + \Delta_{p1}(t), \\ \\ \dot{V_{f2}} = -\nu_1 F_d^*(l^*)[T_f(L,t) - T_f^*(L)]^2 + \nu_1 F_d^*(l^*)[T_f(l^*,t) - T_f^*(l^*)]^2 \\ -\beta_2 \int_{l^*}^{L} [T_f(x,t) - T_f^*(x)]^2 dx - \nu_1 F_d^*(l^*) \int_{l(t)}^{l^*} T_f(x,t) \Big[\frac{\partial T_f(x,t)}{\partial x} - \frac{\partial T_f^*(x)}{\partial x}\Big] dx \\ -\beta_2 \int_{l^*}^{L} [T_f(x,t) - T_f^*(x)] T_f(x,t) dx + \Delta_{f2}(t), \\ \\ \dot{V_{i2}} = \nu_1 F_d^*(l^*) \int_{l(t)}^{l^*} T_p^*(x) \Big[\frac{\partial T_f(x,t)}{\partial x} - \frac{\partial T_f^*(x)}{\partial x}\Big] dx \\ +\beta_2 \int_{l(t)}^{l^*} T_p^*(x)[T_f(x,t) - T_f^*(x)] dx + \Delta_{i2}(t). \end{cases} \tag{5.172}$$

where,

$$\begin{aligned} \Delta_{p1}(t) = -[\xi N(t) - \xi N^*] \int_0^{l(t)} \Big[T_p(x,t) - T_p^*(x)\Big] \frac{\partial T_p(x,t)}{\partial x} dx \\ +\beta_1 [N^2(t) - N^{*2}] \int_0^{l(t)} [T_p(x,t) - T_p^*(x)] dx, \end{aligned} \tag{5.173}$$

$$\begin{aligned} \Delta_{f2}(t) = -\nu_1 [F_d(t,l(t)) - F_d^*(l^*)] \int_{l(t)}^{L} [T_f(x,t) - T_f^*(x)] \frac{\partial T_f(x,t)}{\partial x} dx \\ -\nu_1 [F_d(t,l(t)) - F_d^*(l^*)] \int_{l(t)}^{L} T_f(x,t) \frac{\partial T_f(x,t)}{\partial x} dx \\ +\beta_3 \int_{l^*}^{L} [(T_f(x,t) - T_f^*(x)][N^2(t) - N^{*2}] dx + \beta_3 [N^2(t) - N^{*2}] \int_{l(t)}^{l^*} (T_f(x,t) dx. \end{aligned} \tag{5.174}$$

$$\begin{aligned}\Delta_{i2}(t) = \nu_1[F_d(t,l(t)) - F_d^*(l^*)]\int_{l(t)}^{l^*} T_p^*(x)\frac{\partial T_f(x,t)}{\partial x}dx \\ -\beta_3[N^2(t) - N^{*2}]\int_{l(t)}^{l^*} T_p^*(x)dx\end{aligned} \tag{5.175}$$

Due to asymptotic convergence of $U(t)$, f_p and $l(t)$ it is straightforward to see that $\Delta_{p1}(t) \to 0$, $\Delta_{f2}(t) \to 0$ and $\Delta_{i2}(t) \to 0$ with asymptotic convergence as $t \to \infty$. Integrating (5.172), the limit of the right hand side of

$$V_2(t) \leq V_2(0) + \int_0^t \Delta_{p1}(t) + \Delta_{f2}(t) + \Delta_{i2}(t)dt \tag{5.176}$$

exists and is uniformly bounded and uniformly continuous. Then it is possible to say that $T_p(l(t),t)$, $T_f(l^*,t)$ and $T_p(0,t)$ are bounded and $\dot{V}_2$ is uniformly bounded. Then, from Barbalat's lemma it follows that $\dot{V}_2 \to 0$ as $t \to \infty$. Then it follows from (5.172) that $T_p((l(t),t) \to T_p^*(l(t))$, $T_p((0,t) \to T_p^*(0)$,$T_f((L,t) \to T_f^*(L)$ and $T_f(l^*,t) \to T_f^*(l^*)$ as $t \to \infty$.

- **Case 3:** Where $l(t) > l^*$, therefore $\dot{V}_3 = \dot{V}_{p2} + \dot{V}_{f1} + \dot{V}_{i3}$:

$$\begin{cases} \dot{V}_{p2} = -\xi N^*[T_p(l^*,t) - T_p^*(l^*)]^2 + \xi N^*[T_p(0,t) - T_p^*(0)]^2 \\ -\xi N^* \int_{l^*}^{l(t)} T_p(x,t)\Big[\frac{\partial T_p(x,t)}{\partial x} - \frac{\partial T_p^*(x)}{\partial x}\Big]dx - \beta_2 \int_0^{l^*} \Big[T_p(x,t) - T_p^*(x)\Big]^2 dx \\ -\beta_2 \int_{l^*}^{l(t)} T_p(x,t)\Big[T_p(x,t) - T_p^*(x)\Big]dx + \Delta_{p2}(t) \\ \\ \dot{V}_{f1} = -\nu_1 F_d^*(l^*)[T_f(L,t) - T_f^*(L)]^2 + \nu_1 F_d^*(l^*)[T_f(l(t),t) - T_f^*(l(t))]^2 \\ -\beta_2 \int_{l(t)}^{L} \Big[T_f(x,t) - T_f^*(x)\Big]^2 dx + \Delta_{f1}(t) \\ \\ \dot{V}_{i3} = \xi N^* \int_{l^*}^{l(t)} T_f^*(x)\Big[\frac{\partial T_p(x,t)}{\partial x} - \frac{\partial T_p^*(x)}{\partial x}\Big]dx \\ +\beta_2 \int_{l^*}^{l(t)} T_f^*(x)[T_p(x,t) - T_p^*(x)]dx + \Delta_{i3}. \end{cases} \tag{5.177}$$

where,

$$\begin{aligned}\Delta_{p2}(t) = -\Big[\xi N(t) - \xi N^*\Big]\int_0^{l^*} \Big[T_p(x,t) - T_p^*(x)\Big]\frac{\partial T_p(x,t)}{\partial x}dx \\ -\Big[\xi N(t) - \xi N^*\Big]\int_{l^*}^{l(t)} T_p(x,t)\frac{\partial T_p(x,t)}{\partial x}dx \\ +\beta_1[N^2(t) - N^{*2}]\int_{l^*}^{l(t)} T_p(x,t)dx + \beta_1[N^2(t) - N^{*2}]\int_0^{l^*} \Big[T_p(x,t) - T_p^*(x)\Big]dx\end{aligned} \tag{5.178}$$

$$\Delta_{f1}(t) = -\nu_1[F_d(t, l(t)) - F_d^*(l^*)] \int_{l(t)}^{L} [T_f(x,t) - T_f^*(x)] \frac{\partial T_f(x,t)}{\partial x} dx + \beta_3[N^2(t) - N^{*2}] \int_{l(t)}^{L} [T_f(x,t) - T_f^*(x)] dx \tag{5.179}$$

$$\Delta_{i3}(t) = [\xi N(t) - \xi N^*] \int_{l^*}^{l(t)} T_f^*(x) \frac{\partial T_p(x,t)}{\partial t} dx - \beta_1[N^2(t) - N^{*2}] \int_{l^*}^{l(t)} T_f^*(x) dx. \tag{5.180}$$

Then, because of the asymptotic convergence of $U(t)$, f_p and $l(t)$ it is straightforward to see that $\Delta_{p2}(t) \to 0$, $\Delta_{f1}(t) \to 0$ and $\Delta_{i3}(t) \to 0$ with asymptotic convergence as $t \to \infty$.Integrating (5.177), the limit of the right hand side of

$$V_3(t) \leq V_3(0) + \int_0^t \Delta_{p2}(t) + \Delta_{f1}(t) + \Delta_{i3}(t) dt \tag{5.181}$$

exists and is uniformly bounded and uniformly continuous. Then $T_p(l(t), t)$, $T_f(l^*, t)$ and $T_p(0, t)$ are bounded and $\dot{V}_3$ is uniformly bounded. Then, from Barbalat's lemma it follows that $\dot{V}_3 \to 0$ as $t \to \infty$.Then it follows from (5.172) that $T_p((l^*, t) \to T_p^*(l^*)$, $T_p((0, t) \to T_p^*(0)$,$T_f((L, t) \to T_f^*(L)$ and $T_f(l(t), t) \to T_f^*(l(t))$ as $t \to \infty$.

5.3.4 Controller application to the extrusion process model

The implementation of the controller (5.64) was made using the following PID parameters:$K_p = 0.405$, $T_d = 49.380$ s and $T_i = 8.1 \times 10^3$ 1/s. These parameters were tunned using the Ziegler Nichols method [67]. The plant was simulated using the model of the extrusion process with its geometrical, thermal parameters and viscosity law as shown on Chapter 4. However, as stated before, the extrusion model with constant viscosity is used internally in the controller. The set-points used in this case are constant (time-invariant) temperature profiles obtained from open-loop simulations of the extrusion process model at a screw speed of 800 rpm as it is shown on Fig. 5.1 (red line). The initial temperature profile is also shown on the figure (black line), which corresponds to the steady state temperature profile at 500 rpm.

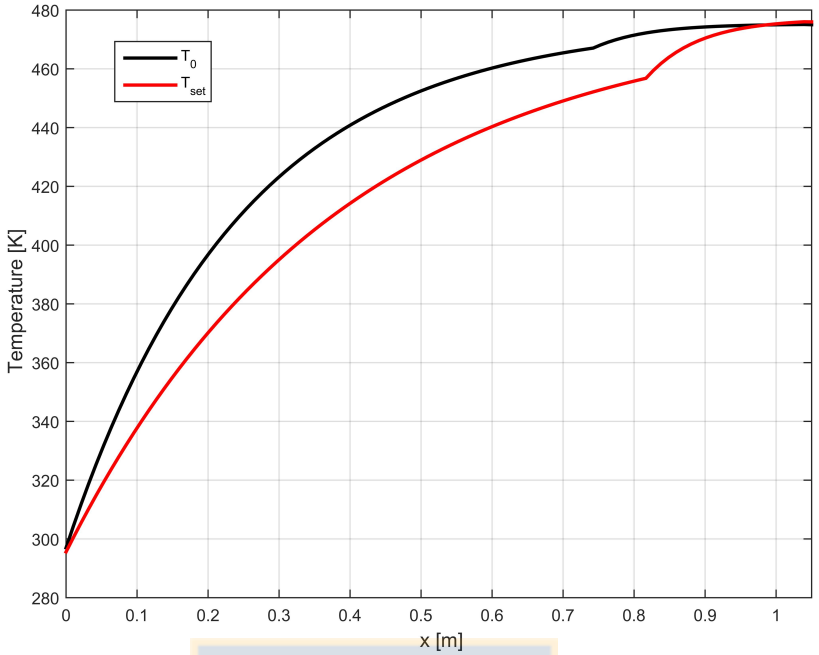

FIGURE 5.1: Temperature profiles used in this study for control purposes. (Source: Personal collection).

Time integration is performed with *Ode*113 routine of *Matlab*® and the plant is simulated using the extruder model with variable viscosity. On the other hand, the energy balance from equations (5.45) and (5.44) with constant viscosity is used internally in the controller.The simulation was made for a period of time of 200 s. The closed-loop starts 10 s after the beginning of the simulation with sampling interval of the control system of 2 s with given set-point temperature profile at 800 rpm. After 100 s of simulation the set-point changes to a new temperature profile at 500 rpm. The following initial conditions with an initial screw speed of $N_0 = 500$ rpm where used:

Initial Filling Ratio	$f_p^0 = 0.2888$
Initial interface Position	$l^0 = 0.7516$ m
Initial input Flow	$F_{in} = 5/3600$ kg/s

TABLE 5.1: Initial values for the simulation test with energy based control. (Source: Personal collection).

Fig. 5.2 shows the evolution of the screw speed according to the changes imposed by the controller while the energy reaches its set-point (Fig. 5.3). Note that the steady state is reached with the controller for both of the set-point profiles proving that it is able to accurately control the temperature and internal energy. In addition, Fig. 5.4 shows the evolution of the integral and proportional and derivative part of the controller during

the simulation period.

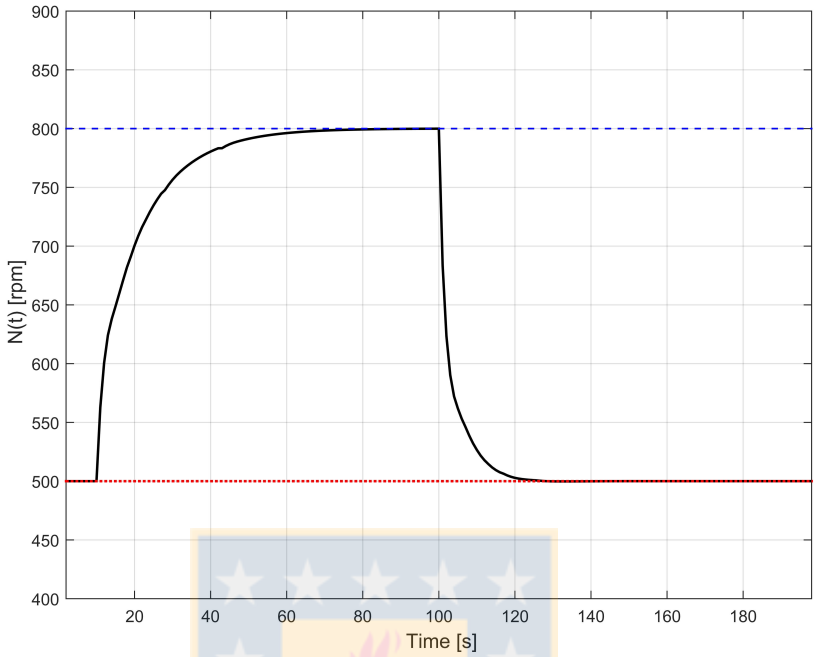

FIGURE 5.2: Screw speed evolution. (Source: Personal collection).

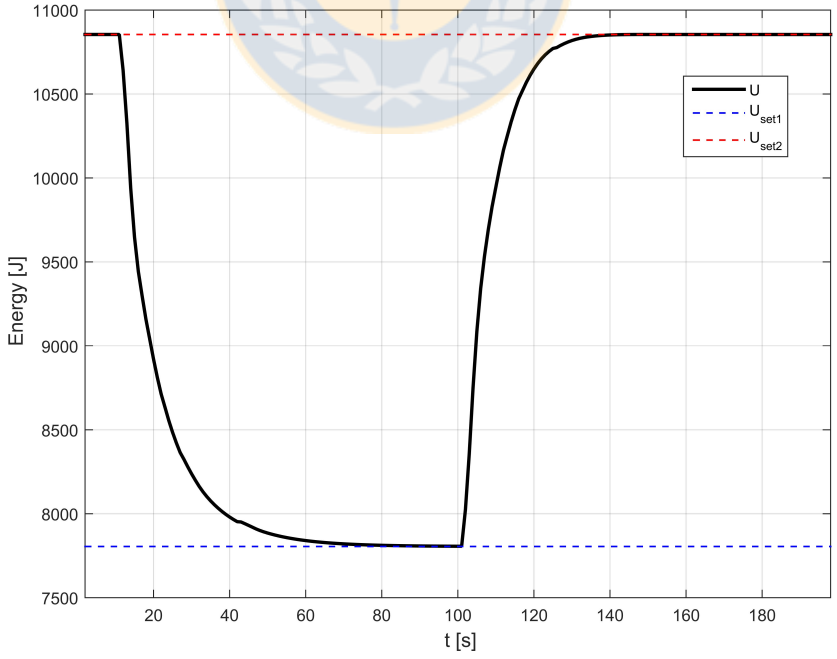

FIGURE 5.3: Internal energy evolution during simulation tests. (Source: Personal collection).

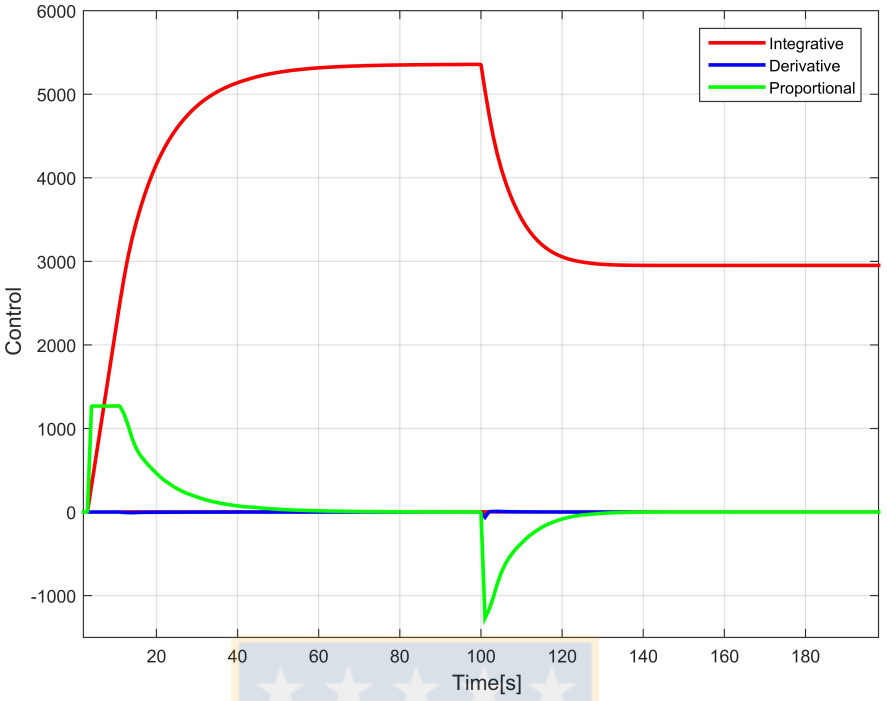

FIGURE 5.4: PID control evolution. (Source: Personal collection).

Fig. 5.5 shows the evolution of the melt temperature at $x_1 = 0.25$ m, $x_2 = 0.5$ m, $x_3 = 0.75$ m and $x_4 = 1.05$ m. Note that for all different positions, the temperature reaches its steady state according to the dynamics imposed by the controller. In addition Fig. 5.6 shows the evolution of the interface position, note that it reaches a steady state accordingly to the evolution of the controller input. The reached equilibrium of the interface position corresponds to the steady state at 800 rpm and 500 rpm. Both the controlled output (temperature along the extruder) and the set-point temperature (at 800 rpm) are shown on. It is clear from those results that the assumption of constant viscosity within the controller does not affect the closed-loop behaviour. Finally, Fig. 5.7 shows the evolution of the temperature along the extruder during fisrt 50 s of simulation, at $t_1 = 10$ s, $t_2 = 20$ s and $t_3 = 40$ s. Note that the control input adjust the temperature of the extruder according to the imposed set-point. In addition, it worth to point out that, even with the complexity of the process (highly nonlinear with moving interface), the controller reaches the set-point accurately in a relatively short time. On the other hand it is clear from the simulation results, that the moving interface, also reaches its equilibrium point thanks to the controller actions.

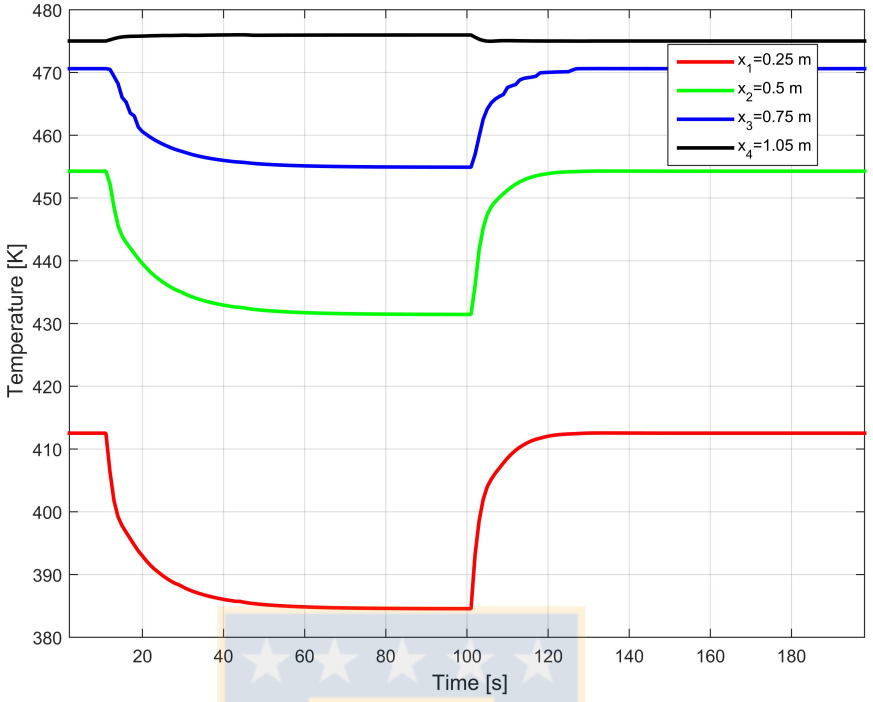

FIGURE 5.5: Temperature evolution along the extruder. (Source: Personal collection).

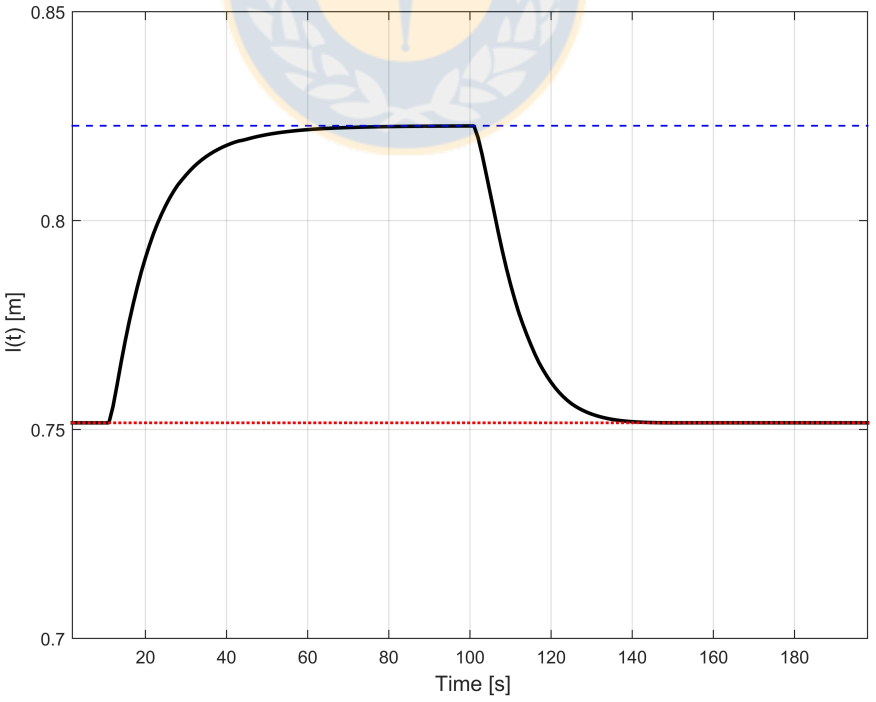

FIGURE 5.6: Interface evolution for the simulation period. (Source: Personal collection).

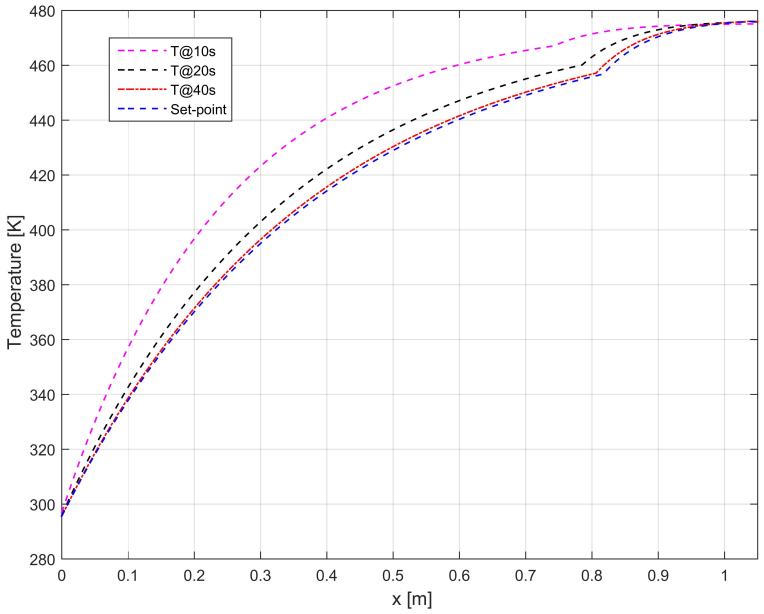

FIGURE 5.7: Evolution of the temperature on the extruder at different periods of time. (Source: Personal collection).

5.4 Summary

In this chapter an entropy balance for both sections of the extrusion process model (*PFZ* and *FFZ*) was presented. This could be the basis of control design based on the balance equation of an availability function which is derived from the entropy balance equation and can be applied for future works. In addition, an energy-based control for the experimentally verified bi-zone model of the extrusion of Polypropylene was presented together with a stability analysis for the interface position, the filling ratio and the melt temperature. The practical usefulness of the method is illustrated by a simulation example showing that it is possible to reach the desired set-point even with the assumption of constant viscosity internally in the controller. The suggested control law requires the computation of the internal energy which in turn requires the knowledge of the temperature and the filling ratio inside the extruder. An estimation of such variables remains as challenge for the control implementation. Therefore, further research could be related to the implementation of the proposed controller on an industrial type twin-screw extruder.

Chapter 6

Conclusions

6.1 General conclusion

This thesis focused on modelling and control of the twin-screw extrusion process. A distributed parameter bi-zone dynamic model with moving interface was presented. The interconnection of the moving interface was performed under the assumption of variable viscosity along the extruder. This assumption is important since, viscosity is well known for being temperature and shear rate dependent, therefore, the complexity of the model increases and new control strategies should be considered in order to deal with a highly nonlinear system. In addition, the moving interface was considered as another challenge in the modelling point of view because of the difficulties that arises with the discontinuity of the variables in the system. An energy-based control was proposed for this extrusion process model. This approach is useful since it allows simple and transparent tunning of the nonlinear controller through some PID parameters, and a stability proof is provided even though the complexity of the model.

Chapter 2 is devoted to the modelling of the twin-screw extrusion process. The proposed model is based on mass and energy balances with the assumption of variable viscosity. The rheological behaviour of the melt strongly depends on several dynamical parameters such as temperature, shear rate and material properties. In this study a Cross-WLF model for viscosity was considered for the extrusion of Polypropylene. The developed bi-zone model was discretized using a finite volume method approach in order to deal with a moving interface. The discretization method for the system was presented taking into account the difficulties of having a highly non-linear coupled system. In Chapter 3 dynamic simulations of the bi-zone model with variable screw-speed and variable input flow was presented. Two different conditions for viscosity have been taken into account:

constant and variable viscosity. The results showed the dynamics of the moving interface, filling ratio and temperature along the process with physical coherence. Also, the importance of the assumption of variable viscosity was proved since the temperature dynamics of the model depends entirely on the rheology of the melt.
In Chapter 4 an experimental validation of the extrusion process bi-zone model adapted to an industrial twin-screw extruder is presented. The extrusion of Polypropylene was chosen because it is a shear sensitive material which physical properties are well known. This is important in the case of variable screw speed since at higher values the shear heating provided by the screw rotation becomes the main heating source. On the other hand the steady state of the extrusion process model was studied through the implementation of an optimization problem using a golden search algorithm. It is worth point out that, on previous works this has not been addressed because of to the complexity of the model. Future work will consider the development of a systematic approach for the identification of the equivalent geometry and a viscosity model of the extrusion process. Improving the instrumentation of the extruder in order to obtain raw temperature measurements will be considered.
Chapter **??** deals with the control of the extrusion process. First an entropy balance for the extrusion process is presented which could be useful for control purposes in future works. Then, an energy-based control for the validated extrusion process is studied. The viscosity is assumed as constant internally in the controller while the plant is simulated with the Cross-WLF model for viscosity. This simplification was made in order to simplify the stability analysis of the controller. The simulation example showed that the model-based controller is able to accurately control the melt temperature and internal energy. However, the suggested control law requires the computation of the internal energy which in turn requires the knowledge of the temperature and the filling ratio inside the extruder. An estimation of such variables remains as challenge for the control implementation.

6.2 Future research

The complexity of the extrusion process and the bi-zone model presented in this study consisting of highly coupled partial differential equations is a topic of constant interest in modelling and control theory. Therefore, the results presented in this study stands as an exploration which suggests many open problems. Regarding to the extrusion process modelling, the problem related to variable viscosity is of major interest for different applications since different rheological models could be tested for several materials. It is worth to point out that a more complex geometry of the screws could be tested, and then several moving interfaces may be considered. Future works will also consider the

development of a systematic approach for the identification of the equivalent geometry and a viscosity model of the extrusion process. Improving the instrumentation of the extruder in order to obtain raw temperature measurements will be considered. On the other hand, reactive extrusion which consider the processing of different raw materials is an interesting challenge because different densities should be taken into account.On the other hand, the assumption of variable viscosity within the controller remains as an important challenge to deal with in the future. In addition, the use of an entropy-balance approach for control purposes is an interesting alternative to be analyzed.

Bibliography

[1] Chamil Abeykoon, Adrian L. Kelly, Elaine C. Brown, and Javier Vera-Sorroche. Investigation of the process energy demand in polymer extrusion: A brief review and an experimental study. *Applied Energy*, (136):726–737, 2014.

[2] M. Hasan Iqbal. *Advanced Control of the Twin Screw Extruder*. PhD thesis, University of Alberta, 2010.

[3] M. Bauser, G. Sauer, and K. Siegert, editors. *Extrusion: Second Edition*. ASM International, 2006.

[4] L. P. B. M. Janssen. Twin screw extrusion. *Chemie Ingenieur Technik*, 50(1):562, 1978.

[5] Z. Tadmor and I Klein. *Engineering Principles of Plasticating Extrusion*. Van Nostrand Reinhold Company, 1970.

[6] B. Vergnes and F. Berzin. Modeling of reactive systems in twin-screw extrusion: challenges and applications. *Chimie*, 9:1409–1418, 2006.

[7] H. F. Giles Jr., J. R. Wagner Jr., and E. M. Mount III. *Extrusion: The Definitive Processing Guide and Handbook*. William Andrew Publishing, 2005.

[8] J. A. Covas and A. Gaspar-Cunha. Polymer extrusion-setting the operating conditions and defining the screw geometry. *In: Optimization in Polymer Processing*, pages 1–35, 2011.

[9] M. L. Booy. Geometry of fully wiped twin-screw equipment. *Polymer Engineering and Science*, 18(12):973–984, 1978.

[10] H. Potente, J. Ansahl, and B. Klarholz. Design of tightly intermeshing co-rotating twin screw extruders. *International Polymer Processing*, 1(IX):11–25, 1994.

[11] L. Wang, S. Smith, and C. Chessari. Continous-time model predictive control of food extruder. *Control Engineering Practice*, (16):1173–1183, 2008.

[12] S. C. Garge, M. D. Wetzer, and B. A. Ogunnaik. Control-relevant model identification of reactive extrusion processes. *Journal of Process Control*, 22(8):1457–1467, September 2012.

[13] Mohammad H. Iqbal, U. Sundararaj, and S. L. Shah. New approach to develop dynamic gray box model for a plasticating twin-screw extruder. *Ind. Eng. Chem. Research.*, C(49):648–657, 2010b.

[14] J. Tayeb, B. Vergnes, and G. Della Valle. A basic model for a twin-screw extruder. *Journal of Food Science*, 4(54):1047–1056, 1989.

[15] D. van Zuilichem, E. van der Laan, and E. Kuiper. The development of a heat transfer model for twin screw extruders. *Journal of Food Engineering*, 11(3):187–207, 1990.

[16] M. K. Kulshrehtha and C. A. Zaror. An unsteady state model for twin screw extruders. *Trans. Inst Chem. Eng*, C(70):21–28, 1992.

[17] M. Diagne. *Modelling and control of systems of conservation laws with moving interface: an application to an extruson process.* PhD thesis, Université d'Lyon, 2013.

[18] J. Rae Elsey. *Dynamic Modelling Measurement and Control of Co-Rotating Twin-Screw Extruders.* PhD thesis, University of Sidney, 2002.

[19] M. K. Das and P. S. Ghoshdastidar. Experimental validation of a quasi three-dimensional conjugate heat transfer model for the metering section of a single screw plasticating extruder. *Journal of Materials Processing Technology*, 120(1-3):397–411, September 2002.

[20] S. Choulak, F. Couenne, Y Le Gorrec, C Jallut, P Cassagnau, and A. Michel. Generic dynamic model for simulation and control of reactive extrusion. *Industrial and Engineering Research*, 43(43):7373–7382, 2004.

[21] K.J. Ganzeveld, J.E. Capel, D. J. van der Wal, and L.P.B.M. Janssen. The modelling of counter-rotating twin screw extruders as reactors for single-component reactions. *Chemical Engineering Science*, 49(10):1639–1649, 1994.

[22] de Ville d'Avray Marie-A, A. Isambert, and S. Brochot. Development of a global mathematical model for reactive extrusion processes in corotating twin-screw extruders. *20th European Symposium on Computer Aided Prcess Engineering-ESCAPE20*, 2010.

[23] M.K. Kulshreshtha, C. A. Zaror, D.J Jukes, and D.L. Pyle. A generalized steady state model for twin-screw extruder. *Trans I Chem E*, 1991.

[24] Chin-Hsien Li. Modelling extrusion cooking. *Mathematical and Computer Modelling*, (33):553–563, 2001.

[25] M. Diagne, V. Dos Santos, F Couenne, B. Maschke, and C. Jallut. Modélisation et commande d'un système d'équations aux dérivées partielles avec frontiére mobile: application au procédé d'extrusion. *JESA*, 7(45):665–691, 2011.

[26] V. Dos Santos. Introduction of a non constant viscosity on an extrusion process improvements. *1st IFAC Workshop on Control of Systems Governed by Partial Differential Equations*, (1):215–220, 2013.

[27] Devesh Tripathi, editor. *Practical Guide to Polypropylene*. Rapra Technology Ltd., 2002.

[28] J. Deng, Kang Li, E. Harkin-Jones, M. Price, N. Karnachi, A. Kelly, J. Vera-Sorroche, P. Coates, E. Brown, and M. Fei. Energy monitoring and quality control of a single screw extruder. *Applied Energy*, 133:1775–1785, 2014.

[29] A. I. Isayev. Injection molding and compression molding fundamentals. *Marcel Decker, New York*, 1987.

[30] Mamadou Diagne, Peipei Shang, and Zhiqiang Wang. Feedback stabilization of a food extrusion process described by 1d pdes defined on coupled time-varying spatial domains. *12th IFAC Workshop on Time delay sysyems TDS 2015*, (48), 2015.

[31] Q. Zheng and Gao Z. An energy saving, factory-validated disturbance decoupling control design for extrusion processes. *Proceedings of the 10th World Congress on Intelligent Control and Automation. Beijing*, pages 2891–2896, July 2012.

[32] Yanping Lin, Jiangguo Liu, and Min Yang. Finite volume element methods: An overview on recent developments. *International journal of numerical analysis and modeling, Series B*, 4(1):14–34, 2013.

[33] F. Harlow and J. Welch. Numerical calculation of time-dependent viscous incompressible flow of fluid with free surfaces. *Physics of Fluids*, (8), 1965.

[34] J.A. Sethian. Level set methods:evolving interfaces in geometry, fluid mechanics, computer vision, and materials science. *Cambridge Monograph on Applied and Computational Mathematics*, pages 1030–1035, 1996.

[35] F. Lotero, F. Couenne, B. Maschke, and D. Sbarbaro. Bi-zone modelling and simulation of twin-screw extrusion process with variable screw speed. *8th Vienna International Conference on Mathematical Modelling*, 8:592–597, 2015.

[36] Takashi Yabe. Universal and simultaneous solution of solid, liquid and gas in Cartesian-grid-based CIP method. volume 19, pages 57–71, 2002. doi: http://dx.doi.org/10.1007/978-3-642-56288-4_5. URL `http://link.springer.com/content/pdf/10.1007/978-3-642-56288-4_5`.

[37] Matlab and Simulink. Choose an ODE solver, 2016. URL `https://www.mathworks.com/help/matlab/math/choose-an-ode-solver.html`.

[38] Purushottam D. Gujrati and Arkadii I. Leonov, editors. *Modeling and Simulation in Polymers*. Wiley-VCH, 2010.

[39] A. Poulesquen. *Contribution á la modélisation de l'extrusion réactive en machine bi-vis*. PhD thesis, Ecole des mines de Paris, 2001.

[40] R. J Crawiford, editor. *Plastics Engineering*. Butterworth Heinemann, 2002.

[41] James E. Mark, editor. *Polymer Data Handbook*. Oxford University Press, 1999.

[42] M.Mahishi. Material characterization for thin wall molding simulation. *ANTEC '98*, page 613, 1998.

[43] E. Fel, V. Massardier, F. Mélis, B. Vergnes, and P. Cassagnau. Residence time distribution in a high shear twin screw extruder. *International Polymer Processing*, 29(1):71–80, 2014.

[44] R. Eymard, T. Gallouët, and R. Herbin, editors. *Handbook of Numerical Analysis*. Elsevier, 2000.

[45] Chamil Abeykoon, Adrian L. Kelly, Javier Vera-Sorroche, Elaine C. Brown, and Phil D. Coates. Process efficency in polymer extrusion:corrlation between the energy demand and melt thermal stability. *Applied Energy*, (135):560–571, 2014.

[46] Chamil Abeykoon. A novel soft sensor for real-time monitoring of the die melt temperature profile in polymer extrusion. *IEEE Transactions on Industrial Electronics*, 61(12):1030–1035, Dec 2014.

[47] M. Trifkovic, M. Choo, K. Sheikhzadeh, and S. Rohani. Model predictive control of a twin-screw extruder for thermoplastic vulcanizate (tpv)applications. *Computers and Chemical Engineering*, 36:247–254, January 2012.

[48] J. Elsey, Jörg Riepenhausen, B. McKay, G. W. Barton, and M. Willis. Modeling and control of a food extrusion process. *Computers chemical Engineering*, 21:S361–S366, 1997.

[49] F. Previdi, S. M. Savaresi, and A. Panarotto. Design of a feedback control system for a real-time control of flow in a single-screw extruder. *Control Engineering Practice*, 14(9):1111–1121, September 2006.

[50] Chamil Abeykoon. A novel model-based controller for polymer extrusion. *IEEE Transactions on fuzzy systems*, 6(6):1413–1430, 2014.

[51] D. Q. Mayne, J. B. Rawlings, C. V. Rao, and P. Scokaert. Constrained model predictive control: Stability and optimality. *Automatica*, 36:789–814, July 2001.

[52] M. K. Kulshrehtha, C. A. Zaror, and D. J. Jukes. Automatic control of food extrusion: problems and perspectives. *Food Control*, 2(2):80–86, 1991.

[53] J.M Greenberg and Li Ta Tsien. The effect of boundary damping for the quasi-linear wave equation. *Journal of Differential Equations*, 52(1):66 – 75, 1984. ISSN 0022-0396. doi: http://dx.doi.org/10.1016/0022-0396(84)90135-9. URL `//www.sciencedirect.com/science/article/pii/0022039684901359`.

[54] T. T. Li. *Global classical solutions for quasilinear hyperbolic systems*. Wiley, 1994.

[55] J. M. Coron, B. d'Andréa Novel, and G. Bastia. A lyapunov approach to control irrigation canals modeled by saint-venant equations. In *1999 European Control Conference (ECC)*, pages 3178–3183, Aug 1999.

[56] J. M. Coron, B. d'Andrea Novel, and G. Bastin. A strict lyapunov function for boundary control of hyperbolic systems of conservation laws. *IEEE Transactions on Automatic Control*, 52(1):2–11, Jan 2007. ISSN 0018-9286. doi: 10.1109/TAC.2006.887903.

[57] Tor A. Johanssen and Camilla Storaa. Energy-based control of a distributed solar collector field. *Automatica*, 38(7):1191–1199, 2002.

[58] Vincent Duindam, Alessandro Macchelli, Stefano Stramigioli, and Heman Bruyninckx, editors. *Modeling and Control of Complex Physical Systems*. Springer, 2010.

[59] Couenne F., Jallut C., Maschke B, breedvel P.C, and Tayakout M. Bond graph modelling for chemical reactors. *Mathematical and Computer Modelling of Dynamical Systems*, 12(2-3):159–174, April-June 2006.

[60] K. Hangos, J. Bokor, and G. Szederkényi. Hamiltonian view on process systems. *AIChE Journal*, 47(8):1819–1831, August 2001.

[61] S. Balaji, V. Garcia Osorio, and B. E. Ydstie. Passivity based control of reaction diffusion systems: Application o the vapor recovery reactor in carbothermic aluminum production. *Chemical Engineering Science*, (65):4792–4802, 2010.

[62] J. K. Johnsen, F. Dörfler, and F. Allgöwer. L2-gain of port- hamiltonian systems and application to a biochemical fermenter model. *2008 American Control Conference*, pages 153–158, June 2008.

[63] G. Hauke, editor. *An introduction to fluid mechanics and transport phenomena.* Springer, 2008.

[64] José M. Ortiz de Zárate and Jan V. Sengers. Chapter 2 - nonequilibrium thermodynamics. In José M. Ortiz de Zárate and Jan V. Sengers, editors, *Hydrodynamic Fluctuations in Fluids and Fluid Mixtures*, pages 5 – 38. Elsevier, Amsterdam, 2006. ISBN 978-0-444-51515-5. doi: http://dx.doi.org/10.1016/B978-044451515-5/50002-8. URL `http://www.sciencedirect.com/science/article/pii/B9780444515155500028`.

[65] N. Ha Hoang and D. Dochain. A thermodynamic approach to the passive boundary control of tubular reactors. *9th IFAC symposium on Nonlinear Control Systems*, pages 383–388, September 4-6 2013.

[66] Martin Ruszkowski, Vianey Garcia-Osorio, and B. Erik Ydstie. Passivity based control of transport reaction systems. *AIChE journal*, 51(12):3147–3166, 2005.

[67] W. Levine, editor. *The control handbook.* CRC Press LLC, 1995.